Turbofan Condition Monitoring using Evolutionary Algorithm based Gas Path Analysis

at KLM Engine Services

T.O. Rootliep

Technische Universiteit Delft

TU Delft

Turbofan Condition Monitoring using Evolutionary Algorithm based Gas Path Analysis

at KLM Engine Services

by

T.O. Rootliep

to obtain the degree of Master of Science
at the Delft University of Technology,
to be defended publicly on Thursday August 27, 2020 at 10:00 AM.

Student number:	4195728	
Project duration:	September, 2019 – August, 2020	
Thesis committee:	Prof. dr. ir. P. Colonna,	TU Delft, chair
	Dr. ir. W. P. J. Visser,	TU Delft, supervisor
	Ir. P. C. Roling,	TU Delft
	Ir. M.C.G. van der Werf,	KLM Engine Services, supervisor

This thesis is confidential and cannot be made public until August 27, 2025.

TU Delft

Executive Summary

The Maintenance, Repair and Overhaul (MRO) industry of aircraft engines is driven by technological advances that aim to reduce costs and increase safety. This master thesis serves as a basis for the exploration of applying hybrid Gas Path Analysis (GPA) tool condition monitoring to on-wing data of modern turbofan engines such as the General Electric GEnx-1B. Three key concepts are addressed: using a soft-computing optimization approach in combination with GPA, utilizing Continuous Engine Operating Data (CEOD), and implementing a Multiple Operating Point Analysis (MOPA).

Gas turbines deteriorate due to the following factors: fouling, abrasion, erosion, corrosion, and object damage. Turbomachinery component condition can be quantified with two 'health' parameters: component efficiency η and component mass flow capacity W_c. In industry, gas turbine maintenance strategies are evolving towards prognostics, allowing for predictive maintenance. KLM Engine Services (ES) still predominantly applies GPA as a compliance test diagnostics tool in the test cell.

The Gas Turbine Simulation program (GSP), a tried and tested object-oriented non-linear GPA modeling environment, is used at KLM ES. The solver uses a Newton-Raphson root-finding algorithm to calculate compatibility equations derived from the conservation laws. An Adaptive Modelling (AM) module is included in GSP to estimate component condition deviations. The AM module is convenient due to its instant implementation into existing GSP models but can be sensitive to sensor noise. Furthermore, the numerical process of GSP AM includes inverting the solution matrix, which requires a square matrix with an equal number of measured parameters M and health parameters N. This is an issue for next-generation turbofan engines as manufacturers tend to install fewer gas path sensors, creating a $M < N$ situation.

The reduction in gas path sensors on these next-generation turbofan engines, including the General Electric GEnx-1B, is compensated by a greater quantity of accessible in-flight data. This is referred to as Continuous Engine Operating Data (CEOD). All sensors are measured with a greater frequency and information on secondary performance parameters like bleed valves, active clearance control systems, power off-take and variable geometry is added. In this thesis a procedure is proposed where the selection of operating points is based on meeting steady-state stability requirements, vicinity to the GSP model design point, and secondary performance parameter outlier filtering. This method is favoured over using GE snapshot data, which are not guaranteed to be near steady-state and exhibit uniform secondary performance parameter values.

The search for the best approach to circumvent the $M = N$ requirement has led to a method called Multiple Operating Point Analysis (MOPA). The principle working mechanism of MOPA is to utilize multiple data sets at different operating points to overcome the problem of underdetermination ($M < N$). By combining an Evolutionary Algorithm (EA) optimization scheme with a GSP engine performance model, the best fit of health parameter deviations can be determined by minimizing the objective function. A sub-form of the EA class named Differential Evolution (DE) has been chosen as the optimizer. Like all EAs, DE is a parallel direct search method which initializes a population of parameter vectors. New parameter vectors are generated using the genetic operations mutation, crossover, and selection. After a predetermined number of iterations, the best output candidate is returned. Despite the heuristic nature of EAs, their ability to escape local minima and deal with noise makes them suitable for on-wing engine condition prediction.

The hybrid GPA tool has been verified using two different GSP engine models. First, it is proven that the tool can work in underdetermined conditions on the simple J85 straight turbojet engine. Subsequently, different simulated deterioration cases are solved using the GEnx-1B GSP model available at KLM. The hybrid GPA tool is able to identify the direction and magnitude of condition deviation of 10 health parameters, using 6 gas path sensors. The hybrid GPA tool has also been validated using historical in-flight data of the GEnx-1B. Both the single and multi-point adaptations are able to track engine component condition for all 10 health parameters and identify events such as turbine blade failure and water washes. However, the relatively large scatter and a few unaccountable deterioration modes indicate that there is still room for improvement.

Combining CEOD with a hybrid GPA model has resulted in a novel approach which has significant potential to improve condition monitoring practise at KLM ES in order to reduce costs. For this purpose, it is recommended to improve the thermodynamic GEnx-1B model, especially in the cruise operating range. Also, optimizing the numerical processes in GSP for use with DEs can contribute to a greater accuracy and lower computation time.

Preface

This master thesis report is the culmination of my year long research at KLM Engine Services and my time as a student at the faculty of Aerospace Engineering at Delft University of Technology. I am grateful for the chance to conduct my thesis work at KLM Engineering & Maintenance, which has been a very inspiring working environment with a positive atmosphere. This I have realized especially in the last few months, when working from home due to COVID-19.

This thesis would not have been the same without the help of others. First of all, I would like to thank Wilfried Visser for his academic supervision and guidance, and Michel Nollet for his support and aero-engine MRO expertise. Furthermore, I would like to thank the other people at KLM involved in my thesis work: Rob Duivis, Asteris Apostolidis, Dirk van den Herik, Lisa Nieuwendijk, and Martijn van Moorselaar. I would also like to thank prof. dr. ir. Colonna and ir. Roling for taking part in my graduation committee.

I would also like to express my gratitude to my direct colleagues at KLM ES, Albert Timmer, Mike Brull, Juan Regueiro, and Martijn van der Werf in particular, for stepping in last-minute to take part in my graduation committee. I would also like to thank my fellow (ex-)interns, Stijn van Vuuren and Bastiaan Röell, for the insightful discussions and enjoyable travels between Delft and Schiphol Oost. Finally, I would like to thank my family and friends for supporting me throughout my student years.

T.O. Rootliep
Delft, August 2020

Contents

List of Figures

List of Tables

Nomenclature

Acronyms

ACC	Active Clearance Control
AGB	Accessory Gearbox
AM	Adaptive Modelling
AMOPA	Artificial Multiple Operating Point Analysis
ANN	Artifical Neural Network
API	Application Program Interface
APU	Auxiliary Power Unit
ARP	Aerospace Recommended Practise
BBN	Bayesian-Belief Network
BDE	Borland Database Engine
BPR	Bypass Ratio
CAI	Booster Anti-Ice
CAI	Cowl Anti-Ice
CCC	Core Compartment Cooling
CDP	Compressor Discharge Pressure
CEOD	Continuous Engine Operating Data
CFD	Computational Fluid Dynamics
CN	Condition Number
DE	Differential Evolution
DI	Diagnostic Index
DLL	Dynamic Link Library
DOC	Direct Operating Costs
DOD	Domestic Object Damage
DP	Design Point
EA	Evolutionary Algorithm
EEC	Electronic Engine Control
EGT	Exhaust Gas Temperature
EGTM	Exhaust Gas Temperature Margin
EGTMHD	Hot Day Exhaust Gas Temperature
EMU	Engine Monitoring Unit
EMWA	Exponentially Weighted Moving Average
ERP	Engine Rating Plug
ES	Engine Services
ESN	Engine Serial Number
EWMA	Exponentially Weighted Moving Average
FADEC	Full Authority Digital Engine Control
FCM	Fault Coefficient Matrix
FFBP	Feed-Forward Back-Propagation
FL	Fuzzy Logic
FOD	Foreign Object Damage
GE	General Electric
GPA	Gas Path Analysis
GSP	Gas Turbine Simulation Program
GUI	Graphical User Interface
HPC	High Pressure Compressor
HPT	High Pressure Turbine
ICM	Influence Coefficient Matrix
IGV	Inlet Guide Vanes
IQR	Interquartile Range

ISA	International Standard Atmosphere
KF	Kalman Filter
KLM	Koninklijke Luchtvaart Maatschappij (Royal Dutch Airlines)
LHV	Lower Heating Value
LLP	Life Limited Part
LPC	Low Pressure Compressor or Booster
LPT	Low Pressure Turbine
MC	Maximum Continuous
MOPA	Multiple Operating Point Analysis
MRO	Maintenance, Repair and Overhaul
N1	Low Speed Rotor System
N2	High Speed Rotor System
NLR	Dutch National Aerospace Laboratory
NSGA	Non-dominated Sorting Genetic Algorithm
OD	Off Design
OEM	Original Equipment Manufacturer
PR	Pressure Ratio
PTO	Power Off-Take
RH	Relative Humidity
rms	Root Mean Square
SFC	Specific Fuel Consumption
SLSQP	Sequential Least SQuares Programming
SVD	Singular Value Decomposition
TBV	Transient Bleed Valve
TIT	Turbine Inlet Temperature
TO	Take Off
UKF	Unscented Kalman Filter
VBV	Variable Bleed Valve
VFSG	Variable Frequency Starter Generators
VSV	Variable Stator Vanes
WF	Fuel Flow
WPG	Workscope Planning Guide

Greek Symbols

α	Smoothing constant	[-]
Δ	Change	[-]
δ	Normalized pressure	[-]
γ	Specific heat ratio	[-]
η	Efficiency	[-]
ρ	Density	[kg/m^3]
Π	Pressure ratio	[-]
σ	Standard deviation	[-]
θ	Normalized temperature	[-]

Roman Symbols

$\dot{m}$	Mass flow	[kg/s]
$\bar{E}$	Error variable vector	[-]
$\bar{v}$	Measurement noise vector	[-]
$\bar{w}$	Control parameter vector	[-]
$\bar{X}$	Health parameter vector	[-]
$\bar{Z}$	Measured parameter vector	[-]
b	neuron bias	[-]
c_p	Specific heat capacity at constant pressure	[-]
c_v	Specific heat capacity at constant volume	[-]
h	performance model	[-]
k	Neuron	[-]
M	number of measured parameters	[-]
m	Number of measured parameters	[-]

N	number of health parameters	[-]
n	Number of operating points	[-]
p	Pressure	[Pa]
R	Universal gas constant	[J/mol K]
T	Temperature	[K]
v	measurement noise	[-]
w	Synaptic weight	[-]
y	neuron output	[-]
A	Area	[m^2]
CR	Crossover constant	[-]
D	Characteristic Diameter	[-]
e	error of a state	[-]
F	Differential Weight	[-]
h	Enthalpy	[J]
I	Moment of inertia	[kg m^2]
J	Jacobian	[-]
N	Rotational speed	[rpm]
NP	Population number	[-]
P	Power	[J/s]
Q	heat	[J]
Re	Reynolds Number	[-]
s	State vector	[-]
u	Internal energy	[j]
V	Volume	[m^3]
v	Velocity	[m/s]
W	Flow Capacity	[kg/s]

Subscripts

0	Total property
1,2,3...	Engine station number, following ARP755
abs	Absorbed
c	Corrected
cc	combustor
$comp$	Compressor
$crit$	critical
del	Delivered
est	Estimated
exp	Expansion
f	fuel
g	Gas power
is	Isentropic
$mech$	Mechanical
mod	Model
pos	Position
ref	Reference
$turb$	Turbine

1 Introduction

The invention of the gas turbine and its introduction into the commercial aircraft sector has revolutionized air transport. Their favourable power-to-weight ratio and modern advances such as the high bypass ratio turbofan have allowed aircraft to fly further while burning less fuel, bringing long-distance travel to the masses and ushering in an era of globalization [1].

High reliability and long operational lifetimes are expected from these aircraft engines. A next-generation turbofan can operate 25,000 hours between major overhauls; equivalent to circling the globe 515 times [2]. Once a Maintenance, Repair and Overhaul (MRO) activity is required, the costs are substantial, adding up to 8.1% of the Direct Operating Costs (DOC) for civil aircraft [3]. An aircraft operator has three options for aircraft engine MRO: outsource the work to the Original Equipment Manufacturer (OEM), send the engine to a licensed third party, or execute the activities in-house. The Air France KLM Group has opted for the last option, with its MRO branch Air France Industries & KLM Engineering & Maintenance. The KLM Engine Services facility located at Schiphol Oost has the capability to perform full overhauls on four engine types manufactured by GE and CFMI; the CFM56-7B, CF6-80C2, CF6-80E1 and the GEnx-1B. During one of these shop visits, aimed at performance restoration, the engine is dismantled and components are inspected, balanced, and repaired or replace as necessary. Afterwards, a performance compliance test is performed in a test cell environment to ensure the engine is safe to fly and meets its performance targets. KLM ES has a on-site test cell capable of testing three of the four engine types, with the exception of the GEnx-1B, which is tested at the Air France Zephyr test cell in Paris. Additionally, the CFMI LEAP-1A and -1B are also in gradual introduction.

1.1. Context & Problem Statement

Reducing DOCs is crucial to ensure competitive advantages for airlines, making effective and advanced engine condition monitoring methods that streamline MRO processes very desirable. Over the years the KLM ES engineering department has used the Gas Turbine Simulation Program (GSP) as a supporting tool to analyze and evaluate engine performance data. Gas Path Analysis (GPA) techniques are used to translate engine performance data, in the form of gas path measurements, into component condition information. The current use of GSP GPA at KLM is mostly limited to engine diagnostics after unexpected behaviour during the outbound test run.

For optimal performance analysis accuracy, parameter inputs from all gas path sensors at the various engine stations are required. With the next generation GEnx-1B and LEAP engine types, the OEM no longer provides the ability to install additional sensors at the various engine stations. However, the other feature that distinguishes these turbofans from their older counterparts is the introduction of Continuous Engine Operating Data (CEOD). Hence the number of sensors is limited, but the amount of measurement data is vast for each and every flight. The former results in reduced potential to accurately analyze performance through GSP's Adaptive Modelling (AM) method. AM relies on the numerical matrix operations that require an equal number of output condition parameters and input performance parameters. Also, GSP AM is not compatible with novel Multiple Operating Point Analysis (MOPA) methods, which can be used to increase condition prediction accuracy when few measurements are available. These issues uncover the need for a new engine prognostics tool, that caters the demands of KLM ES and harmonizes with the newer features of

modern next-generation turbofans.

1.2. Research Objective & Questions

With the problem statement from the previous section in mind, a main project research objective can be formulated as follows:

> *To make the use of Gas Path Analysis techniques at KLM Engine Services future-proof, by developing an accurate on-wing component condition monitoring tool that can operate with few gas path sensors.*

Subsequently, a literature study was performed in order to establish the best path in achieving this project goal. Two main focus points that form the scope of this thesis were identified: using a soft-computing optimization approach in combination with GPA to circumvent an underdetermined system, and utilizing the advantages of CEOD by implementing a multiple operating point analysis. Combining a GSP model with an evolutionary algorithm optimizer and MOPA is a new theory that has not been done before, and could be very valuable for KLM ES and to the field of gas turbine GPA if successful. The main concepts of this thesis can also be developed into sub-objectives, aiding in splitting the workload and structuring it into a logical report:

- Evaluate the current state of the art in gas turbine prognostics.
- Investigate soft-computing optimization techniques, in particular Evolutionary Algorithms, and their use in conjunction with GPA.
- Implement a Multiple Operating Point Analysis and assess the change in accuracy.
- Assess how CEOD can best be processed and used in order to supply consistent near steady-state operating points.

Using the main research objective and sub-objectives, the research question can be set out.

> *How can multi-point gas path analysis with GSP be combined with Evolutionary Algorithm techniques to perform optimal on-wing component condition prognostics for modern turbofan engines?*

The resulting multi-point hybrid GPA tool will be verified with simulated data, and then applied to on-wing data from the GEnx-1B. Using engineering knowledge and gas turbine expertise from within the KLM ES environment, the condition monitoring results will be validated, in order to arrive at an answer for the main research question.

1.3. Report Structure

In this section the structure of the report will be explained. First, gas turbine theory, modelling, maintenance strategies, and novel theories will be investigated qualitatively in chapters 2, 3 and 4. Using this information, a hybrid GPA tool is developed in chapters 5, 6 and 7. Then, chapters 8 and 9 aim to quantitatively answer the research questions. A more detailed description of each chapter is given below.

Chapter 2 describes the principles of gas turbine operation and maintenance. This is followed by how gas turbines can be modelled, in Chapter 3. The non-linear GPA modelling environment of GSP is also described in detail. In Chapter 4 novel GPA methods are described that could aid in making a better condition monitoring tool for the GEnx-1B. Subsequently, Chapter 5 will show a proof of concept of the hybrid GPA tool, which combines a Genetic Algorithm with the existing GEnx-1B GSP model. This tool is tested on a straight turbojet engine model. Afterwards, in Chapter 6, the intricacies of continuous in-flight data are explained, including the method to extract operating points from the CEOD set. Chapter 7 will expand upon reference model techniques necessary to accurately monitoring engine component condition. Then, in the two penultimate chapters, Chapter 8 and Chapter 9, the hybrid GPA tool is applied to simulated as well as real on-wing engine data. General conclusions are drawn along with future recommendations in Chapter 10.

2

Aero Engine Life Cycle Management

This chapter describes the principles of gas turbine performance, operation and maintenance. This background knowledge is necessary in order to fully understand engine condition monitoring, gas path analysis, and the inner workings of GSP. First, the design and operation of an aero engine is discussed, followed by different forms of deterioration present in gas turbines. Then, different maintenance strategies and techniques are discussed, and how they are currently applied at KLM ES. In the last section the engine sensors and subsystems of the GEnx-1B in particular are explained.

2.1. Aero Engine Design & Operation

A gas turbine is a continuous combustion engine, designed to convert heat into usable power. An aero engine is a subcategory of gas turbines, running in an open cycle with air as the working fluid, and with thrust as the output. An aero turbine in its simplest form is shown in Figure 2.1. Atmospheric air is drawn through the gas path continuously. The air is compressed through the compressor, heat is added by the combustion of fuel in the combustor, the hot gas is expanded in a turbine and subsequently ejected into the atmosphere. Part of the power generated by the turbine drives the compressor, and part provides thrust.

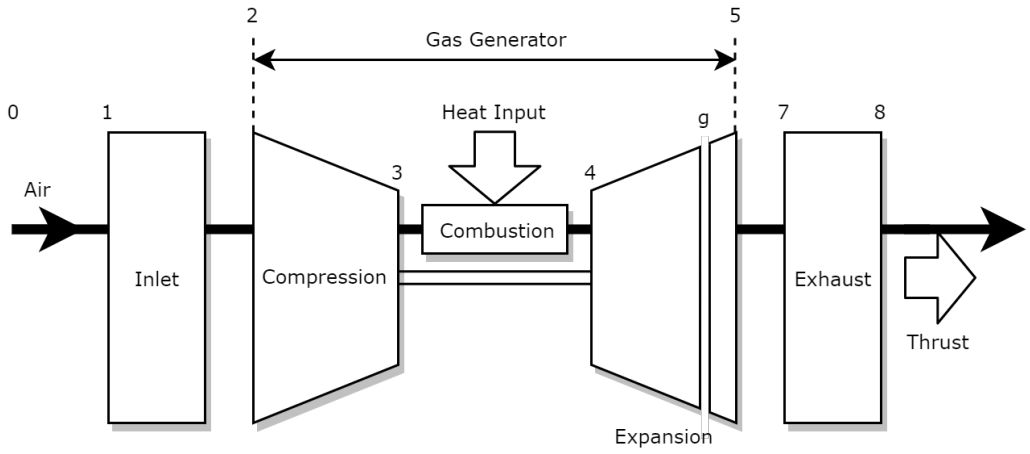

Figure 2.1: Open cycle gas turbine schematic

When adding multiple spools and a bypass flow, the basic aero engine from Figure 2.1 will start to resemble the contemporary engines that power the latest commercial airliners. These so-called turbofan engines are very complex machines, designed for high propulsive efficiency and low weight. A cross-sectional diagram of a typical modern turbofan, the GEnx-1B, is shown in Figure 2.2. The station numbering and major component modules are also indicated, using the Aerospace Recommended Practise (ARP) 755 station designation, which will be used throughout this report [4]. The difference between stations 12 and 2 is that they

indicate the fan inlet tip and hub locations. In the maintenance process, the engine is split up into the following modules: fan rotor, fan stator assembly, Low Pressure Compressor (LPC), High Pressure Compressor (HPC), combustor, High Pressure Turbine (HPT), Low Pressure Turbine (LPT), turbine rear frame, and the accessory drive assembly. The fan and LPC are connected to the LPT via the N1 shaft, while the HPC and HPT are linked with the N2 shaft. In terms of deterioration, the most sensitive components are the HPC and HPT. The fan, LPC and LPT are also key components that determine overall engine efficiency; however they are less sensitive to deterioration according to the GEnx-1B workscope planning guide [5]. However, it is still convenient to include all five of these modules in a condition monitoring system. The combustor module is usually not included, as combustor deterioration is difficult to model.

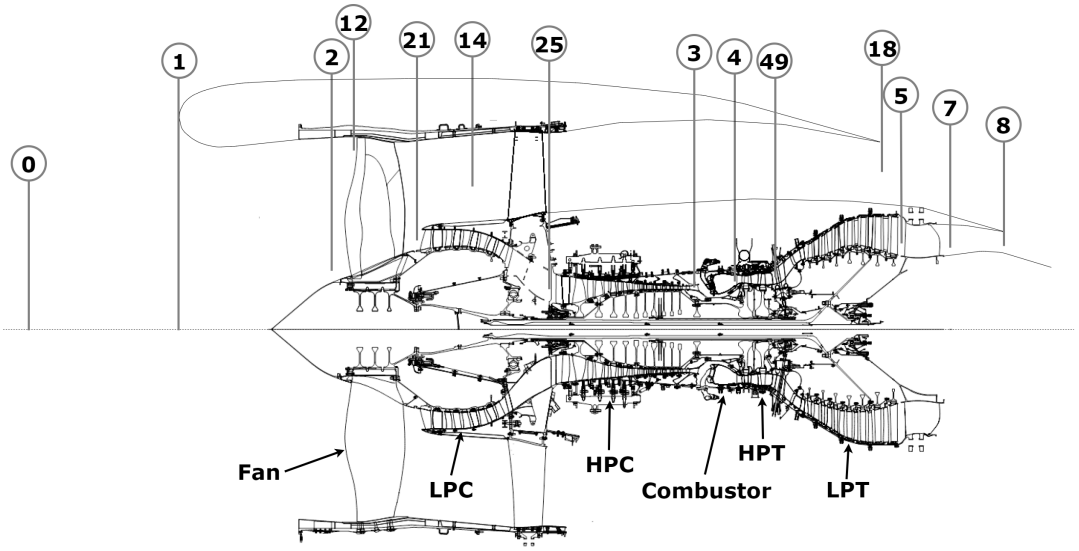

Figure 2.2: Cross-section schematic of the GEnx-1B, marked with station numbering and major component names [adapted from [6]]

2.2. Deterioration

When in operation, gas turbines deteriorate. There are several factors that contribute to a performance loss in gas turbine components; fouling, abrasion, erosion, corrosion, and object damage [7, 8]. These sources can be split up into recoverable and unrecoverable deterioration. All of these factors will be briefly expanded upon below.

2.2.1. Fouling

Fouling is the accumulation of particles that adhere to the internal surfaces of gas path components [9]. These deposits can alter blade profiles and increase their surface roughness. Also, the mass flow area is narrowed when fouling builds up [7]. As a result, fouling reduces the mass flow rate, efficiency and pressure ratio of gas turbine components [10]. In general, fouling is a recoverable process, as it can be reversed to some degree with water washes. During a water wash, detergent and water passes through the gas path of the turbofan, washing away any build up [11]. However, water washes are most effective at removing compressor (cold section) fouling, as particles melt and can be baked to surfaces in hot engine sections [9].

2.2.2. Abrasion

Abrasion occurs when a rotating surface rubs on a stationary surface, wearing off material. Usually, this occurs in a gas turbine in the form of tip clearances and seal wear. In the case of seals, abrasion occurs by design, in order to establish the proper clearance. Seal teeth wear in to an abradable honeycomb material. However, after this seal run-in period, the clearance will continue to gradually increase due to thermal growth, centrifugal growth and turbulence, inducing leakage flows [8]. The same principle influences tip clearances. A gap between the rotating compressor and turbine blades and shroud means that a small portion of the air bypasses these components on which no work is done [8]. Consequently, tip clearances have a large effect on the efficiency of gas turbines. Abrasion is a non-recoverable process, requiring off-wing maintenance and component replacement.

2.2.3. Erosion
Erosion is the wear of surface metal due to mechanical surface action with particles, larger than 10 microns, hitting the flow surfaces [9]. This can change the airfoil shape, contour and surface finish [8]. This form of deterioration is especially important for turbofan engines, as these fly in unfiltered air, as opposed to land-based gas turbines, and can experience hostile environments. Examples of ingested particles are sand, when taking off in desert climates, and volcanic ash, which can be present in the upper atmosphere.

2.2.4. Corrosion
Corrosion is a chemical reaction whereby metals wear away. Corrosion types such as oxidation and sulfidation mainly attack the sections of a gas turbine experiencing elevated temperatures [9]. Higher temperatures act as a catalyst for these chemical reactions, sometimes denoted as hot corrosion. Corrosion will weaken the metal, causing subsurface cracks and increasing the chance of premature failure [9]. Most turbofan engines are outfitted with a protective coating, designed to prevent excessive corrosion. During maintenance activities, this coating can be reapplied.

2.2.5. Object Damage
All of the previous deterioration effects are gradual over time. It is also possible for sudden damage to occur, called object damage. There are two types of object damage: foreign and domestic. In the case of Foreign Object Damage (FOD), debris from the runway or a bird strike may damage the internals of the gas turbine. Domestic Object Damage (DOD) occurs when an internal component becomes loose and travels downstream. In both cases, damage can be severe and gas turbine performance deteriorates abruptly [12].

2.2.6. Quantifying Deterioration
Engine component deterioration must be quantifiable in order to measure any changes over its lifespan. When studying turbomachinery theory, deterioration can be brought back to an increase in one of the three forms of three-dimensional losses [13]:

- **Profile losses**: entropy generation in the boundary layers of solid surfaces. These losses result from streamwise flows only.
- **Secondary losses**: losses due to flows that vary significantly in velocity and direction from the primary flow. Endwall losses are also included in secondary losses.
- **Tip leakage losses**: The clearances between compressor and turbine blades, seals and shrouds will induce flow tip leakages. No angular momentum is transferred to this portion of the flow, and thus no work done.

However, these losses are not quantifyable unless a full 3D CFD model of the gas turbine is developed. Therefore, an alternative method is to relate the deterioration to the parameter groups as described in Section 3.4.2, because these govern the shape of the component performance maps. It is most common to pick the following two, which can subsequently be called "health" parameters or condition deltas [14–18]:

- Change in component efficiency $\boldsymbol{\Delta\eta}$
- Change in (corrected) component mass flow capacity $\boldsymbol{\Delta W_c}$

However, some authors like Gronstedt [19] use component efficiency in combination with the pressure ratio. In all cases, these parameters are determined in terms of a percentage. Thus, when implementing a GPA method, the deterioration of the five components; fan, LPC, HPC, HPT, and LPT, are characterized solely by two parameters, which is convenient and provides sufficient detail when monitoring the condition of a gas turbine.

2.2.7. Effect of Deterioration Modes on Components
Subsequently, it is important to quantify how the deterioration mechanisms explained above affect the individual components. In research conducted by Escher [20], a summary was made, which is shown in Table 2.1. The most important conclusion to take from this summary is that component efficiency decreases for all deterioration modes. Component flow capacity always decreases in compressors, while it usually increases for turbines. This is especially important when creating simulated deteriorated data sets, as well as settings bounds for any search algorithm.

Table 2.1: Change in health parameters per component deterioration mode [20]

Component deterioration mode	$\Delta\eta$	ΔW_c	Ratio $\Delta\eta : \Delta W_c$
Compressor fouling	⇓	⇓	1:3-8
Turbine nozzle guide vane fouling	⇓	⇓	1:2
Compressor erosion	⇓	⇓	1:2
Turbine erosion	⇓	⇑	1:2
Compressor corrosion	⇓	⇓	1:2
turbine corrosion	⇓	⇑	1:2
Blade abrasion	⇓	⇑	0.5:1
FOD	⇓	⇕	1:0.5

2.3. Maintenance Strategies

Engine maintenance can be described as the work required during the service life of an engine to ensure it operates reliably, safely and cost-effectively [21]. There are different strategies that have evolved over time in the MRO industry, illustrated in Figure 2.3. The earliest strategy was corrective maintenance, whereby components are replaced post-failure. This strategy is really only applicable to land-based gas turbines, as it implies major safety issues for aero engines. Preventive maintenance quickly became the next dominant strategy. This takes place on a rigid schedule, where parts are life-limited and maintenance intervals are conducted within a predetermined time frame. With this strategy, it is possible that maintenance is conducted too early, as the actual part condition is disregarded [12]. The next major step, shown in Figure 2.3 by the notations red and blue, is the switch to condition-based monitoring. This is called a predictive maintenance strategy, and it has two further distinctions: diagnostics and prognostics. With diagnostics, fault symptoms are detected by monitoring the performance of a gas turbine using sensor data [12]. Next to fault detection, is it also important to isolate the fault by locating the faulty component, and fault identification, so that the root cause of the fault is found [22]. This is only possible when enough health state parameters are available for the engine. The newest advancement within the field of gas turbine maintenance is prognostics. It is desirable to predict impending failures, in order to streamline the maintenance process as much as possible. A prognostic method forecasts the future state of components by calculating the trajectory of deterioration based on current trending of parameter data. If successful, prognostics is superior to diagnostics. Nevertheless, there are faults such as FOD which cannot be prognosticated.

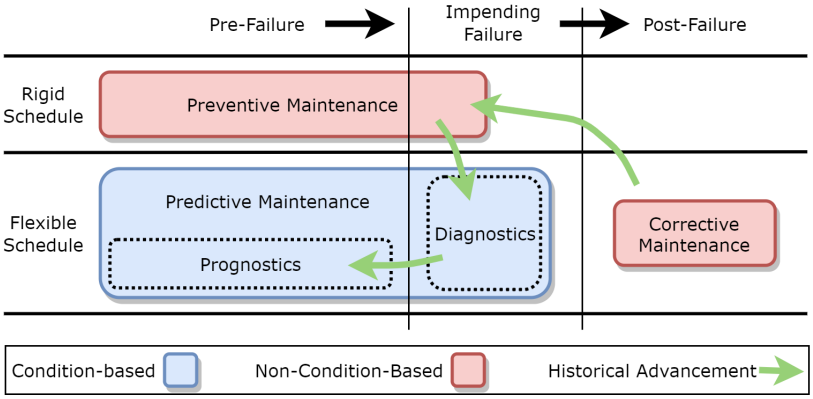

Figure 2.3: Evolution of aero-engine maintenance strategies [adapted from [12]]

2.3.1. Current Maintenance Strategy at KLM ES

Engine maintenance drivers can be categorized into three primary elements: performance loss due to hardware deterioration, the expiration of Life Limited Parts (LLP), and abrupt engine damage [2, 21]. The most important parameter that indicates performance is the Exhaust Gas Temperature Margin (EGTM). EGTM is defined as the difference between the red-line EGT and the peak EGT experienced during takeoff. EGTM can be used as a measure for engine efficiency, as a lower EGTM indicates a degraded engine. During a performance restoration shop visit, the engine is disassembled and components are inspected, balanced, and repaired or replaced as necessary [2]. Part repair and replacement is dictated solely by the engine repair

manual, as formulated by the OEM. The OEM also defines the operating life, measured in number of flight cycles, of LLPs.

However, on-wing engine condition monitoring and workscope management are becoming increasingly important. The in-house tool used by KLM ES for engine monitoring is called PROGNOS. It generates alerts based on engine trending and performance deviation identification using similarity-based modelling. The engineers at Engine Services also have GPA software in the form of GSP at their disposal. This tool is currently applied as a diagnostics tool, in order to identify engine components that contribute to a failed performance compliance test after overhaul [23]. This process is shown in Figure 2.4 by the arrow in red. This can be valuable, as dismantling the entire engine core to find a fault can be avoided. However, GSP is not employed to its full potential this way, which is indicated by the green arrow in Figure 2.4. By using GPA as a prognostics tool as well, engine health can be monitored real-time by accurately tracking gas path deterioration, and predicting when maintenance should take place. If the component condition is known, a tailor-made workscope can be made for each specific engine before it enters the engine shop.

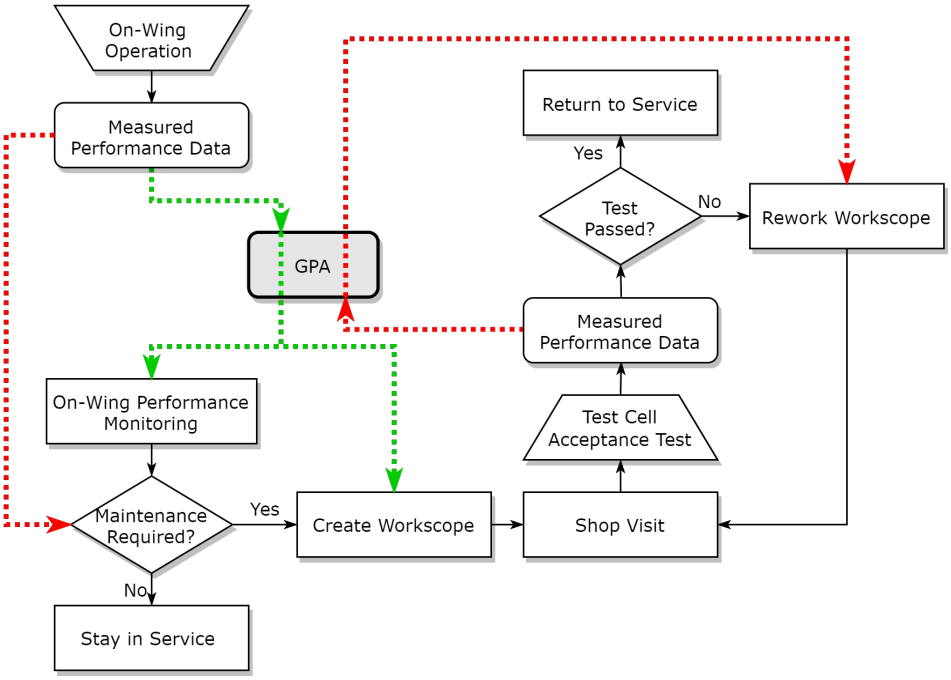

Figure 2.4: Current (red) and future (green) embedding of GPA in the engine maintenance process [Adapted from [16]]

2.4. GEnx-1B Turbofan Engine

After an investigation into general aero-engine operation and maintenance, this section will focus on the GEnx-1B. Later in this report the hybrid GPA tool will be tested specifically on this engine, and for this reason it is important to clarify its major subsystems as well as the engine sensors available for monitoring.

The GEnx-1B is a two-spool, high bypass engine designed for the Boeing 787. Compared to its predecessor it has a higher bypass ratio of 9:1, a 3D CFD core design, and uses composite materials for the fan [24]. The optimized design of the compressor rotors and stators allows for a maximum overall pressure ratio of 48:1 [6]. An illustration of the GEnx-1B without its cowling is shown in Figure 2.5.

2.4.1. Control System

The GEnx-1B Engine Control System is a computer based system with full authority, also called a FADEC. The relevant components include the Electronic Engine Control (EEC), Engine Rating Plug (ERP), Variable Stator Vane (VSV) actuators, Variable Bleed Valve (VBV) actuators, Transient Bleed valve (TBV), High Pressure Turbine Active Clearance Control (HPTACC) Valve; Low Pressure Turbine Active Clearance Control (LPTACC) Valve, Core Compartment Cooling (CCC) Control Valve, engine sensors, and engine starting and ignition components. The system controls the engine following cockpit inputs and provides cockpit indication feedback, maintenance reporting and engine condition monitoring [6]. Values calculated by the performance monitor-

Figure 2.5: General Electric GEnx-1B without cowling [24]

ing tool are GE proprietary and as a result KLM ES does not have access to this data.

2.4.2. Bleed Systems

There are numerous systems which are actively controlled by the EEC in order to optimize the GEnx-1B in-flight performance. These create uncertainties in a GPA model, especially when the modulation in transient operation is unknown. It is therefore important to know how these systems operate. The first are bleed flows are airflows diverted from the core flow path. These can be divided into two categories: internal and customer flows. All technical information in the description below originates from the installation manual [6].

Internal bleed flows interconnect the core flow path with the bypass flow. There are two such systems, controlled by the VBV and TBV. The variable bleed system consists of ten doors located aft of the booster, which can discharge air to the bypass flow in order to prevent compressor stalls. The VBV valves are predominantly active during idle operation and deceleration.

The other bleed system present on the GEnx-1B is the transient bleed system, controlled by the TBV. It is located on the aft HPC case, and discharges HPC air into the bypass stream. This system is used to unload the HPC during starting and acceleration from idle for increased stall margin. In previous research [16, 17, 25], the position of both valves is assumed constant at high power settings, and the effects of internal bleed flows are modeled as constant mass fractions. However, as will be shown in Section 6.3.2, currently available on-wing data does contain VBV and TBV position data, and this could be incorporated into an improved GSP model.

Customer bleed flow, as opposed to internal bleed flow, is air that does not return to the main flow path. As a result, it can be a significant source of loss of work output in a turbofan thermodynamic cycle. Verbist came to the conclusion that GPA diagnostics is also significantly affected by conducting an AM analysis with varying bleed flows [16]. However, as opposed to the the Boeing 787 incorporates a fully electric architecture for the first time, eliminating the need for customer bleed to feed the aircraft environmental control system, wing leading edge anti-ice system, or start the APU.

The only bleed flow that is still supplied for anti-ice purposes is HPC stage 7 air to the outer engine nacelle and the booster. The maximum allowable mass flow for these anti-ice systems varies at different corrected fan speeds. At N1K around takeoff and cruise, the maximum allowable mass flow is 3.3 %.

2.4.3. Cooling Systems

The second type of active systems present on the GEnx-1B are cooling systems. Cooling flows are implemented to permit operation at elevated temperatures. There are both active and passive cooling systems.

The shaft, certain casings and the two stages of the HPT are cooled passively. After these flows have cooled the components, they return to the primary flow. This implies that the core and bypass mass flow stay constant. Therefore, these flows are not additionally modeled in GSP.

Active systems, on the other hand, cannot be ignored when simulating turbofan engine operation. There are three active cooling systems; HPT Active Clearance Control, LPT Active Clearance Control, and CCC. These systems are operated by the EEC with the HPTACC valve, LPTACC valve, and CCC valve, respectively.

During transient operation the tip clearance, or the distance between the rotor and the casing, varies as a result of mechanical and thermal loads. A general example of this phenomenon is shown in Figure 2.6. The case tends to have a faster thermal response to the gas flow temperature than the rotor, due to the difference in mass and material. Large sudden changes in rotor tip radius are caused by centrifugal forces during acceleration and deceleration [26]. These variations indicate the need for an ACC system. This will prevent any potential blade rub, as well as optimize the efficiency by minimizing tip clearances.

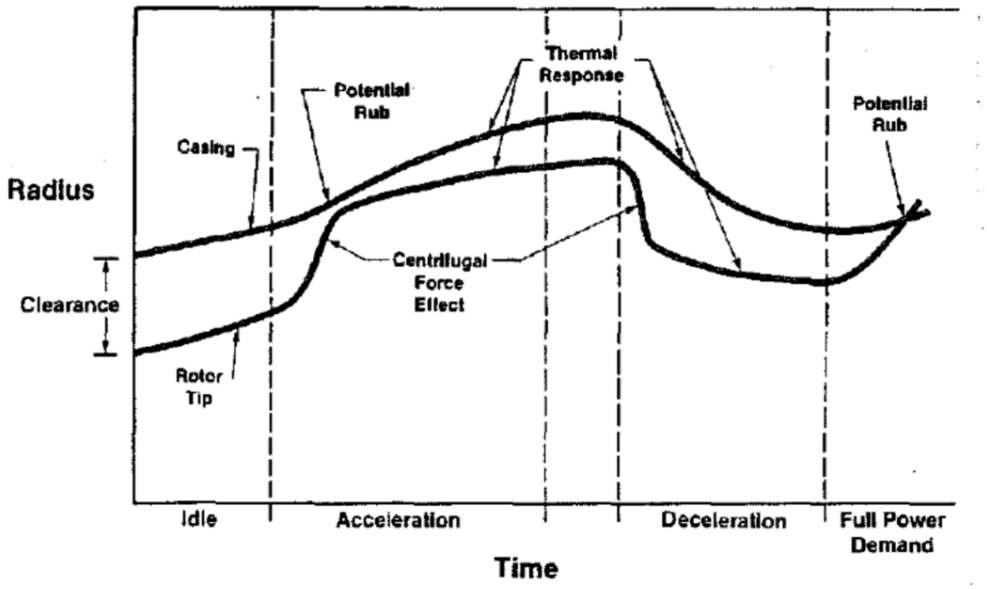

Figure 2.6: General tip clearance variation during transient operation [26]

The GEnx-1B employs an active clearance control system for the HPT and LPT. The EEC controls the amount of fan discharge air through a fuel-operated valve by monitoring sensor inputs. This can pose an issue to a GPA model, as actively varying conditions inside these components are difficult to model. For accurate modelling, all different tip clearances will require a unique component map.

The purpose of the CCC system is to provide cooling airflow to the core under-cowl environment. Fan discharge and VBV air pass through a cooling manifold if the valve is open. This usually occurs at high power settings, but the valve is controlled by the EEC as a function of a variety of sensor inputs. Unlike the HPTACC and LPTACC valve, the CCC valve only has two positions, fully open and completely closed. The CCC cooling air exits the engine through the core engine vent.

2.4.4. Variable Geometry Systems

Lastly, the GEnx-1B employs primary airflow active control systems in order to improve off-design performance. Compressor performance is most critical due to the adverse pressure gradient present. This is why the HPC includes variable geometry in the form of the VSV system. The Inlet Guide Vanes (IGV) and the stages 1-4 stator vanes can rotate on their axis, so that flow angles can vary with spool speed. This is necessary because at low speeds, incorrect axial velocities will cause blade stalling and potential compressor surges [27]. The EEC controls the vane position with the VSV actuator system.

2.4.5. Engine Sensors

One of the major technological advancements of next-gen engines like the GEnx-1B is that its status is monitored constantly by sensors while on-wing. Table 2.2 gives an overview of the most important measured parameters available for condition monitoring on the GEnx-1B.

Table 2.2: Engine sensors present on the GEnx-1B divided by primary and secondary performance parameters

Parameter	Description	Unit
$T_{t,2}$	Total fan inlet temperature	$°C$
$T_{t,25}$	Total HPC inlet temperature	$°C$
$T_{t,3}$	Total HPC outlet temperature	$°C$
$T_{t,49}$	Exhaust gas temperature (EGT)	$°C$
$P_{t,2}$	Total fan inlet pressure	psia
$P_{S,3}$	Static HPC outlet pressure	psia
$N1$	Fan speed	rpm
$N2$	Core speed	rpm
WF	Fuel flow	pph
$HPTACC$	HPT Active Clearance Control Valve Position	%
$LPTACC$	LPT Active Clearance Control Valve Position	%
CCC	Core Compartment Cooling Valve Position	%
TBV	Transient Bleed Valve Position	%
VBV	Variable Bleed Valve Position	%
VSV	Variable Stator Vane Position	%
PTO	Total Engine Horsepower Extraction	hp
CAI	Cowl Anti-Ice Bleed Valve Position	-

These variables can be divided into two groups; gas path sensors and secondary performance parameters, separated by the horizontal line. The compressor inlet static pressure ($P_{s,25}$) sensor was initially also included in the design of the GEnx-1B. However, this sensor has been removed on newer engine serial numbers and its functionality eliminated by a software update in older engines. It is not clear why GE decided to remove this sensor. One possibility is that it reduces the number of components that can potentially malfunction, therefore increasing the reliability of the system. Another option is an additional protrusion could lead to local ice buildup, which could potentially damage the HPC. It is assumed that GE is in possession of the exact component performance maps, and therefore their own need for this sensor is less than it would be for third parties. Another option is that it has been removed to reduce complexity. A pressure sensor at station 25 is less important than at station 3, as HPC stall detection and bleed valve operation is based directly on the $P_{s,3}$ sensor.

The location of the gas path sensors is shown in Figure 2.7. This figure also indicates the desired performance indicators, or health parameters, for each engine component. The choice of performance indicators is explained in more detail in Section 2.2.6. The GEnx-1B has fewer gas path sensors than its predecessors. When compared to the CF6-80C2, also serviced at KLM ES, it lacks pressure sensors at the LPC outlet, HPT outlet, and in the fan bypass duct. Furthermore, a LPT outlet temperature measurement is not available either. As a result, the GEnx-1B has more performance indicators than measured performance variables. As will be explained in more detail in Chapter 3, this forms a problem when performing diagnostics calculations.

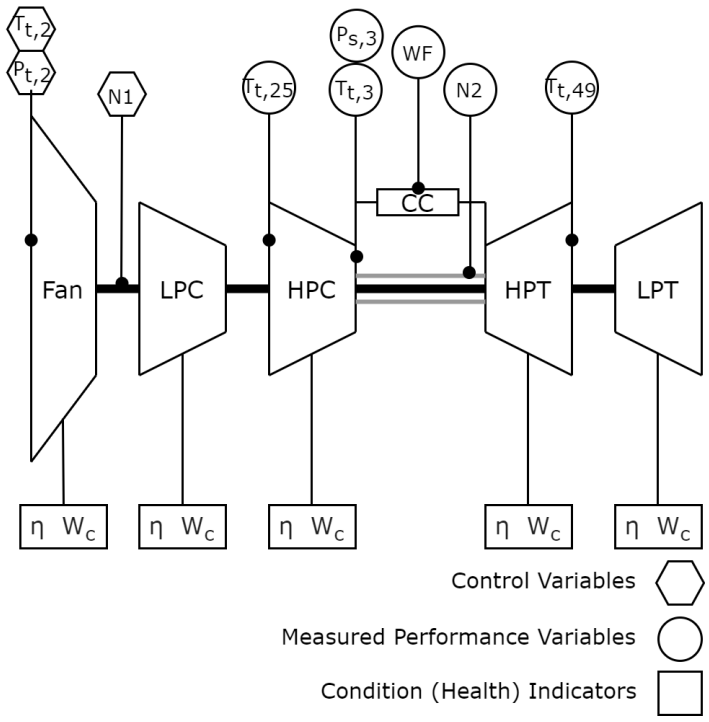

Figure 2.7: Schematic showing component condition indicators and measured performance variables

3

Gas Turbine Modelling & GSP

After a summary of the operation and maintenance of gas turbines in Chapter 2, this chapter will expand on different ways to analytically and computationally model gas turbine performance and deterioration. First, it is explained how the gas turbine can be modelled according to the Joule-Brayton cycle. This is followed by step-by-step design and off-design cycle calculations. Then, different gas turbine modelling techniques are explained. Finally, the non-linear GPA tool GSP is described.

3.1. Ideal Cycle

The first step in setting up a model for an aero engines is to understand its thermodynamic cycle. The gas turbine process follows the Joule-Brayton cycle, and can be expressed in the form of an h-s diagram. In ideal form, this cycle is illustrated in Figure 3.1, consisting of the the following processes between stations 2, 3, 4 and 5:

- Line 2-3: isentropic compression
- Line 3-4: isobaric heat addition
- Line 4-5: isentropic expansion
- Line 5-2: isobaric heat rejection

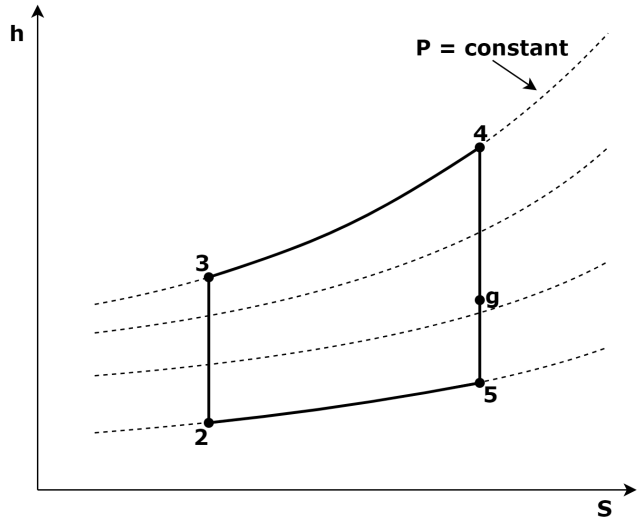

Figure 3.1: enthalpy-entropy (h-S) diagram of an ideal Joule-Brayton cycle

This form of the Joule-Brayton cycle is ideal as there are no losses and no increase in entropy. This is explained in more detail below:

1. The working fluid is an ideal gas, with constant specific heats c_p and c_v. Usually, the thermodynamic properties are expressed in terms of c_p and γ, where γ is the specific heat ratio $\frac{c_p}{c_v} = \frac{c_p}{c_p - R}$
2. There is no change in kinetic and potential energy between the various components.
3. The compression and expansion processes are isentropic. Thus, there is no entropy increase between stations 2-3 and 4-5.
4. The process is a closed cycle, where the atmosphere is modelled as a heat exchanger that cools the working fluid in line 5-2.
5. There are no pressure losses in the combustor, inlet and exhaust. As a results points 1 and 9 lie in exactly the same location as points 2 and 5, respectively. Also, the heat addition between 3 and 4 follows the constant pressure line.
6. Mass flow is constant.
7. There are no mechanical losses in the transmission of power from the turbine to the compressor.

In Figure 3.1, station g is also indicated in the expansion process between points 4 and 5. This marks the point where the distance between 2-3 is equal to 4-g. The residual power, g-5, is called the specific gas power. Gas power is defined as the power that can be extracted from the gas generator. In the case of an aero engine, the isentropic expansion of the gas from stations g to 5 results in the maximum kinetic power, or thrust [15].

3.2. Real Cycle

By reviewing the ideal Joule-Brayton cycle in the previous section, it is possible to adapt it to a cycle that more accurately reflects a real aircraft engine. The changes are summarized below, and can be seen in Figure 3.2.

1. The thermodynamic properties of the working fluid, C_p and γ, are dependent on the temperature, pressure and gas composition. The effects of pressure are negligible. However, both the temperature and the gas composition change significantly between stations, and do need to be taken into account.
2. There are signification changes in kinetic energy between components. Potential energy changes are small and can still be safely ignored.
3. The compression and expansion processes are no longer isentropic. Friction and other losses increase entropy during the process, and as a result the processes are irreversible. This is why lines 2-3 and 4-5 are no longer vertical.
4. The cycle is now open, with no connection between stations 5 and 2. However, cycle entry condition 2 is equal for both open and closed cycles.
5. Friction between the working fluid and gas path walls induce significant pressure losses that cannot be neglected. Also, the addition of heat and mixing between fuel and air causes an additional pressure loss in the combustor. This is why point 4 is located on a lower pressure isobar.
6. Mass flow does not stay constant, since fuel is added in the combustor and bleed flow is used for cooling.
7. There is a mechanical loss in the shaft connecting the turbine and compressor. This will cause the point g to move slightly lower on the 4-5 line.

As a result of the effects stated above, the real cycle deviates significantly from the ideal cycle. These effects also change the equations of a cycle calculation, as will be explained in the following section.

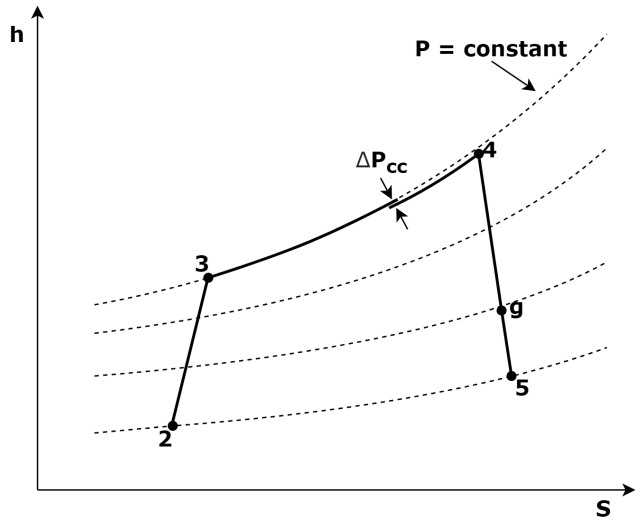

Figure 3.2: enthalpy-entropy (h-S) diagram of the real Joule-Brayton cycle

3.3. Design Point Cycle Calculation

The gas turbine cycle can be modelled as a fully steady-state process, because all its processes are fully continuous [15]. This is in contrast to reciprocating engines, where compression, combustion and expansion take place periodically. In order to understand the workings of a 0D gas turbine simulation program, this section will explain the steady-state real cycle equations used in a design point calculation.

3.3.1. Total Properties

The energy balance of a gas turbine, following the first law of thermodynamics, can be stated as:

$$\dot{Q} = \dot{m}\left(h_2 - h_1\right) + \frac{1}{2}\dot{m}\left(v_2^2 - v_1^2\right) + \dot{W} \tag{3.1}$$

Potential energy is ignored. $\dot{Q}$ denotes the quantity of energy supplied to the system as heat, $\dot{m}$ is the mass flow, h is the enthalpy, v is the velocity, and $\dot{W}$ is the work done by the system. This equation can be simplified to the total enthalpy as follows, by only taking the internal energy part:

$$0 = h_2 - h_1 + \frac{1}{2}\left(0 - v_1^2\right) \tag{3.2}$$

All total properties are defined by the subscript 0. By renaming subscripts the equation becomes:

$$h_o = h + \frac{1}{2}v^2 \tag{3.3}$$

Total enthalpy is defined as the enthalpy level of the fluid if it were brought to a stop adiabatically without any change in work [27]. This total property implicitly states its kinetic energy level, and thus all calculations can be performed without explicitly taking kinetic energy changes into account. This makes cycle calculations less complex. The same can be done for temperature, using the relation between total enthalpy and temperature:

$$h_0 = c_p \cdot T_0 = c_p \cdot T + \frac{1}{2}v^2 \tag{3.4}$$

$$T_0 = T + \frac{v^2}{2 \cdot c_p} \tag{3.5}$$

And pressure:

$$p_0 = p\left(\frac{T_0}{T}\right)^{\frac{\gamma}{\gamma-1}} \tag{3.6}$$

3.3.2. Isentropic Efficiencies

The second important concept in cycle calculations is isentropic efficiency. In order to be able to use the isentropic equations for a real process, an isentropic efficiency term is added. It is defined as the ratio of work for the ideal versus the real process. Isentropic efficiency for a compression and expansion process can be defined as, respectively:

$$\eta_{is,comp} = \frac{T_{0,3,is} - T_{0,2}}{T_{0,3} - T_{0,2}} \tag{3.7}$$

$$\eta_{is,exp} = \frac{T_{0,4} - T_{0,5}}{T_{0,4} - T_{0,5}} \tag{3.8}$$

Then, using the isentropic process relations between temperature and pressure:

$$\frac{T_{0,3,is}}{T_{0,2}} = \left(\frac{p_{0,3}}{p_{0,2}}\right)^{\frac{\gamma_{air}-1}{\gamma_{air}}} \tag{3.9}$$

$$\frac{T_{0,4}}{T_{0,5,is}} = \left(\frac{p_{0,4}}{p_{0,5}}\right)^{\frac{\gamma_{gas}-1}{\gamma_{gas}}} \tag{3.10}$$

Equation (3.9) and Equation (3.10) can be substituted into Equation (3.7) and Equation (3.8):

$$\eta_{is,comp} = \frac{\left(\frac{p_{0,3}}{p_{0,2}}\right)^{\frac{\gamma_{air}-1}{\gamma_{air}}} - 1}{\frac{T_{0,3}}{T_{0,2}} - 1} \tag{3.11}$$

$$\eta_{is,turb} = \frac{\frac{T_{0,5}}{T_{0,4}} - 1}{\left(\frac{p_{0,5}}{p_{0,4}}\right)^{\frac{\gamma_{gas}-1}{\gamma_{gas}}} - 1} \tag{3.12}$$

Equation (3.11) and Equation (3.12) give the isentropic efficiencies of the compressor and turbine, respectively. These equations are true for a constant pressure ratio over the compressor or turbine. This is appropriate when conducting a single cycle calculation. When performing calculations over a range of pressure ratios, the polytropic efficiency is used.

3.3.3. Mechanical Losses

In a cycle calculation, the mechanical losses in the transmission of power between the compressor and turbine are modelled as:

$$\eta_{mech} = \frac{P_{turb} - mechanical\ losses}{P_{turb}} \tag{3.13}$$

The losses of the shaft due to bearing friction and windage is usually very small. However, what is also included is the power needed to drive any ancillary components such as oil pumps [27].

3.3.4. Combustor Efficiency

As stated earlier, losses are associated with the combustor as well. The combustor efficiency is defined by the ratio between the actual energy that is obtained from combustion and the maximum energy that can be extracted from the fuel, using the Lower Heating Value (LHV):

$$\eta_{cc} = \frac{\dot{m} \cdot c_{p_{gas}} \left(T_{0,4} - T_{0,3}\right)}{\dot{m}_f \cdot LHV_f} \tag{3.14}$$

Where $\dot{m}$ is the total mass flow and $\dot{m}_f$ the mass flow of the fuel injected.

3.3.5. Calculation Scheme

Using the definitions in the previous four subsections, an entire gas turbine cycle can be calculated. Also needed are parameters such as the mass flow, component pressure ratios and efficiencies, and the ambient conditions. A steady-state operating point can be calculated for a given turbine inlet temperature or fuel flow.

First, the ambient temperature and pressure are converted to their total properties using Equation (3.5) and Equation (3.6), depending on the velocity or mach number of the aircraft. The pressure loss associated with the inlet is defined as η_{inlet}:

$$p_{0,1} = p_0 \left[1 + \eta_{inlet}\left(\frac{\gamma_{air}-1}{2}\right) M_0^2\right]^{\frac{\gamma_{air}}{\gamma_{air}-1}} \tag{3.15}$$

$$T_{0,1} = T_0 \left[1 + \left(\frac{\gamma_{air}-1}{2}\right) M_0^2\right] \tag{3.16}$$

Next, the flow enters the compression process. These calculations are the same whether the compression takes place in the fan, Low Pressure Compressor (LPC), or High Pressure Compressor (HPC). The temperature increase is given by rearranging Equation (3.11):

$$T_{0,3} = T_{0,2} + \frac{T_{0,2}}{\eta_{is,comp}} \left[\left(\Pi_{comp} \right)^{\frac{\gamma_{air}-1}{\gamma_{air}}} - 1 \right] \tag{3.17}$$

The pressure increases with the given pressure ratio, a component property:

$$p_{0,3} = p_{0,2} \cdot \Pi_{comp} \tag{3.18}$$

For a turbofan engine, part of the flow bypasses the core, and is only compressed by the fan. For a given bypass ratio, the core mass flow is:

$$\dot{m}_{core} = \frac{\dot{m}_{total}}{1 + BPR} \tag{3.19}$$

Using this information, it is possible to determine the power needed to drive a compressor:

$$P_{comp} = \dot{m}_{core} \cdot C_{p_{air}} \left(T_{0,3} - T_{0,2} \right) \tag{3.20}$$

After the compression process, the flow passes through the combustor. The steady-state point is calculated using fuel as the controlling variable in this case. In this case, a given fuel flow is used. Equation (3.14) can be rewritten to give the temperature after combustion:

$$T_{0,4} = \frac{\eta_{cc} \cdot \dot{m}_f \cdot LHV_f}{\dot{m}_{core} \cdot C_{p_{gas}}} + T_{0,3} \tag{3.21}$$

The pressure after the combustor is calculated with the combustor pressure loss in the form of a pressure ratio lower than one:

$$p_{0,4} = p_{0,3} \cdot \Pi_{cc} \tag{3.22}$$

Then, the power delivered by the turbine depends on the power required by compressor:

$$p_{turb} = \frac{P_{comp}}{\eta_{mech}} \tag{3.23}$$

Using this information, the turbine exit temperature can be determined:

$$T_{0,5} = T_{0,4} - \frac{P_{turb}}{\left(\dot{m}_{core} + \dot{m}_f \right) C_{p_{gas}}} \tag{3.24}$$

Furthermore, the pressure is determined by using the equation for isentropic expansion efficiency (Equation (3.12)):

$$p_{0,5} = p_{0,4} \left[1 - \frac{1}{\eta_{is,turb}} \left(1 - \frac{T_{0,5}}{T_{0,4}} \right)^{\frac{\gamma_{gas}}{\gamma_{gas}-1}} \right] \tag{3.25}$$

This procedure is equal for the High Pressure Turbine (HPT) as well as the Low Pressure Turbine (LPT).The LPT provides the power to drive the LPC as well as the fan. The final part of the cycle calculation consists of determining the nozzle critical pressure ratio and subsequently thrust. If the flow velocity exceeds Mach 1 in the nozzle, it is choked. The critical pressure ratio has to be lower than the expansion of the turbine exhaust gases to ambient pressure for the flow to be choked, given by:

$$\frac{p_{0,7}}{p_{amb}} \geq PR_{crit} = \frac{1}{\left[1 - \frac{1}{\eta_j} \left(\frac{\gamma_{gas}-1}{\gamma_{gas}+1} \right) \right]^{\frac{\gamma_{gas}}{\gamma_{gas}-1}}} \tag{3.26}$$

Where η_j is the nozzle efficiency. From this point, only the calculations for choked flow are given, as this virtually always occurs.The nozzle exit pressure and temperature are:

$$p_8 = \frac{p_{0,7}}{PR_{crit}} \tag{3.27}$$

$$T_8 = \frac{2T_{0,7}}{\gamma_{gas}+1} \tag{3.28}$$

Note that these parameters are no longer total properties, as the kinetic energy is needed separately to determine the jet velocity:

$$v_8 = \sqrt{c_{p_{gas}} \cdot R \cdot T_8} \tag{3.29}$$

Then, using flow density and nozzle area, the thrust of the core flow can be determined:

$$\rho_8 = \frac{p_8}{R \cdot T_8} \tag{3.30}$$

$$A_8 = \frac{\left(\dot{m}_{core} + \dot{m}_f\right)}{\rho_8 \cdot v_8} \tag{3.31}$$

$$F_{core} = \left(\dot{m}_{core} + \dot{m}_f\right)(v_8 - v_0) + A_8\left(p_8 - p_{atm}\right) \tag{3.32}$$

The bypass thrust is determined in the same fashion. This concludes a turbofan cycle calculation. Some other important parameters are the thermodynamic efficiency and the EGTM. The first is defined as the rate of addition of kinetic energy to the freestream divided by the rate of supplied energy:

$$\eta_{th} = \frac{\frac{1}{2}\left(\dot{m}_{core} + \dot{m}_f\right)\left(V_8^2 - V_0^2\right)}{\dot{m}_f \cdot c_{p_{gas}}\left(T_{0,4} - T_{0,3}\right)} \tag{3.33}$$

This is the efficiency of the gas generator only, excluding inlets, nozzles, and conversion of power to thrust. The Exhaust Gas Temperature (EGT), is the major performance characteristic of a turbofan engine. The maximum temperature obtained in the core of the engine is directly related to its current state. The maximum temperature location is at the turbine inlet (TIT), but the temperature ranges there are too high for the placement of a temperature sensor. Therefore, the EGT sensor further downstream is used. Component deterioration over time will mean an engine has a higher EGT for the same fan speed (N1). When comparing this parameter with a set maximum for a engine, the EGT margin is obtained:

$$EGTM = EGT_{redline} - EGT \tag{3.34}$$

Values for EGTM which are close to zero or negative usually indicate that a shop visit is necessary for performance restoration.

3.4. Off-Design Cycle calculation

When an operating condition changes, a free running gas turbine, given a fixed engine design, will find a new equilibrium steady-state operating point automatically. This dynamic behaviour can be modelled by solving sets of differential equations, which describe a system of state variables [15]. This involves iteration, unlike for the design point calculation.

3.4.1. Conservation Equations

Any off-design point must still be in thermodynamic equilibrium, and thus must satisfy the three conversation laws: conservation of mass, momentum, and energy. These are in their most basic form given by, respectively:

$$\frac{\partial}{\partial t}\left(\rho A\right) + \frac{\partial}{\partial x}\left(\rho A v\right) = 0 \tag{3.35}$$

$$\frac{\partial}{\partial t}\left(\rho A v\right) + \frac{\partial}{\partial x}\left(\rho A v^2\right) = -A\frac{\partial p}{\partial x} \tag{3.36}$$

$$\frac{\partial}{\partial t}\left(\rho A u\right) + \frac{\partial}{\partial x}\left(\rho A v h\right) = 0 \tag{3.37}$$

where ρ is the flow density, A the cross-sectional area, v the velocity, p the pressure and h the specific enthalpy. By solving these equations for a new input value, an off-design point can be determined.

3.4.2. Component Performance Models

For an off-design calculation, a performance model is required for each component. These 'map' the performance of a component in its entire operating range. In this section, only the compressor and turbine component models are discussed, as these have the most complex characteristics. The performance of these components can be fully described with the nine variables given in Table 3.1 [28].

Table 3.1: list of component performance parameters

Symbol	Parameter	Unit
D	Characteristic Diameter	m
N	Rotational speed	rad/s
$\dot{m}$	Mass flow	kg/s
$T_{0,1}$	Total inlet temperature	K
$T_{0,2}$	Total outlet temperature	K
$p_{0,1}$	Total inlet pressure	Pa
$p_{0,2}$	Total outlet pressure	Pa
Re	Reynolds Number	-
γ	Ratio of specific heat	-

These parameters are based on four physical quantities: length, mass, temperature and time. In terms of calculating with these quantities, it is more convenient to conduct a dimensional analysis and group the variables into parameter groups. This way, there are less independent variables and component characteristics can be drawn in a single map. There are six parameter groups [27, 28]:

Dimensionless Parameter Groups

(a) $\frac{\dot{m}\sqrt{ReT_{0,2}}}{P_{0,2}D^2}$ Mass flow

(b) $\frac{ND}{\sqrt{ReT_{0,2}}}$ Rotor speed

(c) $\frac{p_{0,2}}{p_{0,1}}$ Pressure ratio

(d) $\frac{T_{0,2}}{T_{0,1}}$ Temperature ratio

(e) Re Reynolds number

(f) γ Ratio of specific heats

These parameter groups can be simplified further. It is assumed that the variations of gas properties is small, and that the effects of viscosity of the fluid in a normal operation range can be neglected [15]. Thus, parameter groups (e) and (f) can be ignored. Furthermore, the equation for isentropic efficiency, Equation (3.11), is only dependent on the the temperature ratio and the pressure ratio. Therefore, group (d) can be replaced by the isentropic efficiency [28]. Now, the characteristics that define component performance is reduced to four parameters.

From these fully dimensionless parameter groups, other commonly used groups can be derived. The first set is formed when excluding the ratio of specific heats and the characteristic diameter, which is is the case when the working fluid and the geometry are fixed:

Quasi-dimensionless Parameter Groups

(a) $\frac{\dot{m}\sqrt{T_{0,2}}}{P_{0,2}}$ Mass flow

(b) $\frac{N}{\sqrt{T_{0,2}}}$ Rotor speed

(c) $\frac{p_{0,2}}{p_{0,1}}$ Pressure ratio

(d) η Efficiency

Finally, these parameter groups are corrected to ISA standard sea level conditions, which makes them independent of inlet conditions [15]. Using:

$$\theta = \frac{T_{0,1}}{T_{std}} = \frac{T_{0,1}}{288.15} \tag{3.38}$$

$$\delta = \frac{p_{0,1}}{p_{std}} = \frac{p_{0,1}}{101325} \tag{3.39}$$

the corrected parameter groups can be defined as:

Corrected Parameter Groups

(a) $W_c = \frac{\dot{m}\sqrt{\theta}}{\delta}$ Corrected mass flow

(b) $N_c = \frac{N}{\sqrt{\theta}}$ Corrected rotor speed

(c) $PR = \frac{p_{0,2}}{p_{0,1}}$ Pressure ratio

(d) η Efficiency

These four parameter groups can be plotted in a single map, and thus the entire performance characteristic of a compressor or turbine can be determined when any two of the first three groups (a), (b) or (c) is known [27].

Compressor Map

A generic compressor map is illustrated in Figure 3.3. Here, the pressure ratio is plotted against the corrected mass flow. Areas of equal efficiency are depicted by the gray dotted lines, while the black lines indicate lines of constant rotor speed. The middle black dotted line, called the operating line, is where the compressor runs at equilibrium (steady-state). These can also be seen on the related Figure 3.4. For constant speed lines, there is a convex curve of varying corrected mass flow which lead to a maximum local isentropic efficiency, indicated by the black dot. These correspond to operating line steady-state points. The constant speed line with the highest efficiency peak is the most favourable design running speed of the compressor.

At each of the speed lines there is a maximum attainable pressure ratio. At this ratio, a symptom called surge occurs, illustrated by the top black dotted line in Figure 3.3. During surge, the relative velocity of the flow over the compressor airfoils becomes too large, with separation as a result. The compressor stalls, not able to support the adverse pressure gradient, and the flow reverses. This quickly lowers the outlet pressure, the operating point moves down the speed line, stopping the flow reversal. This continues in a repeating cycle, which could be destructive for the compressor. During normal operating conditions, an engine will never reach the surge line, as a surge margin is always maintained with variable compressor geometry.

Another phenomenon clearly visible is choking at high corrected mass flows. This is a critical condition where a shock wave forms at the location with the smallest cross-sectional area, when the flow reaches Mach 1. At this point, a maximum mass flow is reached no matter the reduction in pressure ratio.
These maps are the visual representation of a multi-dimensional table in a computer model. The component operating point is then determined by interpolating in the table from the input parameters [15].

Turbine Map

Turbine maps follow the same approach as the compressor maps, with the four corrected parameter groups. In this case, it is appropriate to plot the efficiency and corrected mass flow against the pressure ratio, as depicted in Figure 3.5. Similar to the compressor, a choking line is visible where constant speed lines merge. The shock wave commonly occurs in the nozzle throat, restricting the mass flow.

The top part of Figure 3.5 shows that the turbine efficiency is dependent on the the rotational speed. The efficiency is nearly constant for a wide range of rotational speeds and pressure ratios. This is because the expanding nature of the flow allows turbine blades to operate effectively over a wide range of flow incidence angles [27].

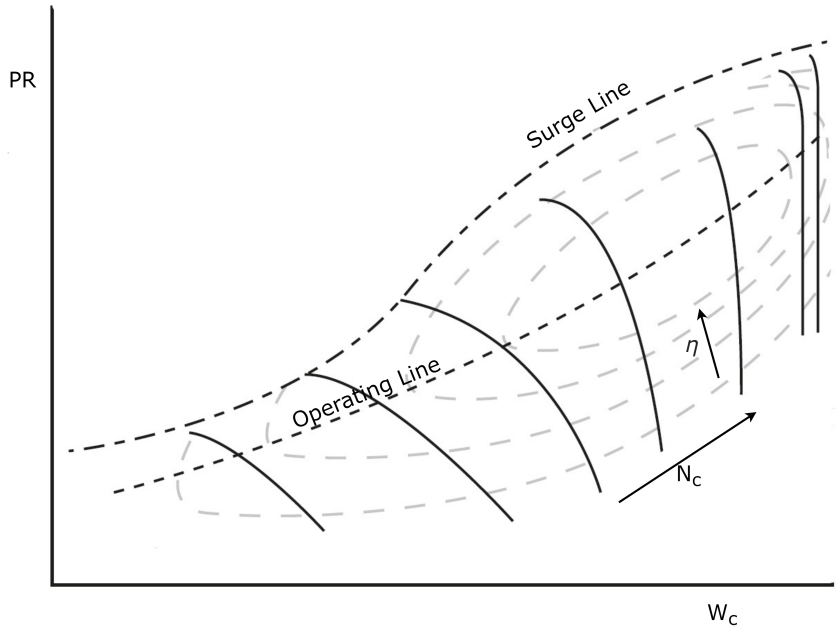

Figure 3.3: typical compressor map

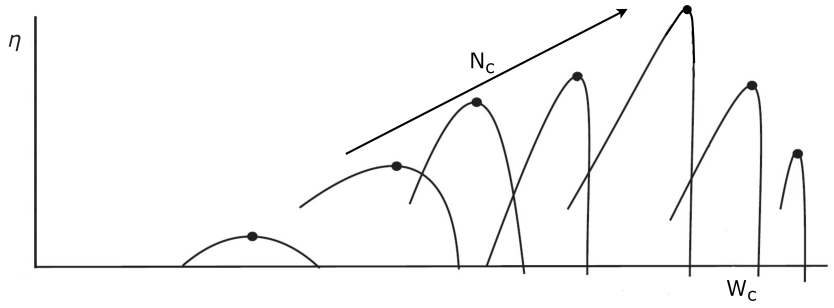

Figure 3.4: compressor map showing efficiency vs mass flow for different speed lines

3.4.3. Calculation Scheme

Using the conservation equations and component performance models, an off-design point calculation can be performed. The component performance models explained previously are linked together to form a single system. This means that the operating points of each individual component must be matched to each other, which is an iterative process. It requires successive guesses of component operating points, while minimizing error in the conservation equations from Section 3.4.1.

There are two ways of going about this process: a nested loop and a matrix iteration. Both are too complex to perform by hand, and require a computer model. The methodology below will explain a simple nested loop calculation, while a matrix operation procedure is shown in Section 3.6.

1. Begin with initial guess of engine power setting and compressor operating point.
2. Complete one pass of the cycle calculation as previously explained in Section 3.3.5, matching the compressor operating point to the turbine operating point.
3. Determine error between the calculated values of the matching constraints (for example shaft rotational speed) and the initial guess.
4. Alter component map operating points slightly and repeat steps 2-3, until the error is between a fixed tolerance limit.
5. The last iteration gives the off-design operation point.

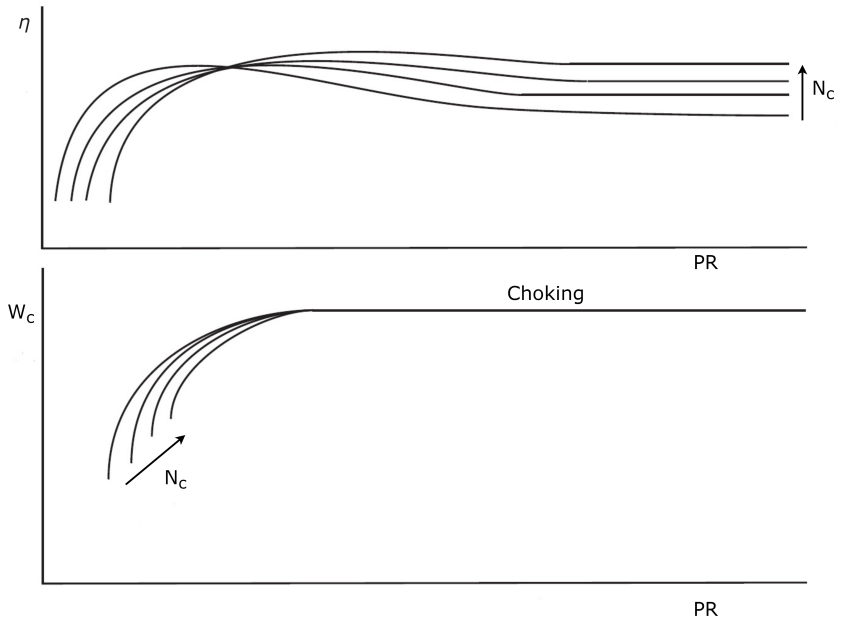

Figure 3.5: typical turbine map

This method is not very efficient when considering 2-spool turbofan engines. These more complex gas turbine systems will require solving a system of equations simultaneously in matrix format, utilizing iteration approaches such as the Newton-Raphson method.

3.5. Modelling Gas Turbine Performance & Diagnostics

Turbofan engine predictive condition-based maintenance can be performed in a number of ways. The monitoring methods can be classified in three groups: model-based methods, soft computing methods, and hybrid methods. The focus of this section is on model-based methods, while empirical methods will be investigated in Section 4.5.

The first step in modelling a gas turbine is defining the spatial dimensions. This can be done in four different ways, increasing in complexity but also accuracy. A short description of each is given below [29]:

- **0D**: The flow properties are only calculated at the inlet and outlet points of components in the flow path. At these points, the flow properties are averaged. This method is the most widely used for performance modelling, as it does not require major computing power or a detailed description of engine geometry.
- **1D**: The flow properties are calculated continuously throughout the engine in one dimension, usually in the direction of flow. These are still averaged properties, but not at discrete points.
- **2D**: The flow dynamics are now calculated in a two-dimensional plane. This usually requires a CFD analysis. The entire engine can be modelled by making the model axi-symmetric.
- **3D**: By adding the third spatial parameter to the 2D model, a complete model is formed, where exact flow behaviour is known at every location in the engine. Such a model is rarely used for an entire engine due to the extremely high complexity and computing time.

3.5.1. Linear GPA

The simplest model-based method is linear gas path analysis. It consists of linearised thermodynamic relations inside the gas turbine that are solved using matrix operations. The thermodynamic relationship between measurement parameters and condition parameters can be expressed as: [30]

$$\bar{Z} = H \cdot \bar{X} \tag{3.40}$$

Where $\bar{Z}$ is the measured parameter vector, $\bar{X}$ the health parameter vector, and H the Influence Coefficient Matrix (ICM). Similarly, the deviations of these parameters can be related as:

$$\Delta\bar{Z} = H \cdot \Delta\bar{X} \tag{3.41}$$

However, for the purposes of condition monitoring it is necessary to have the component condition deviations as an output. Hence, the inverse of H is calculated and Equation (3.41) becomes:

$$\Delta\bar{X} = H^{-1} \cdot \Delta\bar{Z} \tag{3.42}$$

The inverse of H is called the Fault Coefficient Matrix (FCM). It is important to note that Equation (3.42) can only be solved if the number of measurable parameters M is equal to the number of component health parameters N, $M = N$, so that H is invertible. A linear gas turbine model is a powerful tool, as analysis is fast. However, the assumption of linearity only holds near the design point. As indicated in Figure 3.6, this can cause errors of large magnitudes when going beyond this region [16]. At larger deltas, a linear model diverges from reality, making it impossible to detect faults.

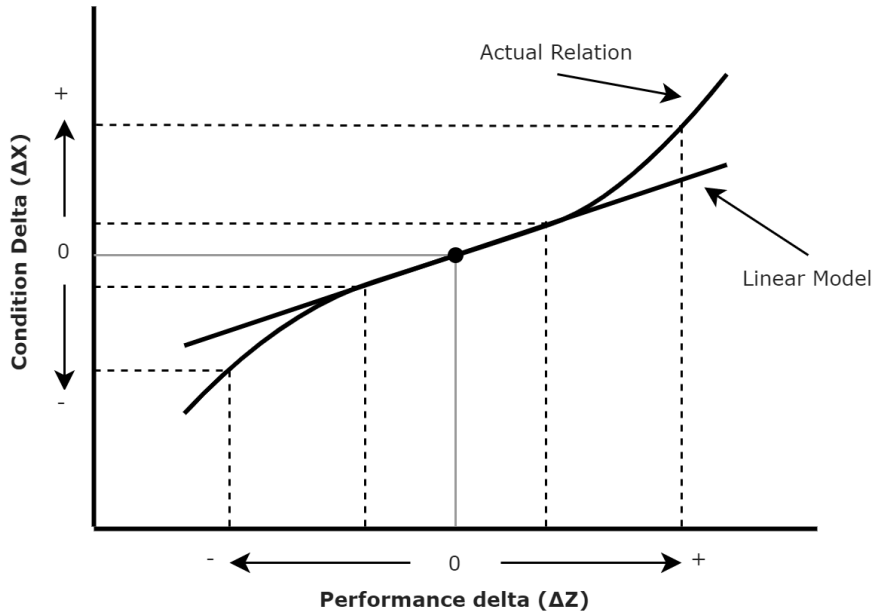

Figure 3.6: accuracy discrepancy between an arbitrary linear model and reality. [16][redrawn]

3.5.2. Non-Linear GPA

In order to accurately model a larger region of the operating range of a gas turbine, nonlinear GPA must be implemented. One method, proposed by Escher and used in his Pythia program [20], is to apply the linear method repeatedly with an iterative process such as the Newton-Raphson method. Corrections are added to the solution vector, described in Equation (3.43), in order to iterate towards convergence.

$$\bar{X}_{new} = \bar{X}_{old} + \Delta\bar{X} \tag{3.43}$$

This method still has its limits in replicating the complex behaviour of gas turbine components. For greater accuracy, the entire engine model has to be adapted in order to match the measured performance. This approach, first proposed by Stamatis et al. [31], is called Adaptive Modelling (AM) and relies on nonlinear thermodynamic relations and altering calibrated component performance maps. This form of nonlinear GPA can have a factor 10 smaller error when compared to linear GPA [12]. The program which utilizes this nonlinear GPA approach with adaptive modeling is described in the following section.

3.6. Gas Turbine Simulation Program

The nonlinear GPA tool used at KLM Engine Services is the Gas Turbine Simulation Program (GSP) [32]. GSP is a modelling environment created by the Dutch National Aerospace Laboratory (NLR) in conjunction with

the Delft University of Technology [33]. It has been successfully used in simulating various gas turbines, and the capability to create customized model topologies makes it ideal for KLM ES applications [34]. It is possible to run design point, steady state off-design point and transient simulations. Since the focus of gas turbofan modelling at KLM Engine Services is on the thermodynamic performance of a turbofan engine, the emission and heat transfer models are not used nor explained in this section.

3.6.1. Components

Individual blocks representing component models can be arranged to form the desired gas turbine configuration. All of the components are 0-dimensional, except for some kinetics in the combustor, which means that parameters such as temperature and pressure are averaged between gas path stations [15].

The design point performance of components can be specified by inputting design parameters in the design tab of the component. For example, for a compressor these could include the parameter groups pressure ratio, rotor speed or efficiency. It is also possible but not necessary to specify geometrical areas, in order to calculate static conditions. Using these parameter groups and the inlet conditions, exit flow and gas conditions are calculated [15].

Off-design component performance is determined by turbomachinery performance maps as well as the aero-thermodynamic relations. Compressors and turbines require these maps, while ducts, inlets and exhausts can be specified with relations. The performance maps have been explained in detail in Section 3.4.2, while the conservation relations will be expanded upon below. GSP uses files with arrays called beta lines which describe and load a performance map into the program. If an operating point is located in between these beta lines, a linear interpolation is used to find the solution. Hence, the solution space is discrete, and not continuous.

3.6.2. Conservation Equations

In order to calculate the engine operating point, the three conservation laws from Section 3.4.1 need to be satisfied. In GSP, these are derived further into compatibility equations between work, mass flow and rotational speed. For the conservation of mass through a component:

$$\frac{dM_v}{dt} = W_{in} - W_{out} \tag{3.44}$$

Where M_v indicated the mass of the volume inside the component. Using the ideal gas law and expressing mass as a function of volume V and density ρ, the change in mass inside a volume becomes:

$$\frac{dM_v}{dt} = \frac{V}{\gamma RT} \cdot \frac{dp}{dt} \tag{3.45}$$

Where V is the internal component volume. Next, from the conservation of energy law, Equation (3.37), the following relation is derived:

$$\frac{dM_v}{dt} \cdot u + M_v \cdot \frac{du}{dt} - Q = w_{in} \cdot h_{in} - w_{out} \cdot h_{out} + P_{abs} \tag{3.46}$$

Where u is the internal energy, Q the heat absorbed by the component, h the enthalpy, and P_{abs} the power absorbed by the component. This equation cannot be solved in one step in GSP. First, the left terms are assumed zero while calculating the power, which is subsequently corrected for when calculating the left-hand side of the equation [15]. The conservation of energy for a driveshaft is slightly different, given in terms of angular velocity ω and moment of inertia I:

$$I \cdot \frac{d\omega}{dt} \cdot \omega = P_{abs} + P_{del} \tag{3.47}$$

The subscripts abs and del indicate absorbed and delivered power. Lastly, the conservation of momentum as used by GSP is given by Equation (3.48) [15]:

$$\sum \left(w_{in} \cdot c_{in} + A_{in} \cdot p_{s\,in} \right) + F_x = w_{out} \cdot c_{out} + A_{out} \cdot P_{s\,out} \tag{3.48}$$

Where c is the flow velocity and F_x a non-linear function not specified here. The conservation of momentum is used for joining flows and calculating the thrust [15]. All of these compatibility equations are given with the time derivative, making transient simulations possible.

3.6.3. Numerical Process

Due to the non-linear differential equations involved, the solution methodology explained in GSP is not as straightforward as the cycle calculation explained in Section 3.3.5. First, a state vector is formed that fully describes the state, or current operating point, of the gas turbine model:

$$\bar{S} = \begin{bmatrix} s_1 \\ s_2 \\ \vdots \\ s_n \end{bmatrix} \tag{3.49}$$

Where s_n are the individual state variables. Then, a component calculation order will be determined, and a 0-D simulation executes the cycle calculation in this order [15]. This generates the error variable vector $\bar{E}$, with the error of each state e_n:

$$\bar{E}(\bar{S}) = \begin{bmatrix} e_1 \\ e_2 \\ \vdots \\ e_n \end{bmatrix} \tag{3.50}$$

If all of the errors are equal to zero, the compatibility equations are exactly satisfied. In GSP, the error for which a solution is converged is set to a default value of 0.001. An iterative method is required in order to converge to a solution. GSP uses the Newton-Raphson method, a root-finding algorithm given by:

$$x_{i+1} = x_i - \frac{f(x_i)}{f'(x_i)} \tag{3.51}$$

x_0 is the initial guess for the root of the function $f(x)$, and using the derivative of the function, $f'(x)$, the x-intercept of the tangent line is taken as the next guess for the root. For adequate initial guesses, the Newton-Raphson method will converge to the solution iteratively. As there are multiple state variables in the case of a cycle calculation, a multi-variable form of the Newton-Raphson method is used. First, the Jacobian is defined as J in Equation (3.52), and is given by Equation (3.53):

$$\Delta\bar{E} = J \cdot \Delta\bar{S} \tag{3.52}$$

$$J = \begin{bmatrix} \frac{\partial e_1}{\partial s_1} & \cdots & \frac{\partial e_n}{\partial s_1} \\ \vdots & \ddots & \vdots \\ \frac{\partial e_1}{\partial s_n} & \cdots & \frac{\partial e_n}{\partial s_n} \end{bmatrix} \tag{3.53}$$

The matrix values in Equation (3.53) can be seen as the linearized approximation of the sensitivity of each error for a change in each state [15]. Now, the next iteration of the state vector can be described by Equation (3.54), where $\Delta\bar{S}$ is a small step change.

$$\bar{S}_{i+1} = \bar{S}_i + \Delta\bar{S} \tag{3.54}$$

By rearranging Equation (3.52), an expression for $\Delta\bar{S}$ is found:

$$\Delta\bar{S} = J^{-1} \cdot \Delta\bar{E} \tag{3.55}$$

By inserting this expression into Equation (3.54), the multi-variate form of Equation (3.51) is as follows:

$$\bar{S}_{i+1} = \bar{S}_i + f \cdot J^{-1}\Delta\bar{E}_i \tag{3.56}$$

This is how GSP solves for the state vector, $\bar{S}$, updating every iteration by using the inverse Jacobian Matrix J^{-1}. Also note that the iteration control parameter f is included, which limits the magnitude of the correction steps. This factor can be user controlled, as well as automatically adapted by GSP. It also allows the same inverse jacobian to be used for multiple steps, decreasing computing time. This can be done as long as the convergence progress is sufficient, otherwise J^{-1} is recalculated [15].

3.6.4. Adaptive Modelling

It is common practise to calculate deterioration and fault effects using Adaptive Modelling (AM) [31, 33, 35–37]. An AM module is implemented in the code of GSP. Adaptive models 'adapt' reference engine data to the measured performance data to estimate component condition deviations [37]. A flow diagram illustrating this procedure is given in Figure 3.7. The measurement data of a deteriorated engine is compared to the baseline engine model, and using adaptive modeling the condition data of this deteriorated engine is calculated on a component level.

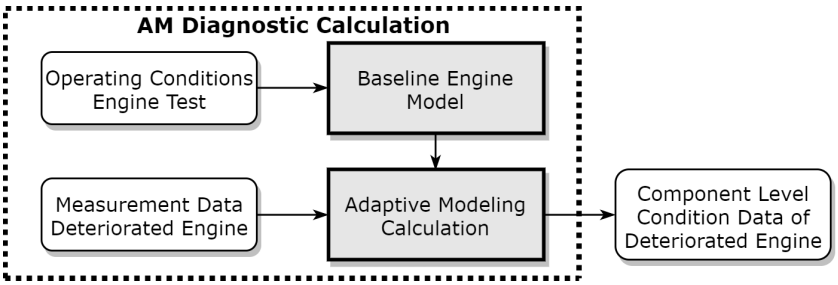

Figure 3.7: Adaptive Modeling procedure as implemented in GSP [33] [Redrawn]

As seen in the previous section, GSP operates by solving a set of non-linear differential equations using the Newton-Raphson method [15]. In adaptive modeling, the additional equations of the deteriorated (adapted) engine are added to the matrix, and then it is iterated towards a solution [37]. The component health parameters from Section 2.2.6 are the so-called map modifiers, and are used to change the compressor and turbine maps. Thus, the system of equations will look as follows [15]:

$$\begin{array}{cccc|ccc|ccc} f_1(s_1)+ & \dots & f_1(s_n)+ & f_1(s_{c1})+ & \dots & f_1(s_{cm}) & = & \varepsilon \\ \vdots & \ddots & \vdots & \vdots & \ddots & \vdots & = & \vdots \\ f_n(s_1)+ & \dots & f_n(s_n)+ & f_n(s_{c1})+ & \dots & f_n(s_{cm}) & = & \varepsilon \\ \hline f_{m1}(s_1)+ & \dots & f_{m1}(s_n)+ & f_{m1}(s_{c1})+ & \dots & f_{m1}(s_{cm}) & = & \varepsilon_{m1} \\ \vdots & \ddots & \vdots & \vdots & \ddots & \vdots & = & \vdots \\ f_{mm}(s_1)+ & \dots & f_{mm}(s_n)+ & f_{mm}(s_{c1})+ & \dots & f_{mm}(s_{cm}) & = & \varepsilon_{mm} \end{array} \tag{3.57}$$

The horizontal and vertical line split the system of equations into its different parts for easier understanding, as explained by Pieters [38]. The upper left section consists of the basic engine model error equations based upon the conservation laws with unknown states s_1 to s_n. The terms in the upper right segment represent the effect of the altered component maps on the calculated engine equilibrium, where scalars s_{c1} to s_{cm} represent the unknown condition factors. The bottom half of the system consist of equations f_{m1} to f_{mm}, that are added by the adaptive modeling component. Of these equations, the terms on the left are the effect of the state variables on the additional error equations, while the terms on the right are the effect of the altered component maps on the additional error equations. The iteration tolerance ε is a set value for off-design calculations, while ε_{m1} through ε_{mm} are the tolerances for each condition factor, and are set manually. It is clear that all of the segments influence each other, which makes solving this system a complex task.

Furthermore, it is important to keep the number of measured parameters and the number of output health parameters equal, otherwise the matrix is not invertible. The solution methodology from this point onwards is the same as for a standard off-design calculation, as explained in the previous section. Since adaptive modeling does not involve any external iteration to find the solution, its convergence speed is much higher than any soft computing method.

3.6.5. Advantages & Drawbacks of Adaptive Modelling

Combining information from the previous sections, the advantages as well as disadvantages to using Adaptive Modelling as a condition monitoring tool for gas turbines are summarized below:

Advantages:

- Simple implementation in existing GSP models

- High adaptability to any kind of GSP model
- User-friendly GUI
- Ability to capture nonlinear behaviour of gas turbine
- Low computational cost, high convergence speed

Disadvantages:

- M=N requirement
- Results only as accurate as reference model
- Not compatible with a MOPA method
- Stability and accuracy issues when data is contaminated with noise and bias, due to deterministic nature
- Multiple (unrealistic) solutions possible, especially with few sensors (risk of smearing: overall engine performance drop caused by a faulty component is inappropriately assigned to other components)

The drawbacks to adaptive modeling indicate that it may not be the best method for condition monitoring of next-generation engines at KLM Engine Services, particularly due to the $M = N$ constraint. This limits the number of condition parameters that can be determined. In order to make a useful diagnosis using only a few measurements, $M < N$, different methods from literature are explored in Chapter 4 are explored.

4

Literature Research

This chapter forms a summary of previous thesis work at KLM, and the current state of the art regarding GPA and gas turbine condition monitoring. First, relevant elements of GPA work at KLM will be investigated, from which a list of advanced engine prognostic requirements can be made. Then, different novel methods from literature are described, and how they relate to the prognostic system requirements.

4.1. GPA at KLM ES

KLM ES has significant heritage in the field of gas path analysis for aero-engine applications. In partnership with NLR and the Delft University of Technology, a long line of students have performed their thesis work at KLM ES, utilizing GSP's capabilities. This section will describe the relevant elements of these projects.

4.1.1. AM Functionality in GSP

The first application of GSP GPA at KLM Engine Services has been performed by Oostveen [39], in association with NLR. He implemented a generic AM module, following the methodology explained in Section 3.6.4, in GSP with the same flexible modeling structure and GUI. Oostveen has proven the functionality of AM by succesfully isolating component faults in simulated deterioration data. When noise is added to the input data, GSP is mostly able to find the correct solution. As a last step, the AM functionality was validated by running test cases with the CF6-50E2 engine in the KLM test cell facility. GSP AM was able to distinguish faulty components from actual engine measurements, but in some cases the parameter selection has to be altered. Optimal sensor selection is performed using the parameter offset method. Even though this is a lengthy procedure, it is of utmost importance for a valid evaluation of the engine condition, according to Oostveen.

Oostveen has also recommended a MOPA to be added to the AM functionality. It was deemed to be too complex and unstable to be implemented at the time. This method will be explained in greater detail in Section 4.4.

Using the AM module from Oostveen, El Bouazzaoui [40] developed a diagnostics tool for the CFM56-7B. The GSP model was developed for take off conditions, and compared with test cell performance data for 3 engines with different engine ratings. The model is shown to be relatively accurate close to the design point. A further analysis is conducted in order to increase the model accuracy in off-design operating conditions by running a transient simulation. However, due to limited information available on the effect of variable geometry systems active during transient operation, the results could not be validated. This thesis marked the first successful implementation of AM as a diagnostics tool at KLM ES, but many issues and shortcomings of the method were also uncovered. These will be summarized at the end of this chapter.

Further post-overhaul performance issues for this engine have been studied by Geris [41], namely the drop in Hot-Day EGT margin after overhaul. This proved difficult as the only flow parameter measured on-wing for the CFM56-7B was the EGT. Using GSP GPA, Geris was not able to find a definitive answer to the research question.

4.1.2. Baseline Calibration Method

In 2009, van Dorp [42] set out to create a GSP diagnostics tool with a dedicated GUI that would be more accurate than TEMPER, the program used by KLM ES at the time. TEMPER uses linear GPA and was only able to detect small condition parameter deviations. Three case studies were conducted, on the CF6-50E2 and CF6-80C2 engines, and the GSP tool gave more insight into the thermodynamic background of the performance issues than TEMPER.

Van Dorp also improved off-design model accuracy using a baseline calibration method. This method goes a step further than the procedure explained in Section 7.1.5 by introducing a set of calibration factors. These alter the model so that it matches the baseline engine over a wider operating range, as shown in Figure 4.1. The advantage of this method is that model off-design accuracy is increased without the need for multiple engine models, a method described further in Appendix B.

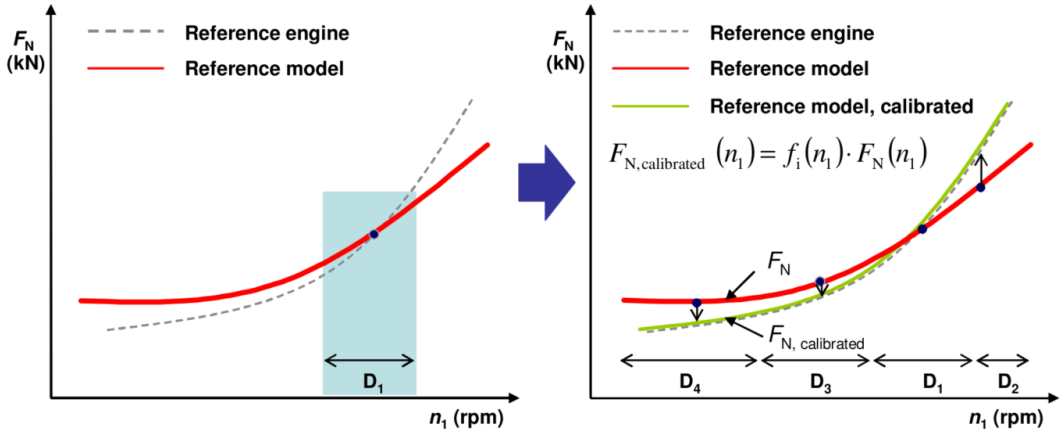

Figure 4.1: Increase in off-design model accuracy by using the baseline calibration method [42]

Subsequently, van Dorp exploits this method by performing the AM calculation for multiple operating points. The condition deviation results are then averaged to form a final solution. This method is simpler than a real MOPA, as no minimizing problem is performed. MOPA would require an alteration of the AM algorithm.

4.1.3. Tuning Compressor Maps

In 2010, den Haan [25] focussed his research on building a proper functioning GSP model of the CF6-80 engines. In contrast to van Dorp, den Haan tuned component maps in order to improve the off-design behaviour of the model. This resulted in suitable accuracy between Maximum Continuous (MC) and Take Off (TO) power. One of the major findings by van Dorp was that GSP AM analysis is enhanced significantly by integrating the LPC component with the fan core component. There are no measurement sensors located between the fan-core section and the LPC, which makes it difficult for GSP to match map modifiers to the LPC only. By looking at the fan core section as an integral part of the LPC on the N1 shaft, the performance parameter changes are more proportional to the actual component deviation. How this is modeled in GSP is illustrated in Figure 8.1.

Following up on the recommendations made by van Dorp, Beishuizen [43] went into deeper detail on this subject by improving the compressor maps of the CF6-80C2. In reality there is no correlation between component efficiency and flow capacity and thrust setting (N1 speed), around a set operating point. However, most GPA models do exhibit such a relation. Beishuizen set out to remove this correlation by utilizing test cell and on-wing data. By fitting a curve to these data points, the speed lines in the compressor maps can be redrawn. More speed lines where added in order to increase the resolution of the map in the operating range. This resulted in more accurate compressor maps. Beishuizen did not alter the turbine maps, as these showed very little correlation to different spool speeds. Overall, Beishuizen succeeded in improving the CF6-80C2 model initially created by den Haan by removing the relation between condition deviation and spool speed.

4.1.4. Enhanced Condition Monitoring

A major step towards the systematic use of GSP GPA in the MRO process was made by Verbist in his dissertation [16]. Verbist is the first to apply a GSP GPA model to on-wing data, for condition monitoring purposes,

and thus his work is highly valuable. The three main subjects addressed are: improving GPA reliability and accuracy, using the available performance data more effectively, and creating an information system concept.

A lack in GPA reliability can be attributed to four factors: measurement error, missing gas path measurements, inaccurate component maps, and incorrect model calibration. The first factor is discussed in greater detail in Section 6.2. The missing gas path measurements issue is difficult to solve. Using proxy parameters as alternative temperature or pressure measurements will amplify real measurement errors, and thus give the resulting parameter deviations and inherently large uncertainty. One of the major differences between test cell and on-wing sensors is the lack of a thrust measurement on-wing. Verbist uses the fan bypass pressure, or $P_{s,14}$, as an alternative, as the bypass flow generates the majority of thrust. However, as is also discussed by Moorselaar in his thesis [17], the GEnx-1B does not have this sensor.

Verbist illustrates effective performance data usage in a number of ways. By first comparing the performance indicators to the EGT and SFC margin, it is possible to see which components affect the overall engine performance the most. The two strongest correlations are present between the HPC condition and EGT, as well as between the HPT flow capacity and EGT margin. Using this information, the relative importance of maintenance on particular components can be established. Next, Verbist conducted a case study to trend the component performance indicators of engines in between maintenance intervals. The case study is successful in monitoring engines on-wing, as engine problems are diagnosed before a shift in the EGT trend is visible. Lastly, Verbist suggests that using an on-wing reference data set will improve the quality of engine condition monitoring results, as it eliminates differences in installation effects between on-wing and test cell data.

The third major area of research was creating a GPA database, for easier long-term condition monitoring. This database is designed to include the following data: on-wing vs test cell distinction, workscopes, measurements, GPA results, and calibration factors, all sorted by Engine Serial Number (ESN). A specialized data importing tool was developed to import performance data into the database. The entire database with all its features is implemented into the GSP AM component, with a similar user interface. Verbist has used this information concept with succes for the CF6 engine types, but it can also be used with GEnx performance data in the future.

Verbist concludes by stating that if GPA is used systematically to analyze operational and post-overhaul performance data, it can be very beneficial to the MRO industry. GPA enables performance prognostics, estimating a cost-effective maintenance workscope before a shop visit, which will restore engine performance to the desired level [16].

4.1.5. Conclusions from Existing GSP GPA Research

Several conclusions can be drawn from the research previously conducted on GSP GPA. The most important and relevant are summarized below:

- Most research has been conducted in a limited engine operating region, from MC to TO power settings
- All reference model tuning is done using test cell data, due to the controlled environment and added measurement capabilities
- A decrease in available engine measurements on newer engines is compensated by a greater quantity of available on-wing data
- Sensor selection plays an important role in the accuracy of GSP analysis
- Off-design performance model accuracy is limited by the availability of turbomachinery component characteristics
- The effect of measurement errors is small when compared to incorrect model calibration and missing gas path measurements
- Using a single, fixed reference data set to analyze multiple engines introduces errors
- Engineering judgment is always required with GSP GPA, as it can return unrealistic solutions even though they are thermodynamically correct.
- Systematic use of GPA in the aero-engine maintenance process remains limited, despite it being recognized as a valuable tool in the industry

Currently, GSP GPA at KLM ES is mismatched to next-gen engines and CEOD. The AM tool can only solve for as many health parameters as there are input measurements. Next-generation turbofan engines have fewer available sensors than older engine models. Thus, not all health parameters can be estimated using AM. Unless the subset of components containing the fault is known, the fault may be attributed to other components (smearing). Therefore, it is worthwhile to investigate other methods that can overcome this issue.

4.2. Advanced Engine Prognostics Requirements

As a starting point for conducting research into novel methods, a list of requirements for an advanced engine prognostics system can be compiled. Meeting these requirements will lead to accurate condition monitoring tool for next-generation engines at KLM Engine Services.

- Predict nonlinear gas turbine behaviour in an operating range from cruise to takeoff
- Model must be robust and stable for all inputs
- Able to deal with measurement noise and sensor bias
- Make a useful diagnosis using only a few measurements ($M < N$)
- Capable of detecting component performance deviations
- Capable of predicting component performance deviations
- Must not be too computationally intensive

4.3. Combinatorial GPA

The first method investigates is combinatorial GPA, which allows for predicting the necessary condition indicators with a limited instrumentation set. This method was first proposed by Aretakis et al. [44], and has also been implemented by Pieters [33, 38]. The full procedure is as follows:

1. Define all different health indicator combinations, for the given set of performance parameters
2. Filter combinations with good observability on the basis of the condition number of the linearized form of the system of equations. This is explained further in Section 8.2
3. Feed these combinations through an adaptive diagnostic model (GSP AM)
4. Calculate the mean and standard deviation of the data set for each performance indicator
5. Calculate a value distribution of each performance indicator and fit a normal distribution over it based on the mean and standard deviation from the previous step
6. Reject all data points outside a 95% confidence interval
7. Combine all health parameters to form a fault signature. Calculate the diagnostic index (DI) for each component using:

$$DI_i = \sqrt{\left(\frac{|\overline{\eta}_i|}{\sigma_{\overline{\eta}_i}}\right)^2 + \left(\frac{|\overline{W}_{c_i}|}{\sigma_{\overline{W}_{c_i}}}\right)^2} \tag{4.1}$$

   Where absolute value of the mean is divided by the standard deviation for each performance indicator. The subscript i indicates the component
8. The faulty components correspond to the largest DI values
9. Now that a diagnosis has been achieved, perform a second pass containing only the faulty components in order to verify the solution and produce a more accurate deviation magnitude

This approach is successful if the subsets include all of the faulty root causes, whereas subsets that do not include all root cause faults contaminate the averaged end result due to smearing. The elimination of incorrect subsets must be done manually, according to engineering judgement. Given that the number of faults (deteriorated condition indicators) is smaller than the number of performance parameters, this method has been proven to return accurate solutions [33, 44]. In the paper by Pieters ([33], GSP GPA results were compared to actual conducted maintenance, and seemed to show agreement in most cases.

4.4. Multipoint Techniques

When looking at new trends in the area of GPA, a promising alternative is conducting a Multiple Operating Point Analysis (MOPA). The principle working mechanism of a MOPA is to utilize multiple data sets at different operation points to overcome underdetermination. The assumption is made that health parameters are independent of the engine operating point. In theory, this results in more detailed engine component condition prognostics. In a study conducted by Loboda [45], the probability of a correct single fault classification is 17% higher when comparing one-point and multi-point diagnosis, increasing from 73% to 89%. This difference increases to 21% for multiple fault classification. Stamatis [46] also verifies the higher accuracy of MOPA.

4.4.1. Single-Objective MOPA

Single-objective MOPA relies on an optimizing scheme in combination with an existing performance model in order to set a diagnosis. The starting point is the relationship for a certain operating point [47]:

$$z = h\big(x, w\big) + v \tag{4.2}$$

Where z is the measurement vector, and the function h varies non-linearly with the health parameters x and control variables w, which include ambient conditions and the parameter used for the engine power setting. In addition, vector v is present to account for measurement noise. Now a minimization function is needed in order to produce a maximum likelihood solution for the nonlinear problem in Equation (4.2). This leads to the following objective function, as developed by Gronstedt [19] from the classic objective function propose by Zedda [48]:

$$f(x) = \sqrt{\frac{\sum_{i=1}^{m}\sum_{j=1}^{n}\left(\frac{z_{i,j}-h_i(x,w_j)}{z_{i,j}\sigma_i}\right)^2}{m\cdot n}} \tag{4.3}$$

where n represents the number of operating points while m is the number of measured parameters within an operating point data set. $z_{i,j}$ describes the measured data, while function h represents the performance model. The standard deviation σ_i is included to scale the influence of each measurement, i, in order to correct for measurement noise v. More information on calculating these standard deviations can be found in Section 6.2.1. The theoretical number of health parameters that can be determined by this technique corresponds to $m \cdot n$, the number of operating points multiplied by the number of measured parameters [19]. With MOPA, there is no longer a distinction between design point and off-design points. Moreoever, it has been claimed that higher accuracy is obtainable when operating points are far from each other [49]

For MOPA to be effective, data from significantly different operating points is required [50]. Hence, MOPA based on data with different power settings, for instance takeoff and cruise, is promising. As such, MOPA combines very well with on-wing snapshot data and CEOD.

Going one step further, an entire portion of flight data could be compared to a transient GSP calculation, with a cumulative objective function [51]. This would come at a cost of computing time. For example, the trajectory of CEOD during acceleration can be compared to simulated transient data in order to measure performance deviation [51, 52]. Li [53] suggests that component deterioration is magnified in transient processes, when compared to steady-state conditions. In practise, however, transient GPA has to be divided into a discrete time series, and thus is can be seen as a very elaborate multi-point analysis.

In order to find the global minimum of the objective function, an optimizing algorithm is required. By far the most popular option in literature is a Genetic Algorithm (GA) [19, 47, 49, 54], as it is able to escape from local minima and deal with noisy data. More detail on GAs can be found in Section 4.5.5.

4.4.2. AMOPA

MOPA has been the subject of constant improvement, with methods that aim for increased result accuracy. One of these variants, named Artificial Multiple Operating Point Analysis (AMOPA), has been proposed by Stamatis [46, 55]. The thinking behind this method is to remove the risk of a wrong diagnosis due to the assumption of health parameter non-variability by implementing artificial extra operating points based on only one engine operating point.

Following the convention from Equation (4.2), an operating point is defined as a vector z containing both measured values x and control variables w. The control variables define the operating point location, and in a standard MOPA procedure would contain (fan) spool speed and ambient conditions. Then an artificial operating point would be created by taking an operating point with different control variables. For example, spool speed is replaced by fuel flow. The spool speed would then be included in the measurement vector x, so that the dimension of y remains the same. Supposing a health parameter deteriorates, the idea of this method is that results with taking the variation of spool speed by keeping fuel flow at the value of intact condition enhances the results when spool speed is constant and fuel flow variation is observed [46]. This is illustrated by Figure 4.2, where a third artificial operating point is present with compressor discharge pressure as a controlled variable. More artificial operating points can be created with measured values that affect the health parameters. According to Stamatis, prediction is improved when more artificial operating points are considered.

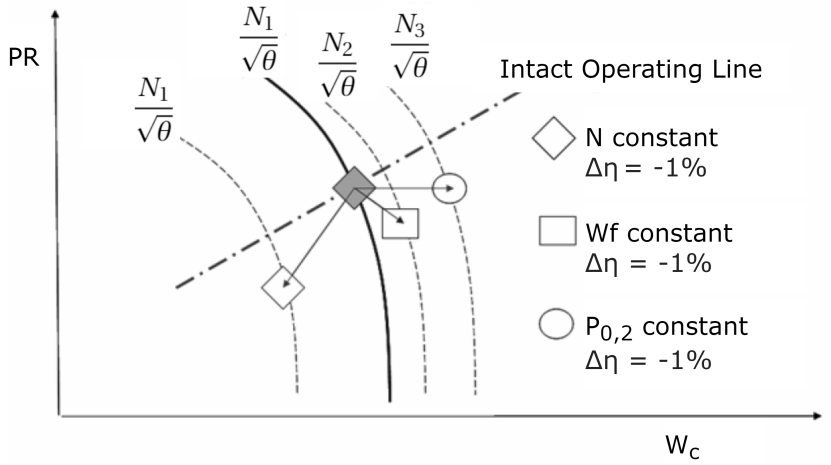

Figure 4.2: Artificial operating points with different control variables in a compressor map for compressor efficiency deterioration [46][Redrawn]

4.4.3. Multi-objective MOPA

Multi-objective MOPA is another variation, where the focus lies on increasing the accuracy through a more elaborate objective function. In the method described in Section 4.4, the objective function outputs for each operating point are simply averaged. This is a simple yet effective way, in most cases, for the optimizing algorithm to deal with multiple points. However, it can occur that the algorithm finds a local minimum, caused by a low objective function value for one operating point, and is subsequently not able to escape this local minimum. If another population member is in a position from where the global minimum can be found, but has a higher average objective function value, there is a lower probability of its survival to the next generation.

A solution to this problem is proposed by Sampath [49] in the form of a Non-dominated Sorting Genetic Algorithm (NSGA) procedure. This method makes use of the concept of Pareto optimality. A Pareto optimal or non-dominated solution is defined as a solution whereby none of the objective functions can be improved in value without degrading any of the other objective values [49]. This concept has been specifically tailored to gas turbine condition monitoring, by sorting all the individuals of a GA population into dominated and non-dominated solutions. Non-dominated solutions will form a Pareto front, as shown in Figure 4.3, and are given higher fitness values. More fronts follow behind this front, with slightly lower fitness values, until the entire population is processed. The advantage of this method is that diversity is maintained within the population, with a greater chance that the optimizer finds the global minimum for the data set.

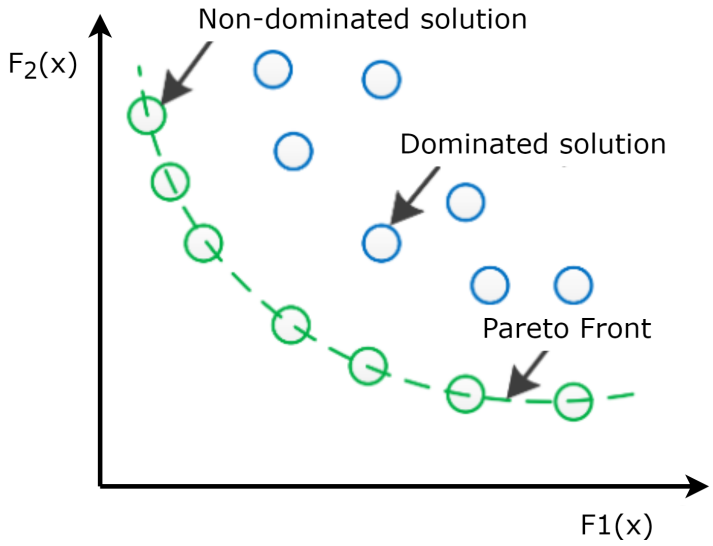

Figure 4.3: Solution space of a dual objective function optimization problem illustrating a Pareto front [56][Redrawn]

4.5. Engine Condition Monitoring with Empirical Methods

An entirely different approach to take for gas turbine diagnostics is to employ purely empirical methods. The main advantages of these methods over model-based methods are that they do not require detailed engine information such as component performance maps, and are able to deal with noise and sensor bias. They usually apply Artificial Intelligence (AI), and approach engine sensor measurement data sets as a pattern recognition problem. Examples include expert systems, Kalman filters, fuzzy logic, Neural Networks and Bayesian-Belief Networks [3, 57]. These will be explained briefly below, along with hybrid methods that combine GPA with heuristic optimization.

4.5.1. Expert Systems & Fuzzy Logic

An Expert System (ES) is a computer program that solves problems by reasoning with specialist subject knowledge [57]. First, a data base is assembled, from which an interpreter inference engine solves problems. For gas turbine monitoring purposes, rule-based systems are most prominently used. These rules must be defined by the program developer, and thus requires some prior knowledge of gas turbine operation. This makes an ES the least sophisticated soft-computing method, with considerable effort needed to maintain and improve the monitoring system. An example of an Expert System within the KLM maintenance environment is PROGNOS. PROGNOS automatically reads on-wing data after it has been downloaded from Engine Monitoring Unit (EMU) after each flight, and generates alerts when any rule output dips below a pre-defined threshold.

In contrast to an ES, which uses a true or false Boolean approach on which computers are normally based, Fuzzy Logic (FL) is a method of computing that can handle 'partial truths' [3]. It is not a stand-alone method, but instead is usually implemented in another soft-computing method for better results. In literature, it has been combined with expert systems [58] and neural networks [59].

4.5.2. Artificial Neural Networks

An Artificial Neural Network (ANN) attempts to replicate the human brain by working with distributed processors that work in parallel as neurons. These neurons can be trained to map inputs to outputs via a nonlinear framework, called the learning phases, and subsequently solve for problems in the operating phase [3]. Among the various different networks, Feed-Forward Back-Propagation (FFBP) Neural Networks are most commonly used for gas turbine diagnostics, and is illustrated in Figure 4.4. For neuron k, w is the synaptic weight, b the neuron bias, and y the neuron output. The training of a neural network refers to the iterative process of adjusting w and b [60]. The NN can also be expanded to include multiple hidden layers.

One of the drawbacks of an ANN is that it cannot operate outside of the range of data to which they have been exposed. This implies that a large data set with all foreseeable fault conditions is required [3].

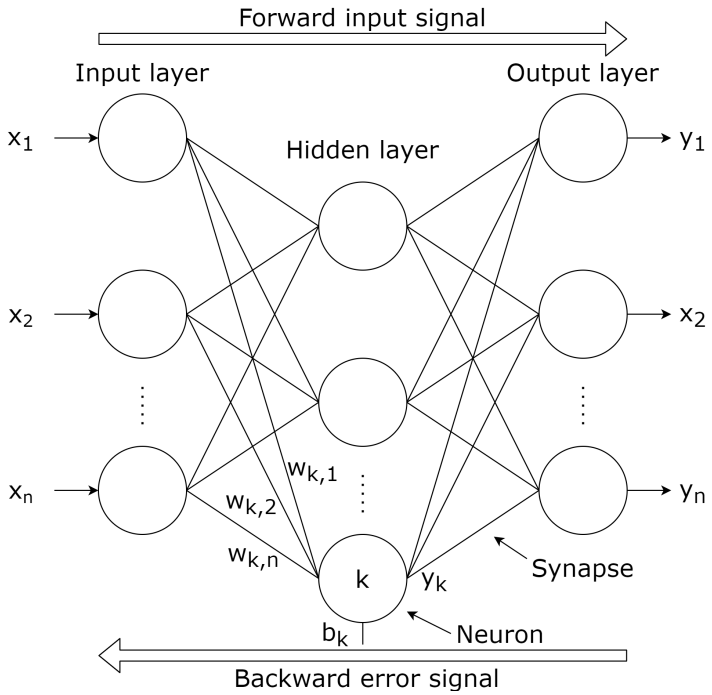

Figure 4.4: Schematic diagram of a Feed-Forward Back-Propagation network [60][Redrawn]

4.5.3. Bayesian-Belief Networks

A Bayesian-Belief Network (BBN) is a hierarchical model that used conditional probabilities, expressing a *degree of belief*, in order to forecast solutions [22]. A turbofan engine is split up into multiple system levels. The flow of fault information moves up system levels, and engine deterioration on a system level (the highest level) is influenced by changes that occur in components lower levels. Degradation signals, or engine measurements, are modelled at all these levels. A health index is computed, which is an indication of the current engine state. By tracking any changes in the health index as well as its covariates from different levels of hierarchy, a prediction of the multiple deterioration trajectories can be made. [61] Like the ANN, this method can return good results within the well-defined bounds of the problem space [22]. Another advantage is that built-in error terms and noise variance mean that a BBN is well-equiped to manage sensor noise [61].

4.5.4. Kalman Filter

A Kalman Filter (KF) utilizes the linear filtering method first developed by Kalman [62] to form a recursive data processing algorithm. A KF uses all available measurement data as prior knowledge of the system, in order to produce an estimate with the statistically minimized error. It can deal with the presence of noise and sensor bias [57]. Other versions are the nonlinear Extended Kalman Filter (EKF) and the Unscented Kalman Filter (UKF), which is more robust to large sensor noise [22].

4.5.5. Hybrid Methods

Hybrid methods combine model-based GPA with a soft computing method in order to either find the component condition deviation or generate component maps. The first case is particularly useful for circumventing the $M = N$ restriction of a nonlinear GPA method.

For example, a heuristic optimizer can be used to replace the iterative matrix operation, and instead form a population of engine design points, which is compared in terms of fitness to the measured data vector every generation. As a result, it is possible to predict more condition parameters than there are measurements. Another advantage is that a heuristic optimizer is more competent in converging to a solution than a stand-alone nonlinear GPA model when the measurement data is contaminated with noise [47]. Contaminated data may lead to a non-physical engine operating point, which an Adaptive Modelling procedure would not be able to solve. When using a heuristic optimizer, on the other hand, methods that deal with noise can be built into the objective function. In the case of single-objective MOPA, the standard deviation σ is used to scale for measurement noise in Equation (4.3).

4.6. Conclusions from Literature Research

The aim of this literature research was to assess the current state of the art in gas turbine condition monitoring and come up with the method best suited for use as a prognostics tool at KLM Engine Services. First of all, it can be concluded that keeping a non-linear GPA program in the form of GSP as part of the tool is the best option for this project, even if GSP is flawed in some aspects. The amount of effort and research that has gone into modelling with GSP, especially at KLM ES, has resulted in a tool that can be very accurate. Another major factor in choosing to keep a physics-based model when analyzing gas turbine performance, as opposed to empirical methods, is that a GSP model of the GEnx-1B is already available. Moorselaar [17] has created a working GSP model that returns accurate results, especially around the takeoff operating range. Although empirical methods, especially ANNs and BBNs, can lead to excellent results in literature, it is uncertain if such results can be achieved within the time span of this thesis project. This is an unnecessary risk to take, especially when a GSP model is already available. Another factor in this decision was the fact that KLM ES itself is heavily invested in GSP, paying license fees every year.

The drawbacks of using a GPA model-based method, however, still need to be addressed. Overcoming the $m < n$ underdetermination requires either a combinatorial or different multi-point approaches. Between these two options, it can be concluded from literature that MOPA has higher potential to return more accurate results. Advantages include introducing a greater number of measurements from multiple operating points, less chance of smearing, and the ability to account for measurement noise. Subsequently, the choice was made to start with a single-objective MOPA, and expand the tool to a multi-objective procedure if sufficient time was available. This turned out not to be the case, and for this reason implementing a multi-objective optimizer is reserved for future recommendations, found in Section 10.2.

In conclusion, a multi-point hybrid GPA tool will be developed for next-generation turbofan engines at KLM ES. The development of this tool will be described in Chapter 5.

5

Multi-Point Hybrid GPA Model

Following from theoretical background in Part I, an advanced condition monitoring tool is developed in Part II, starting with the model itself in this chapter. First, the workings of GSP API is described, followed by a description of the GSP test model. Then, different optimizing algorithms are tested and one is chosen. Finally, the entire multi-point hybrid GPA model is illustrated graphically in the form of a flowchart.

5.1. GSP API

GSP can be used as a stand-alone engine condition monitoring tool when utilizing the built-in AM module. However, for the purposes of this project, it is required to be able to use the GSP simulation capabilities externally. For this reason, a license of the GSP Application Program Interface (API) version was obtained from NLR. This makes interaction and remote calls from other software possible. It comes with a Dynamic-Link Library (DLL) written in the language C++, which contains the functions that are used as the interface between GSP and a high-level programming language such as Matlab or Python. The choice is made to use Python for this project, as it is the standard programming language used at KLM ES. GSP API is only compatible with 32-bit programs, and for this reason a 32-bit version of Python must be used.

5.1.1. Simulation Process

How the communication between Python and GSP works is shown in Figure 5.1. First, the GSP model must be created from within the stand-alone GSP environment. Using the API interface block, inputs and outputs can be defined. Then, Python is used to load the model, communicate the inputs, run the model, and retrieve the simulation outputs. These outputs are subsequently used by the optimizing algorithm.

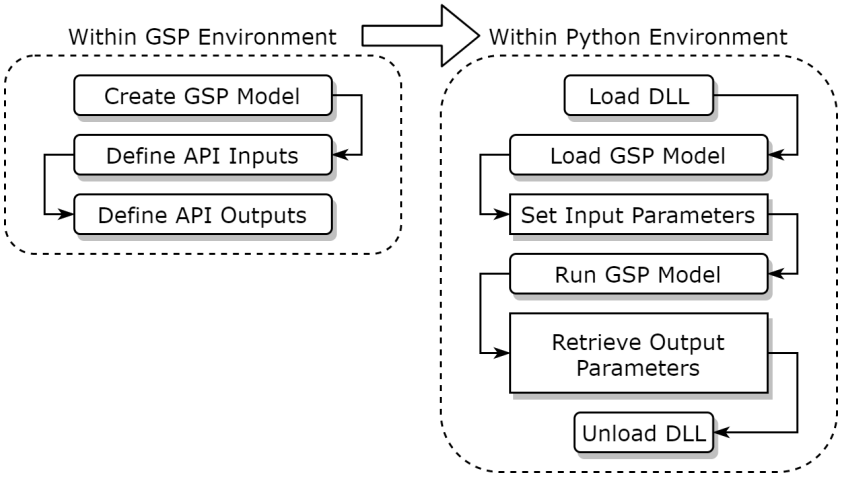

Figure 5.1: Flowchart illustrating the simulation process using GSP API functions

5.1.2. J85 turbojet GSP Model

Before the specifics of the optimizing algorithm is explained, a GSP model is needed as a starting point on which to test the hybrid tool functionality. In order to initially keep the complexity of the hybrid tool to a minimum, a simple single-spool turbojet is chosen in the form of the GE J85 turbojet. This is the go-to standard model within GSP, and its topology is shown in Figure 5.2.

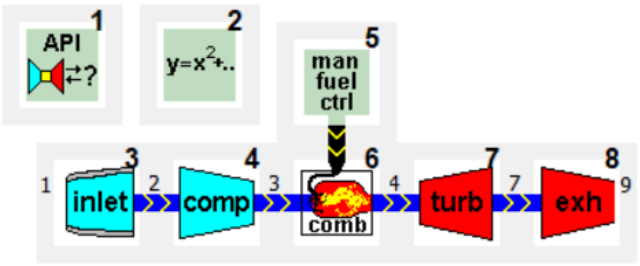

Figure 5.2: Block components which form the GE J85 (TJET) GSP model

Block 1 is called the API interface window, and this is where the inputs and outputs of the model have to be defined. In order to control the model power setting, the spool speed is set using the equation scheduler in block 2. This means that the manual fuel control, block 5, is in a free state. In GSP, it is possible to apply component deterioration effects in the form of three map modifiers: delta correct flow capacity, delta efficiency and delta pressure ratio. As explained before in Section 2.2.6, the first two are used as health parameters. Thus, following the notation from Equation (4.2), the API inputs and outputs for the J85 model are:

Inputs

- 4 health parameters, or vector $\bar{x}$: compressor delta efficiency, compressor delta flow capacity, turbine delta efficiency, and turbine delta flow capacity. The values of these health parameters are constrained, so that the GSP model is not confronted with illogical inputs.
- 1 control parameter, or vector $\bar{w}$: Spool speed N1. Due to the fact that ambient conditions are kept constant anyway, these are not explicitly stated.

Outputs

- 5 engine measurements to start with, vector $\bar{z}$: fuel flow, compressor outlet temperature, compressor outlet pressure, turbine outlet temperature, and turbine outlet pressure.

As this is an ideal model with simulated data, the measurement noise vector $\bar{v}$ is not included. Once the GSP API tool is functional, the number of output measurements can be decreased in order to arrive at a $M < N$ situation. The goal of the python script is to input a certain health parameter combination which returns a measurement vector $\bar{z}$ which is as close as possible to the given (simulated) deteriorated data set. In the next section, different algorithms are tested for this purpose.

5.2. Choosing an Optimizing Algorithm

This section will elaborate on the algorithm used as the optimizer for the objective function Equation (4.3) found in the hybrid GPA tool. There are three main options: a brute-force search, gradient-based optimization and gradient-free optimization. The first method is discarded immediately, as solving for every possible solution in the search space is not feasible for this kind of a problem. For the second method, the search direction is defined by the gradient of the function at the current point. This also requires the problem to be differentiable. If the search space is homogeneous, this provides a fast and efficient way of finding the global minimum of an objective function. However, when local minima are present, there is a high risk that this method will not converge to the optimal solution. Gradient-free optimizers, also called metaheuristics, make few to no assumptions about the problem being optimized. This allows such algorithms to escape from local minima. A drawback of heuristic methods is that there is no guarantee that the global minimum is found.

5.2.1. Gradient-based Optimization

First, a gradient-based optimizer is tested. A logical first choice is the Newton-Raphson method, which produces successively better approximations to roots of a function in an iterative fashion. This method is given by:

$$x_{n+1} = x_n - \frac{f(x_n}{f'(x_n)} \tag{5.1}$$

In order to apply this theorem into the Python program, a Sequential Least SQuares Programming (SLSQP) function is chosen. This is technically a quasi-Newton method, as the Jacobian matrix of the first derivative is not computed explicitly but approximated instead, for increased computational speed. For more specifics regarding the SLSQP algorithm, consult the paper written by Kraft [63]. This method is tested on a simple deterioration case first, where only compressor deterioration is present in the form of a 1% decrease in efficiency and 2% decrease in flow capacity. These values have been determined using Section 2.2.7, where the ratio of efficiency to flow capacity is usually 1:2. The simulation was performed with two operating points, at 95 and 100% spool speed, and bounds that ranged from -2.5 to 1% for the compressor efficiency, compressor flow capacity, and turbine efficiency. Whereas for the compressor the flow capacity usually decreases due to fouling, the turbine flow capacity usually increases, as material burns away to the high temperatures. Therefore, the bounds for the turbine flow capacity range from -1 to 2.5%. Furthermore, all five output measurements are assumed available for this case, so that the problem is not underdetermined, and thus fully solvable for a GSP AM procedure. The results are shown in Figure 5.3. In order to quantify the accuracy of the algorithm, the root mean square error is computed as follows:

$$rms = \sqrt{\frac{\sum_{j=1}^{n} \left(x_j - x_{est}\right)^2}{n}} \tag{5.2}$$

Where x_j is the actual jth health parameter and x_{est} the estimated jth health parameter. For this case, the rms is 0.71, or every predicted health parameter is 1.38% away from the actual health parameter on average.

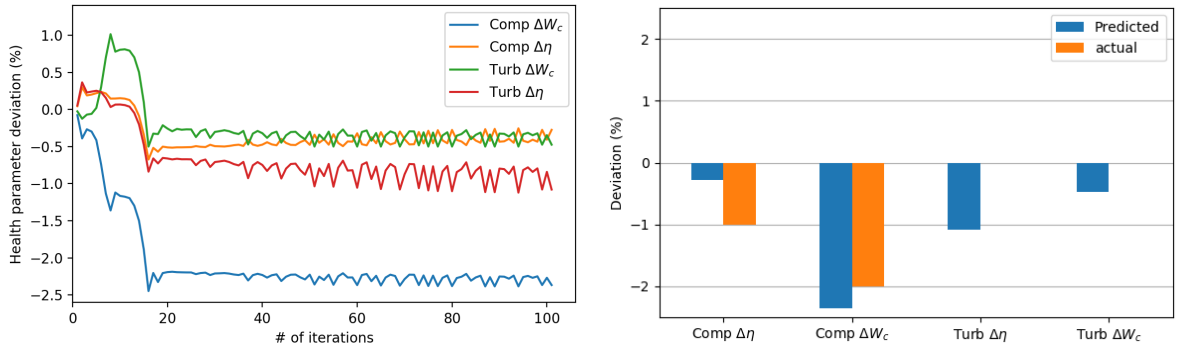

(a) Progression of health parameter deviation per iteration

(b) Actual deterioration vs predicted deterioration

Figure 5.3: Results of the Newton-Raphson optimization method with two operating points

Confirming results from literature, gradient-based optimization is not able to converge to the correct solution in a gas turbine diagnostics-type problem. As suspected beforehand, the algorithm gets stuck in a local minimum. In order to investigate this problem further, the solution space of the deteriorated compressor case from above is plotted in Figure 5.4. As the algorithm varies four different variables and has an output objective function value, the solution space is five-dimensional. This is difficult to display in graphical form. The best option is two three-dimensional graphs, with a colormap as an added fourth dimension. Due to computational restraints, the resolution is only 14x14. Figure 5.4a shows the compressor health parameters vs turbine efficiency, and Figure 5.4b the compressor health parameters vs turbine flow capacity. Although this strictly does not convey the complete search space, the plots still give a good idea of the local minima. It is clear that this search space is too complex for a gradient-based method to reliably traverse. Another thing to consider is that the search space would become even more nonhomogenous when more sensor measurements are removed and more complicated deterioration cases are considered.

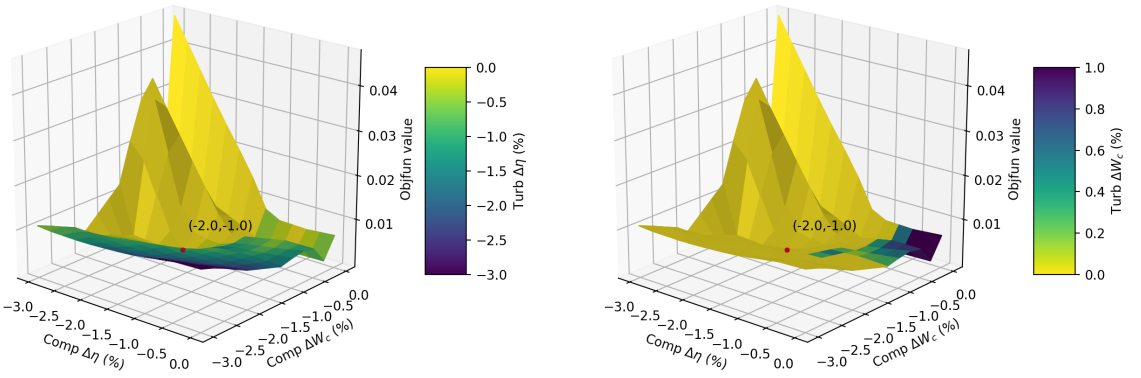

(a) Compressor solution space with turb $\Delta\eta$ as third dimension

(b) Compressor solution space with turb ΔW_c as third dimension

Figure 5.4: Deteriorated J85 model solution space (case: -2% comp $\Delta\eta$, -1% comp ΔW_c)

5.2.2. Heuristic Optimization

As explained before, heuristic optimization is able to escape from local minima. This makes it ideal for gas turbine diagnostics problems, which exhibit complex multi-dimensional search spaces.

The predominant method used in literature as a heuristic optimizer is the family of Evolutionary Algorithm (EA). An EA used mechanisms inspired by biological evolution, including a population of multiple candidate solutions [22]. The most popular type of EA is the Genetic Algorithm. Using principles of selection, crossover and mutation, the population will eventually cluster around the optimal solution [19]. In the selection operation, the individuals for the next generation are chosen based on their objective function value. Crossover creates new individuals by swapping parts of the parameter vector, while mutation introduces new information by applying random changes [64]. Mutation prevents the algorithm from getting stuck in local minima.

However, running a GA in its traditional form for gas turbine diagnostics is not ideal, as it functions with individuals encoded as binary strings [19]. The genetic operators (selection, crossover and mutation) are then applied on these binary representations. Binary strings are used to complete the analogy of biological evolution, mimicking genotypes. However, as also noted by Gronstedt [19] and Houck et al. [65], encoding a GA with floats can give an order of magnitude in performance improvement.

For this reason, a Differential Evolution (DE) procedure will be applied in this thesis. First developed by Storn and Price [66], the candidate solutions are considered as real vectors. The selection, crossover and mutation operators, however, are still present like in a Genetic Algorithm. The DE strategy is described below, following the paper by Storn and Price [66]:

Initialization

DE is a parallel direct search method which initializes NP parameter vectors x with dimensions D, also called agents, as a population for each generation G:

$$x_{j,i,G}, \qquad j = 1,2,..,D, \qquad i = 1,2,...,NP \tag{5.3}$$

This initial vector population is chosen at random and covers the entire search space. D is the amount of health parameters that are investigated. An initial guess is not available for gas turbine diagnostics, but the health parameter bounds can be varied according to previous knowledge of the system. This will be explained in more detail in Section 6.5.

Mutation

The next step is to generate new parameter vectors. This operation is called mutation, and can be described by:

$$v_{i,G+1} = x_{r_1,G} + F \cdot \left(x_{r_2,G} - x_{r_3,G}\right) \tag{5.4}$$

Where $r_1, r_2, r_3 \in \{1, 2, ..., NP\}$ are randomly chosen, mutually different integers. These integers must also be different from i. As a result, the minimum population size of a DE must be greater than or equal to 4. $F \in [0, 2]$ is the differential weight which controls the amplification of the differential variation $(x_{r_2,G} - x_{r_3,G})$.

Crossover
Crossover is introduced to increase the diversity of the new parameter vectors. A trial vector is formed:

$$u_{j,i,G+1} = \left(u_{1,i,G+1}, u_{2,i,G+1}, ..., u_{D,i,G+1}\right) \tag{5.5}$$

Then, in the crossover process parameter mixing occurs. At random, a number of parameters from the trial vector are replaced by parameters from the mutant vector. This works as follows:

$$u_{j,i,G+1} = \begin{cases} v_{j,i,G+1} & \text{if } \left(randb(j) \leq CR\right) \text{ or } j = rnbr(i) \\ x_{i,j,G} & \text{if } \left(randb(j) > CR\right) \text{ and } j \neq rnbr(i) \end{cases} \tag{5.6}$$

where $randb(j)$ is the jth evaluation of a random number generator with an outcome between 0 and 1. CR is called the crossover constant, and is a user-determined fixed value also between 0 and 1. $rnbr(i)$ is a randomly chosen integer between 1 and D, which ensures that at least one parameter within the trial vector is mutated. The crossover process is illustrated in Figure 5.5.

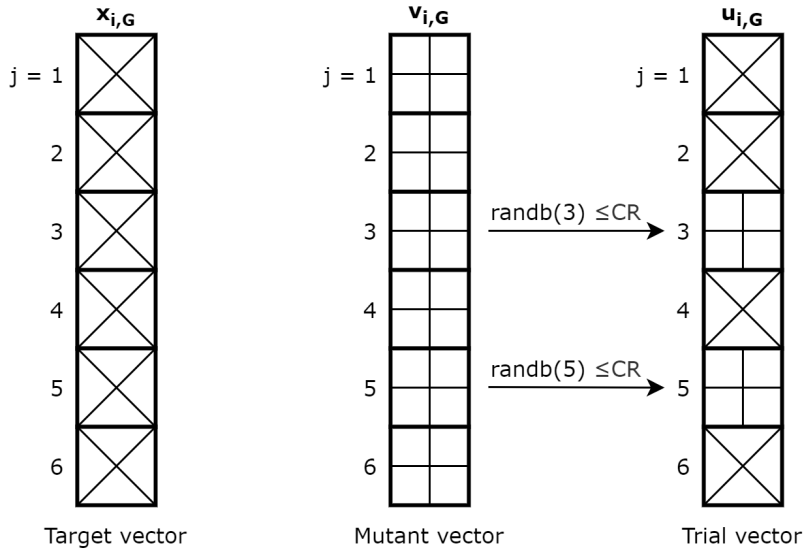

Figure 5.5: Illustration of the crossover process, with D=6 parameters [66][Redrawn]

Selection
The last operation is called selection. If the trial vector $u_{j,i,G+1}$ from the crossover operation has a lower objective function value than the target vector $x_{j,i,G}$, it replaces the target vector in the next generation $G+1$. Otherwise, the old vector $x_{j,i,G}$ is kept. As all population members serve as a target vector one time NP competitions take place every generation.

5.2.3. Choice of DE Control Variables

There are three DE control variables; F, CR, and NP, which can be altered to improve optimization performance. Increasing the mutation constant F will increase the search radius, but slow down convergence. This trade-off can be removed entirely by employing dithering. Dithering randomly changes F on a generation to generation basis. The theory behind this process is that dithering can inject enough mutation in a certain generation to escape local minima if necessary, while in other generations maximise the solution vectors in a small radius around a potential global minimum. According to Storn & Price, values of F smaller than 0.4 and greater than 1 are only occasionally effective [66].

The effects of altering population size NP are straightforward. By introducing more candidate solutions the search radius is widened, but the convergence time is increased. A rule of thumb proposed by Storn & Price is that NP lies between $5 \cdot D$ and $10 \cdot D$ [66].

The crossover constant CR determines the number of parameters from the mutant vector that progress into the trial vector. Increasing CR will speed convergence greatly, but comes at the risk of population instability. Storn & Price suggest high values of CR, around 0.9, as a first try in order to see if a quick solution is possible [66].

Another useful addition to the DE algorithm is continuously updating the best solution vector within a single generation. This can lead to faster convergence as the trail vectors take advantage of the continuous improvements of this vector. Also, a polishing optimizer can be employed after the DE algorithm has finished. This is usually a gradient-based optimizer, running on the assumption that the DE came sufficiently close to the small concave search space around the global minimum.

In a combination of testing and knowledge from literature, the Differential Evolution settings that are used in the final engine model are compiled:

- NP = 40
- F = [0.4, 1]
- CR = 0.7

5.3. Differential Evolution Results

In this section, the differential evolution method is tested on the J85 GSP model. Just like before, a deteriorated compressor is simulated. The optimizer is tested on an engine model with 5, 4 and 4 engine sensor outputs. One of the potentially problematic characteristics of an EA is that it performs slightly differently every time. In order to decrease the chance that any of the following results were merely a lucky fluke, they were run multiple times. It was confirmed that none of these results were not representative of the hybrid tool's function-solving capability. Also, all of the simulations were run for a fixed number of 20 iterations.

The first simulation includes the full sensor set, which makes it in essence an overdetermined problem. The results are shown in Figure 5.6. Unlike the gradient-based optimizer, the DE has no issues converging to the actual solution, with an rms of just 0.05. The solver is able to converge to the area of the global minimum within 5 iterations.

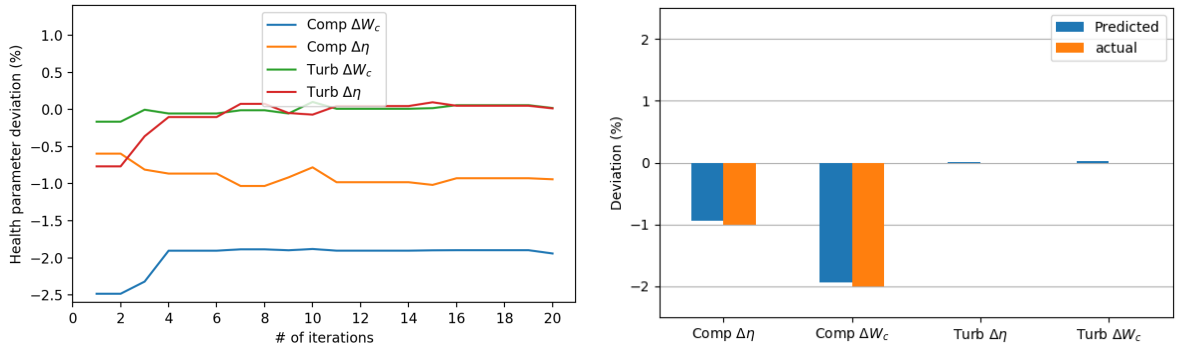

(a) Progression of health parameter deviation per iteration

(b) Actual deterioration vs predicted deterioration

Figure 5.6: Results of the DE optimizing method for 5 measurement parameters

For the second run, the turbine outlet pressure sensor is removed, leaving four measured parameters in the J85 engine model. The results of this simulation are shown in Figure 5.7. When comparing this simulation with the previous case, the rms is slightly higher, at 0.09. However, the hybrid GPA tool is not inhibited much by the decreased sensor amount, as it is still clearly able to converge to the correct solution.

Finally, the compressor outlet temperature sensor is also removed. This situation would replicate a real next-generation turbofan case, whereby the number of performance parameters is less than the number of health parameters. The results in Figure 5.8 show that a DE optimizer is still proficient in prediction engine condition, with an rms of 0.12. Unlike the cases before, smearing is a little more present. An overshoot in compressor efficiency deterioration is compensated by a turbine efficiency deviation above zero.

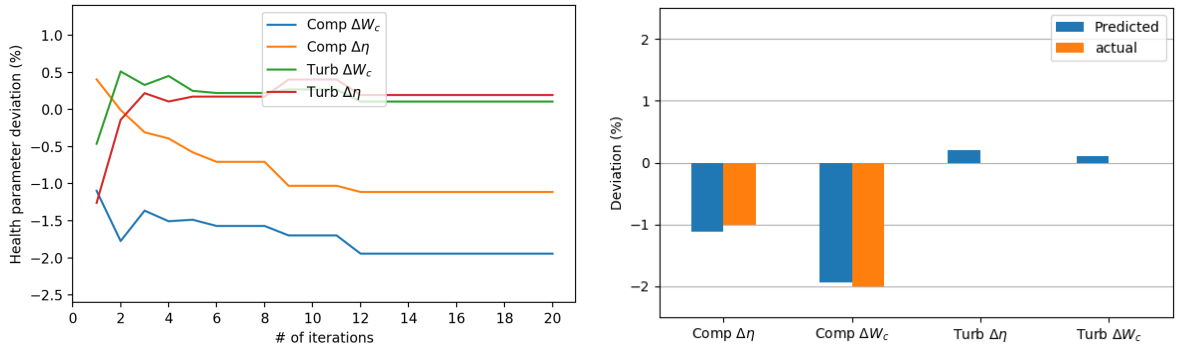

(a) Progression of health parameter deviation per iteration

(b) Actual deterioration vs predicted deterioration

Figure 5.7: Results of the DE optimizing method for 4 measurement parameters

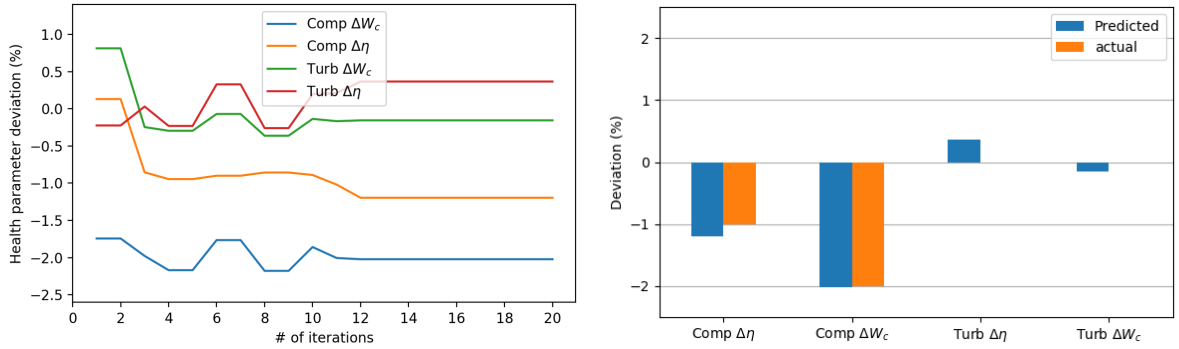

(a) Progression of health parameter deviation per iteration

(b) Actual deterioration vs predicted deterioration

Figure 5.8: Results of the DE optimizing method for 3 measurement parameters

5.3.1. Smearing

Having conducted numerous different cases at different combinations and levels of deterioration, it became apparent that occasionally, smearing occurs. Smearing is a mechanism where a condition deviation of a deteriorated component is inappropriately assigned to other components. This is especially prevalent when few gas path measurements are available, resulting in ill-defined components. Such a case is shown in Figure 5.9, where turbine deterioration was simulated. When looking at the engine as a whole, the total deterioration of both efficiency and flow capacity is predicted accurately. However, it is clearly visible that half of the actual efficiency drop is assigned to the compressor, and half to the turbine. This suggests that this model outcome gives an objective function value very close to the actual case, and that is why the algorithm converges to this local minimum. Through experimentation, it was also noted that smearing tends to only occur with efficiency health parameters.

5.4. Flowchart

This chapter is concluded by implementing the DE algorithm into a generic GPA tool which is able to co-function with any GSP model. The operating of such a tool is best shown in the form of a flowchart, Figure 5.10. First, a population of NP candidate solutions, or agents, is initialized. Then, the steps of mutation and crossover are undertaken to form NP trial vectors. The fitness of both the initial agent vectors and trial vectors is then determined by running them as off-design points in GSP, and subsequently comparing the outputs to the measured engine data through an objective function. On the basis of fitness, it is determined whether the agent vector is replaced or not. This process is repeated in new generations until a solution vector meets the convergement criteria, or the maximum number of iterations is exceeded. As a final result, the program returns the set of health parameters with the best fit to the measured engine data set.

One of the limitations of this set up is the amount of time it takes to run the DE scheme. Since a DE has a large population size, calculations can be run in parallel. Thus, in theory, using multiple cores would speed

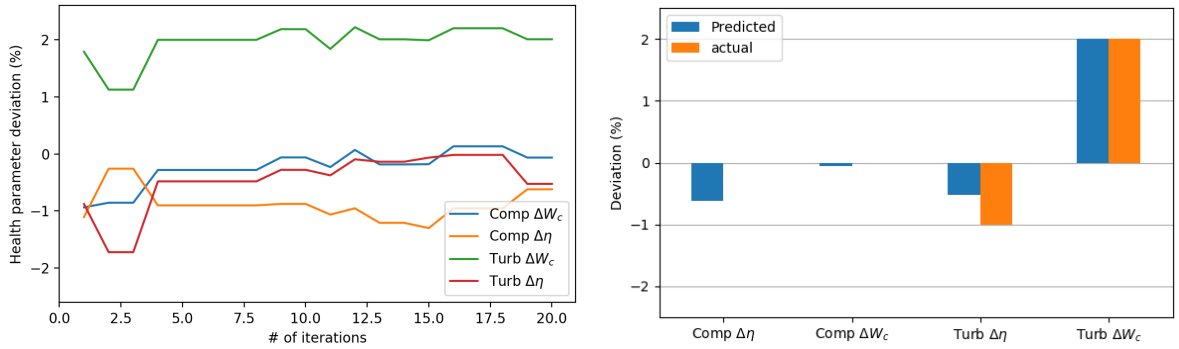

(a) Progression of health parameter deviation per iteration

(b) Actual deterioration vs predicted deterioration

Figure 5.9: Illustration of smearing for a J85 with a deteriorated turbine

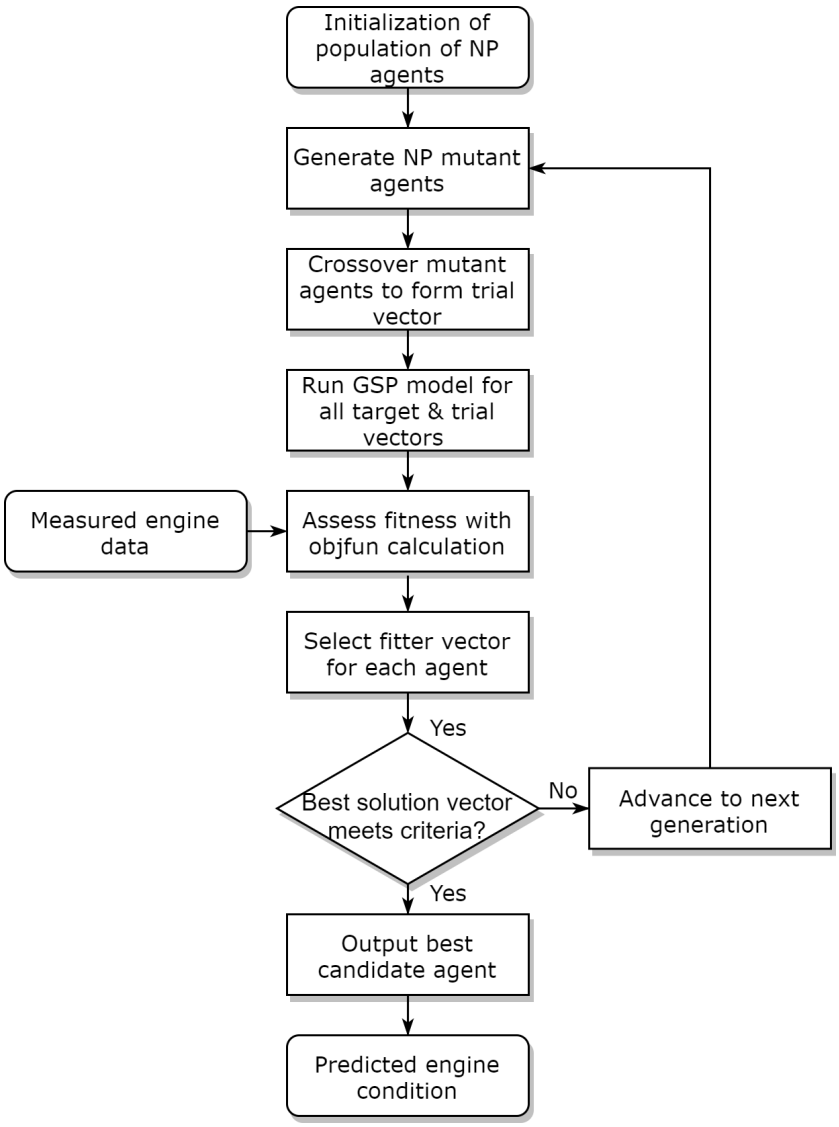

Figure 5.10: Flowchart of hybrid GPA tool

up the program significantly. However, this is not possible as multiple instances of GSP API cannot be opened due to map database limitations [67].

6

On-Wing Data Acquisition & Processing

Previously, most GSP GPA analyses have been conducted using test cell data. This has many advantages, as the test cell is a controlled environment, allowing for better steady-state operation of turbofan engines. However, in order to monitor engine component deterioration, GPA must be applied to on-wing data. This chapter will explain the installation effects present when operating an engine on an aircraft, followed by transient operation systems. Subsequently, on-wing measurement uncertainty is discussed. Finally, the subjects of snapshot data, continuous engine operating data, and data processing are discussed.

6.1. On-wing Installation Effects

The differences between engine performance in the test cell and operating on-wing are called installation effects. These can influence GPA condition monitoring, especially when the baseline GSP model is tuned using test cell data and subsequently used for on-wing data trending.

6.1.1. Power Off-Take

The Boeing 787 is designed with a fully electrical architecture, and as a result the GEnx-1B is required to provide a certain amount of electrical power in addition to thrust. In the test-cell, no additional customer power is required and the two Variable Frequency Starter Generators (VFSG), connected to the N2 shaft via the Accesory Gearbox (AGB), solely generate electrical loads for the accessory systems. On-wing, the target load is around 400 horsepower per engine. GE assumes a VFSG efficiency of 92.8% [6].

6.1.2. Inlet & Exhaust Nozzles

The second installation effect stems from different inlet and exhaust nozzles being installed in the test cell and on-wing. The bell mouth inlet used in the test cell is designed for minimal losses, with an optimal inlet airflow [16]. The on-wing inlet, on the other hand, is designed to ensure stable inlet flow over a wide range of inlet angles of attack. Though these differences may compromise GPA results, they are virtually impossible to investigate and quantify.

6.1.3. Engine Anti-Ice System

The Engine Anti-Ice (EAI) system extracts stage 7 HPC bleed air to supply heat to the engine inlet and the booster, in order to prevent any ice buildup. Ice on the cowling leading edge or booster splitter lip could disrupt a steady airflow into the engine, as well as potentially causing damage if ingested. For this thesis, the focus lies on the Cowl Anti-Ice (CAI) system, as the Booster Anti-Ice (BAI) system valve lies downstream of the CAI valve. The exact time this system is switched on varies from flight to flight, as it is regulated by the outside air temperature sensor. According to the GEnx-1B installation manual [6], the maximum airflow that can be extracted is 3.3% of the total core airflow at cruise/takeoff fan speeds.

6.1.4. Unsteady Conditions & Thermal Stability

GSP GPA assumes steady-state performance of a gas turbine when performing a design point calculation. When using test cell data for calibrating a GSP model, this assumption is mostly valid, as the engine is properly

warmed up for 10 minutes, and allowed to settle before recording a measurement [68]. However, for on-wing measurements this is not the case. Take off is commenced after a short idle taxi period, and the take off snapshot is taken before the engine has reached a thermally stable point. According to research done by Röell [68], this difference can lead to a 7.5-10 $°C$ variation in EGT. CEOD gives more freedom in picking an operating point for GPA modeling, and allows for an analysis in deciding a preferred data point for steady-state performance.

6.2. On-Wing Measurement uncertainty

Measurement uncertainties can have an effect on GPA results, and have been quantified by Verbist [16] and Moorselaar [17] using a Monte Carlo analysis. Verbist analysed 1500 trials of simulated sensor errors added to measured performance parameters of a healthy CF6-80C2 engine, in order to analyse sensor error propagation. The values for the sample mean converge to zero deviation, corresponding to an engine with no component condition deterioration. Furthermore, the narrow probability distributions in the results suggest that random sensor noise has a small effect on AM calculation results, except for change in LPC efficiency, which had a larger standard deviation. Verbist states this is due to the lack of a temperature sensor in the fan bypass outlet duct or a pressure measurement at the LPT outlet. Moorselaar came to a different conclusion with the GEnx-1B model, which is logical as the measuring sensor set is different. The GEnx-1B showed a greater sensitivity to sensor noise in the N2 system when subjected to the same Monte Carlo simulation. This is also contributed to a lack of sensors, in this case the HPC inlet and LPT outlet pressure ($P_{S,25}$ and $P_{S,49}$). As these sensors are missing, the inlet and outlet conditions of the N2 system are not fully defined.

However, it can be assumed that overall, the effect of sensor noise is small. As for sensor bias, as long as data from the same engine is used for performance trending, any bias is constant and makes no relative difference. When taking a single reference engine as a baseline for multiple other engines, it must be made sure that no sensor bias is present by checking if these fall in reasonable ranges. Another possibility is the occurrence of a sensor fault during flight, which will be visible when trending engine performance in between maintenance intervals.

6.2.1. Sensor Accuracy

In order to investigate measurement uncertainty and scatter, it is important to know the accuracy of each sensor. The performance parameters are measured by different types of sensors. Spool speeds are measured by rotational sensors, temperatures by thermocouples, pressures by pressure inducers, and the fuel flow by a flow meter. The range and accuracy of these sensors are summarized in Table 6.1.

Table 6.1: Sensor types with their accompanying range and accuracy [69]

Sensor type	Parameters	Range	Accuracy	Unit
Frequency interface	N1, N2	0 - 13,750	±0.12	RPM
Thermocouples	$T_{t,2}, T_{t,25}, T_{t,3}, T_{t,49}$	-54 - 1137	±1.1°C or ±0.4%	°C
Pressure transducer	$P_{t,2}$	1.6 - 20	±0.01	psia
	$P_{s,3}$	5 - 750	±0.36	psia
Flow meter	W_f	400 - 30,000	±3.5%	pph

It can be noted from Table 6.1 that the spool speed measurements have the highest accuracy, while fuel flow measurements have the lowest. One area of application of this information is selecting the control variable. Of the two usual choices, fuel flow and fan speed, the latter is the better option when looking at the sensor accuracy.

Knowing the accuracy of each sensor can be very valuable in quantifying the potential noise contamination of each measurement. As explained in Section 4.4.1, noise is modelled by a standard deviation added to each measurement. The sensor accuracy is assumed to be two times the standard deviation (2σ) of the data set, in a Gaussian distribution. This means that 95.45% of all measurements do not exceed the 2σ noise level. This method is implemented in Chapter 9.

6.2.2. Humidity

On-wing, the air humidity is not measured. Humidity can have a large effect on turbofan performance, as it influences the thermodynamic properties of the working fluid, resulting in a different engine operating point. This effect has been researched by Röell [68] and van Vuuren [70], both of whom have matched airport

humidity data to takeoff snapshots. In other literature [15–17, 43], a relative humidity value of 60% is taken as a fixed value. Van Vuuren has conducted an analysis to quantify the effect of humidity on off-design performance. His results show that for more humid conditions, the corrected mass flow decreases by 1% while the corrected spool speed increases by 1% for both compressors and turbines. The outlet temperature of the compressor decreases, while the opposite is true for the turbine. Finally, a decrease in thrust is expected when operating in humid conditions. These variations will influence component condition deviation per flight for the same engine, and thus can return incorrect results when performing multi-flight condition monitoring. On the other hand, as altitude increases, absolute humidity decreases. According to [29], absolute humidity is negligible above 6000 meters. One could argue that for this reason, a cruise data set has less added uncertainty than takeoff data.

6.3. On-wing Data

It is not possible to determine engine deterioration between maintenance intervals without on-wing data. This is why early GPA research was mainly focused on post-acceptance test troubleshooting. However, all current engines in the KLM fleet collect performance data in-flight. This is done in two different ways, which will be described below.

6.3.1. Snapshot Data

Snapshot data consists of two data sets per flight, consisting of takeoff and cruise [16]. These are made available for the airline, but it is unknown how GE exactly processes this data. It is suspected that the takeoff snapshot is taken at the point of peak EGT during takeoff, and that both snapshots are averaged over 10 seconds.

These snapshots give KLM an extensive database of on-wing performance data for various engine types that has been utilized in previous research [16, 17, 43, 68, 70]. However, in all of these cases the methodology still includes initially creating the GSP model with test cell performance data en subsequently calibrating it with on-wing snapshots. This is due to the fact that more measurements are available in the test cell environment. The primary performance parameters available from snapshot data is summarized previously in Table 2.2. Note that the secondary performance parameters are not all available in snapshot data. In the test cell, the net thrust and relative humidity are also measured. The lack of a $P_{s,14}$ measurement makes the thrust measurement in the test cell particularly valuable.

6.3.2. Continuous Engine Operating Data

One of the major technological advancements of next-gen engines like the GEnx-1B is that their status is monitored constantly by sensors while on-wing. Because of this, a vast amount of data for condition monitoring is available. Continuous data is raw data received in a csv file format. It contains all information collected during a flight, resulting in more than 600 parameters and a few hundred thousand data points. A a result, a data set from CEOD is much more complete than a GE snaphot. This is illustrated in Table 6.2, where the extra performance parameters are shown. CEOD gives detailed information on secondary performance parameters like installation effects, bleed flows, cooling flows, and variable geometry. These are all parameters not available in previous GPA investigations, and can aid in creating the most detailed GPA model at KLM ES to date.

The terminology used by GE for CEOD parameters varies. The first word "selected" refers to the parameter which the EEC has selected to be shown in the flight deck display system [6]. When compressor is mentioned, GE implies the high pressure compressor. Also, in CEOD the temperature sensor at station 12 must be used for the $T_{t,2}$ measurement, as the latter is not available. For further information regarding the difference between these two stations refer to Figure 2.2.

The last three rows in Table 6.2 indicate parameters which cannot be implemented in GSP directly, but still provide potentially useful information. The first, the calculated core airflow, is a GE proprietary parameter. It is unknown how it is calculated, but it can be applied in the verification and validation process by comparison with the core airflow as calculated by GSP. The takeoff peak EGT value can be used in order to prove or disprove the hypothesis that the takeoff snapshot is taken at this moment in time. Finally, the core speed rate of change, $\Delta N2$, could be a useful parameter as it indicates when the core speed is near to constant. This could aid in picking the best point for a near steady-state data set.

Table 6.2: Parameters available from CEOD [17]

Parameter	Description in CEOD	Unit
$T_{t,2}$	Selected Total Temperature at Station 12	$°C$
$T_{t,25}$	Selected HP Comp Inlet Total Temperature	$°C$
$T_{t,3}$	Selected Compressor Delay Total Temperature	$°C$
$T_{t,49}$	Selected Exhaust Gas Temperature	$°C$
$P_{t,2}$	Selected PT2 Pressure	psia
$P_{s,3}$	Selected Compressor Discharge Static Pressure	psia
$N1$	Selected Fan Speed	rpm
$N2$	Selected Core Speed	rpm
W_f	Selected Mass Fuel Flow	pph
$HPTACCV_{pos}$	Selected HP Turbine Active Clearance Control Valve Position	%
$LPTACCV_{pos}$	Selected LP Turbine Active Clearance Control Valve Position	%
$CCCV_{pos}$	Selected Core Compartment Cooling Valve Position	%
TBV_{pos}	Selected Transient Bleed Valve Position	%
VBV_{pos}	Selected Variable Bleed Valve Position	%
VSV_{pos}	Selected Variable Stator Vane Position	%
PTO	Total Engine Horsepower Extraction	hp
CAI_{pos}	Selected CAI (Cowl Anti-Ice) Bleed Config	-
$\dot{m}_c$	Calculated Core Airflow	pps
$T_{t,49_{peak}}$	Takeoff Peak EGT Value	$°C$
$\Delta N2$	Core speed rate of change	$\%N2/s$

6.3.3. Advantages & Drawbacks of GPA with On-Wing Data

This section can be summarized by noting the pros and cons of using CEOD in a gas path analysis. A comparison is made to both test cell data and on-wing snapshot data.

Advantages

- All data is measured under similar circumstances, eliminating on-wing installation effects
- Availability of secondary performance parameters, allowing for a more precise and specified GPA model
- Allows for multi-point calibration and MOPA using multiple data points at different power settings
- More freedom in picking data points when compared to snapshot data

Disadvantages:

- Difficult to find near steady-state data points, especially in takeoff conditions
- Fewer primary performance parameters (thrust and relative humidity)
- On-wing installation effects introduce errors
- Operating conditions vary widely

It can be concluded that utilizing CEOD is a step forward in GPA, and is suited well to apply novel methods like MOPA. A succesfull implementation, however, depends on how well noise can be filtered out of the data and if picking quality near-steady state points is possible.

6.4. Data Preprocessing

CEOD will require some data preprocessing before it is usable in GPA, as opposed to test cell data. For this reason, a software tool is developed that is able to convert CEOD files into 2 operating point data sets for every flight. This procedure follows the following steps:

1. Check validity of CEOD files and remove unnecessary parameters from data set

2. Reduce data set for faster analysis time, to a time offset where all relevant parameters are measured. This reduces the data frequency from 0.06 to 0.96 seconds.
3. Pick operating points based on three criteria:
   (a) Relevant flight phase (takeoff/climb or cruise)
   (b) Core speed rate of change between -0.2 and 0.2 $\%N2/sec$
   (c) N1k closest to desired design operating point
4. Check if there are any outliers in the secondary performance parameters using the Interquartile Range (IQR) method, explained in Section 6.4.1
5. Replace operating points where outliers are present with the next best N1k operating point, for which the secondary performance parameters fall within the interquartile range.

When executing step 3(a), it is important to understand aircraft flight phases. This is illustrated in Figure 6.1, were a typical flight is shown. The starting and ending points of these flight phases are predetermined by GE, and show a small delay, visible in the takeoff insert graph. This is not deemed to have a significant effect on the analysis. The horizontal black line indicates the GSP model takeoff design point. This N1k speed is predominantly reached during the takeoff, initial climb and/or climb phases. This is where the tool will search for an adequate takeoff operating point. Then, the vast majority of time, the engine is in the cruise phase at a lower N1k.

By filtering out the data with a high core speed rate of change, the operating point will be near steady-state. Also, matching the corrected fan speed N1k with the GSP model design point is optimal for the functioning of GSP, as the component maps are tuned around this point. By removing any secondary performance outliers, these variables are controlled and do not influence the investigation into the relationship between the independent (primary performance parameters) and dependent (health parameters) variables. GE applies a smoother by averaging data points between a short period of time. It was decided not to implement such a method, as time-averaging can result in a non-physical set of performance parameters, and subsequently innacurate GPA outcomes.

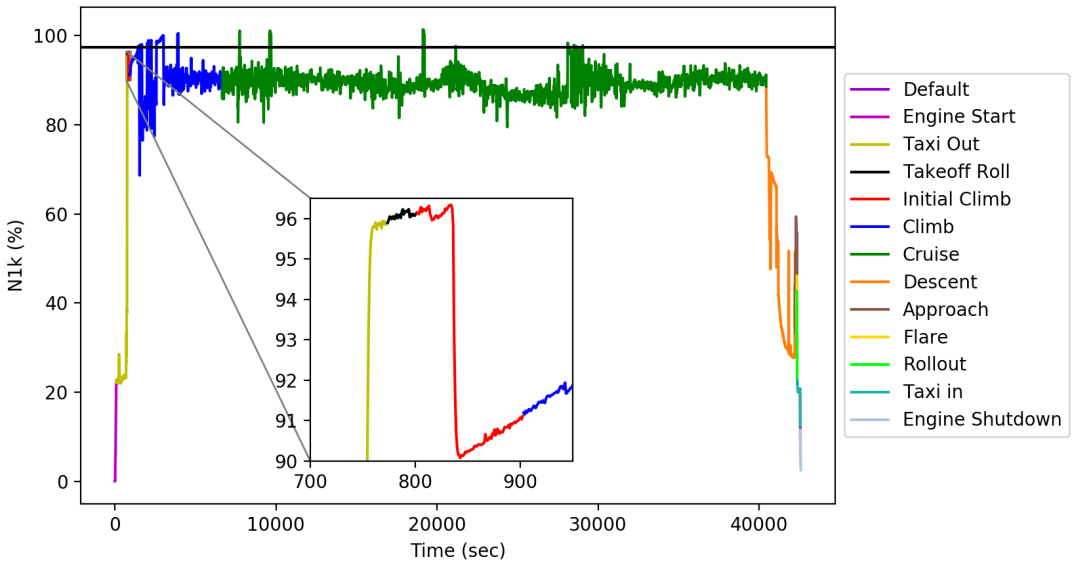

Figure 6.1: Corrected fan speed variation during all aircraft flight phases of a typical flight

6.4.1. Outlier Filtering using IQR Method

This section will expand on steps 4 and 5 in the data preprocessing tool procedure. In order to reduce the variability of operating points, a novel step within gas turbine diagnostics is taken to control the secondary engine performance parameters. As CEOD permits the choice of any operating point, specific points can be picked for which all secondary performance parameters fall within the same range. This range, and the

outliers that lay outside the range, is established using the well-known IQR method. In this method, the dataset can be summarized with five numbers: the minimum, 25th percentile, median, 75th percentile, and the maximum [71]. The 25th and 75th percentiles are also called the lower and upper quartiles, respectively. The Interquartile Range is then defined as the distance between the lower and upper quartiles [71]:

$$IQR = Q_3 - Q_1 = q_n(0.75) - q_n(0.25) \tag{6.1}$$

The IQR specifies the middle half of the dataset, and is a robust measurement of the variability of the data set. It is also used to determine when a point is qualified as an outlier:

$$outlier \begin{cases} < Q_1 - 1.5 \cdot IQR \\ > Q_3 + 1.5 \cdot IQR \end{cases} \tag{6.2}$$

When a data point is more than 1.5 times the IQR beyond the middle half of the data set, it is classified as an outlier. The preprocessing tool then automatically picks the next best operating point from within the CEOD dataset, which does fall within the required range. This analysis can also be visualized effectively in the form of a box-and-whisker plot. These will be used for the on-wing analysis in Section 9.2.

It must be noted that removing outliers from operating point data can also have negative effects. The possibility exists that results are filtered out that indicate a fault in the engine. This will be investigated in greater detail in Chapter 9. Also, there is a trade off between removing outlier and picking the most optimal N1K point.

6.4.2. Data Smoothing

Finally, consecutive flight data will require a form of noise filtering. The simplest and most widely employed method of noise filtering is taking an Exponentially Weighted Moving Average (EWMA) [17, 23]. It filters out high frequency fluctuations due to flow distortions, and is defined by:

$$A_i = \alpha \cdot x_i + (1 - \alpha) A_{i-1} \tag{6.3}$$

Where x_i is the current observation, while A_i is the current smoothed value. A smoothing constant α is also included, in order to manually control the filtering. This method is used when trending data which is continually being updated.

In some cases where all of the data is already available, a centered moving average gives better smoothing, as the problem with an EWMA that it only depends on past and present points, and as a result introduces lag relative to the input data. This can be corrected by using a non-causal filter in the form of a symmetrical window function of a Gaussian function, centered around the current value. By taking into account equal past and future inputs, the lag can be removed. The Gaussian window is defined as:

$$w(n) = e^{-\frac{1}{2}\left(\frac{n-\frac{1}{2}N}{\sigma \cdot \frac{1}{2}N}\right)^2} \tag{6.4}$$

Where n is the current value, N the maximum window sample size, and σ the standard deviation of the data set.

6.5. Variable Bounds Method

A novel concept introduced in this thesis, made possible by the availability of CEOD, is a variable bounds method. The genetic algorithm requires lower and upper bounds to be set for each condition parameter. These bounds define the search space that the algorithm is constrained by in finding the best-fit solution. A major problem encountered when adapting the hybrid GPA tool from simulated data to real on-wing data was these bounds. Setting them too constrictive creates the danger of the actual solution falling outside the search space, while setting an extremely wide range makes it difficult for the GA to converge to a solution.

For this reason, an automatic adapting bounds method was developed, based on the EGT Hot Day Margin (EGTMHD). The EGTMHD is defined as the EGTM corrected for hot day conditions. This parameter was chosen as it best represents total engine condition and is available without any further calculation, as it is provided by GE. It is assumed that for EGT margins close to those of the reference engine model ($EGTM_{ref}$), the overall condition deviation of the engine components is closer to zero. When the EGTMHD is higher or lower than the reference engine, the condition parameter bounds are adjusted accordingly. The hybrid GPA tool follows the ranges as shown in Figure 6.2. These ranges have been constructed from general knowledge

of turbofan deterioration, such as the fact that deviation rarely exceed 5%, and testing multiple operating points.

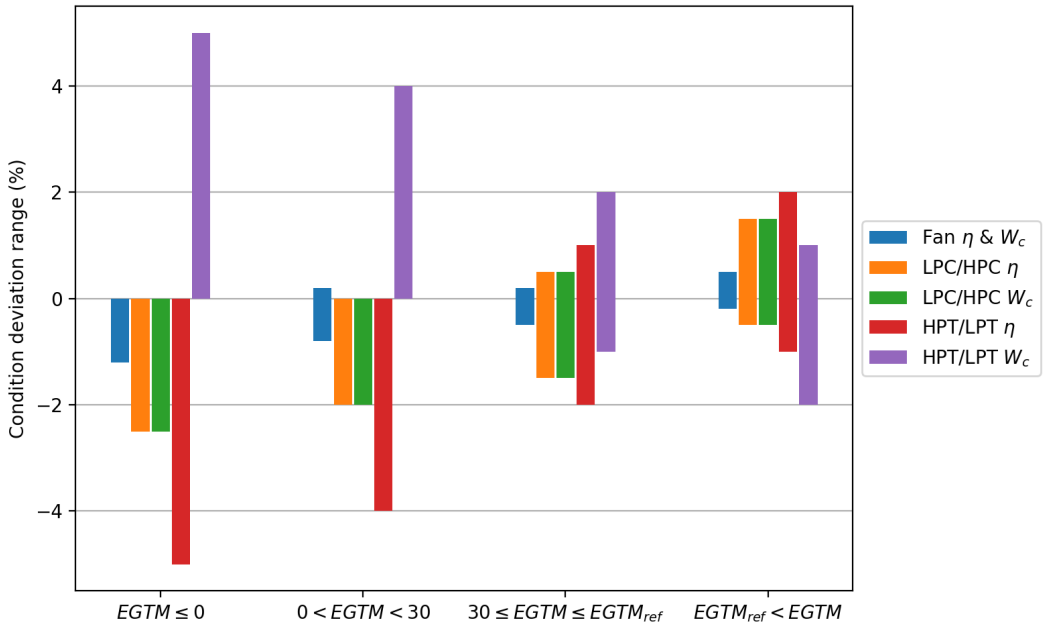

Figure 6.2: Range of bounds of component condition parameters used by hybrid GPA tool

7

GPA Reference Models

Prediction of component deterioration is limited by the ability of the GPA performance simulating model in replicating the actual healthy engine state. Every turbofan engine contains small geometrical differences which causes a performance scatter [72]. Therefore, it is necessary to calibrate the general model to specific engine cases. This is one of the major problems that has been uncovered by Moorselaar [17] among others [15, 16, 38]. Therefore, creating an accurate reference performance model is vital for effective engine prognostics. First, different reference model techniques are discussed.

7.1. Reference Model Techniques

In order to fully understand the procedure of creating a GPA model and subsequently applying it to specific engine data, it is important to define the relevant nomenclature:

- **Baseline model**: the GSP performance model made to match the performance of a specific engine class or type. This is usually done with baseline performance specifications or picking the most average engine data set.
- **Reference engine**: an actual engine measurement data set, portraying the initial (healthy) engine condition, from which any deviation can be measured.
- **Reference model**: The performance model which has been calibrated or tuned to the reference engine data set. This is sometimes also called the **calibrated model**. The goal of a reference model is to represent a specific engine more accurately than the baseline performance model.

Current standard practise at KLM Engine Services is to take test cell take-off data as the design point for the baseline model [16, 17, 25, 39, 43]. The engine is selected with the most average performance. Then, an off-design analysis is conducted, in which generic component maps available in open literature are tuned to match the operating line of the most average engine [73]. This concludes the creation of the global baseline model. This model is then adapted to each individual engine case using calibration factors, which matches the model to the specific engine design point.

7.1.1. Tuning Component Performance Maps

One of the major limitations of GPA, being a physics-based method, is the accuracy of the component performance maps. For a non-OEM enterprise such as KLM ES, exact component maps and other performance data is not available. This is the reason that component maps from the public domain have to be tuned. This simplest method is to simply relabel and relocate the speedlines in publicly available maps relative to a reference point. A more complex and accurate method is to iteratively relabel speed lines, which if done manually is a time-intensive process. An attempt was made to partially automate this process in a paper by Verbist [74], using AM. The condition deviation parameter set was determined with an adaptive modelling procedure every time after a speed line relabelling. Then, an rms was calculated using this data set. This enabled the generation of a best fit curve, with the speed line that results in the optimal rms value. This process converges to the optimal speed lines. This method has also been applied to the existing GEnx-1B GSP model, developed by Moorselaar [17].

7.1.2. Reference Engine Data Set Selection

There are two options when selecting a reference engine data set for on-wing GPA. The first is the test cell performance data during the most recent post-overhaul acceptance test. This is accurate and reliable data due to the controlled operating conditions. Also, more performance parameter measurements are available. However, it is possible that an offset will occur, also noted by Verbist in his research, due to installation effects [16]. The other option is to use the first on-wing measured data set when the engine enters service or after a major overhaul. This option will most likely produce more accurate results, as the condition deviation over time is initially centered around a zero mean. However, initial engine run-in fluctuations make the selection of an initial data set difficult. One option is reduce this problem is to average the data of multiple cycles. Röell [68] suggests using the first 10 cycles, while according to Aretakis et al. [18] the first 50 cycles represent a steady healthy engine condition. The issue with averaging multiple performance parameters, however, is that the end result is an unphysical situation. This is especially prevalent when on-wing data is used, where installation effects are different every flight.

7.1.3. Multiple vs Average Reference Data Set

The approach applied by Verbist is to use multiple reference engines [16]. The set is defined using the 10 engines with the best overall condition according to their EGT margin. Then, for each performance data set, the AM calculation is performed 10 times, with each different reference engine. Then, the AM results are averaged, providing a more reliable result than those obtained with a single reference data set. However, Verbist recognizes that a high EGT margin is no guarantee for good individual component condition.

Another method Verbist has experimented with is averaging the reference engines before the AM calculation. The advantage in doing this is that the AM calculation only needs to be run a single time, reducing computational time. However, creating such an averaged reference set could result in an unphysical model from a thermodynamic standpoint. However, Verbist proves in a case study that this method returns similar results when compared to multiple reference engines averaged.

Both of these methods can be described as a inter-engine approach. This term has been coined by Clifton [75], along with its counterpart; the intra-engine approach. A more detailed explanation of this concept is given in the following subsection.

7.1.4. Inter- vs Intra-Engine Approach

In the inter-engine approach, a generic model is created for a specific engine type, in this case the GEnx-1B, and this model is assumed to represent the normal behaviour of all engines in that class. This model is subsequently calibrated to match an individual engine. In an intra-engine approach, the baseline model is constructed from the outset for a single engine, which is then kept for individual engine prognostics. This way, all deviation in performance is exclusively due to deterioration, instead of potentially incorrect calibration. The difference between an inter-engine and intra-engine approach is visualized in Figure 7.1. The figure shows a generic data space with two variables, x_1 and x_2, where region A corresponds to normal behaviour for an entire engine class. A single engine from that class has less variant behaviour corresponding to region B, a subset of region A. Region C represents a deteriorated data set belonging to engine B. If region A is used to generate the reference model, the deteriorated data set C would fall inside normal behaviour for that engine, just like data set B. However, if data set B is used to generate the model of normality, data set C would correctly be classified as abnormal or deteriorated for that engine.

This generic example illustrates how an intra-engine approach may provide a better characterization of an individual engine, increasing the condition monitoring capability. This conclusion is also verified by other research, where using a generic model rather than an engine specific model negatively affects the quality of the diagnostic information obtained [16, 18, 54, 73]. The reason an intra-engine approach is not currently the industry standard is that it is very time-consuming and laborious to tune component performance maps.

7.1.5. Calibration Factors

A built-in feature in the GSP AM tool are calibration factors. Every engine is slightly different, and for this reason the global baseline model does not always match the reference model, resulting in false indications of deterioration. In order to solve this problem, calibration factors are introduced, which can be used to align the global baseline model to the engine of interest. A calibration factor is given by:

$$f_c = \frac{P_{i\,ref}}{P_{i\,mod}} \tag{7.1}$$

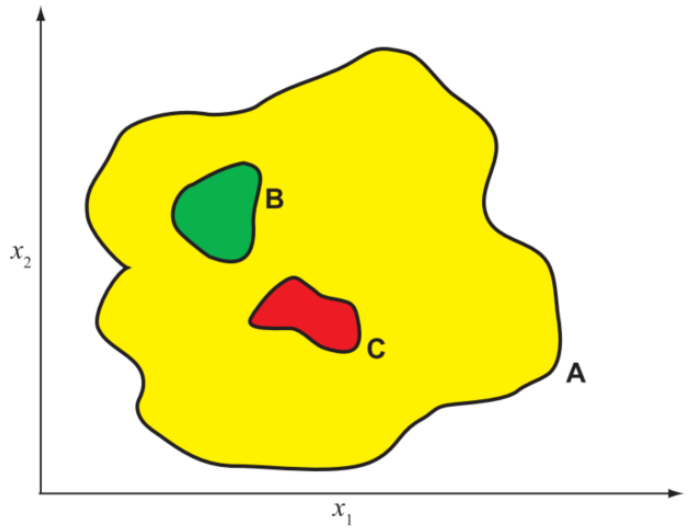

Figure 7.1: Visual depiction of the inter- versus intra-engine approach [75]

Where P_i is a performance parameter, and the subscripts ref and mod indicate the reference design values and model values, respectively. Design point values as well as the operating conditions, including power setting, can be aligned in this manner. According to Visser and Verbist, calibration factors improve the stability and results of the AM module significantly [15, 16]. However, this method has its limitations, as also acknowledged by these authors. A linear interpolation is not always accurate, even around the design point, and as a result the accuracy can suffer from second-order deviations [15].

This is especially prevalent when there is a mismatch in power setting between the reference engine and model. This is illustrated by Figure 7.2, which shows a design point model calculation for equal and unequal power settings. Model calibration can lead to a good match between the measured values and the reference model when the operating power setting is equal, as shown in Figure 7.2a. By introducing a calibration factor for the power P, the calibrated model (dashed line) behaves like the actual engine (solid line) near the design point. However, when the data from the reference engine is measured at a different power setting than the model is designed and tuned for, inaccurate results occur. The reference model data is essentially off-design. In reality, this scenario will occur often when working with on-wing data, where the power setting fluctuates much more than in a controlled test cell facility setting.

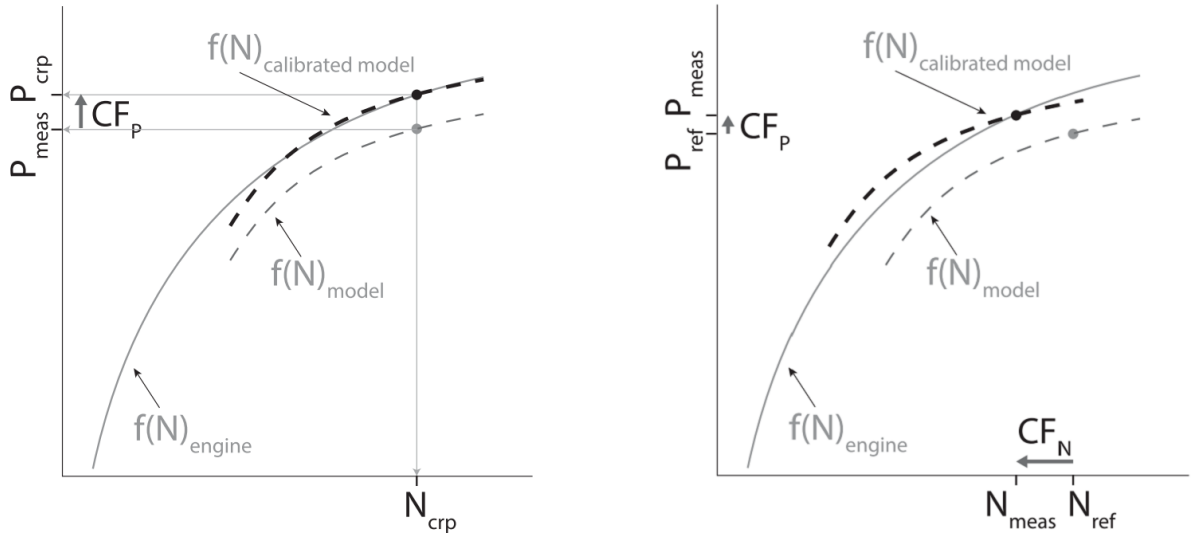

(a) Calibrating model at equal power settings

(b) Calibrating model at unequal power settings

Figure 7.2: Calibration factor effects on a design point calculation [16]

A solution to this problem is the off-design calibration method, developed by Verbist [16]. By first running the reference model at the power setting of the reference engine data, essentially off-design, and calculating the calibration factors with that data, the accuracy of the calibration is improved. This is shown in Figure 7.3, indicating a better fit than in Figure 7.2b.

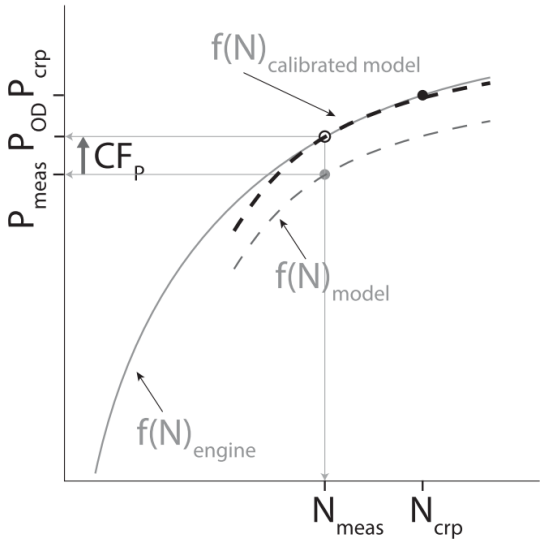

Figure 7.3: Graphical illustration of Verbist's off-design calibration method, at unequal power settings [16]

7.2. Implementation in Hybrid GPA Tool

In the previous section, several different options in terms of developing a GPA reference model have been described, which could be implemented in the hybrid GPA tool. As the primary objective of this research project was not to develop an extremely accurate GSP baseline model, but rather to demonstrate the feasibility of a hybrid GPA tool, it was decided not to develop the existing baseline GSP model for the GEnx-1B any further. The component performance maps were not additionally tuned, which means that the model is most accurate at high power settings.

Secondly, the first on-wing data set is used as the reference engine. On-wing installation effects deter the use of any test-cell data sets, even though more parameters are available in the test cell. Additionally, it was chosen not use any data set averaging, due to the unphysical thermodynamic data sets that could occur, and the large number of uncontrollable variables on-wing.

In early stages of this project, using an intra-engine approach as described in Section 7.1.4 was seen as a very promising addition to the hybrid GPA tool in order to increase condition monitoring accuracy. However, due to time constraints, it was not implemented.

The off-design calibration factor method, as used in GSP AM, was also adopted in the hybrid GPA tool. It is a relatively straightforward implementation, and adequate given the timespan of this project. In any case, the CEOD preprocessing step, explained in Section 6.4, also entails that power setting fluctuation is brought to a minimum.

The two problems with this method are that calibration factors do not always capture the exact nonlinear state of an individual engine, and that the reference model is only accurate in a close area around the calibration point. It was outside the scope of this project to solve these issues and develop a better option than the calibration factor method. An ideal situation would be to automatically generate component maps in an intra-engine approach. How this could be done is described in Appendix B.

7.2.1. Multi-Point Adaptation

Now that the choice of model calibration technique has been determined, this section will elaborate on adapting the calibration factor method to a multi-point analysis. As the component maps have been tuned for the takeoff/climb operating range, taking a single calibration would create large deviations in the cruise operating range. For this reason, calibration factors are used in both portions of the operating range, using two

reference engine data sets from the same flight. In essence, this creates multiple reference models, improving off-design model accuracy. This can be done for as many operating points as are used in the multi-point analysis. The result of such a procedure is illustrated in Figure 7.4, as proposed by van Dorp [42].

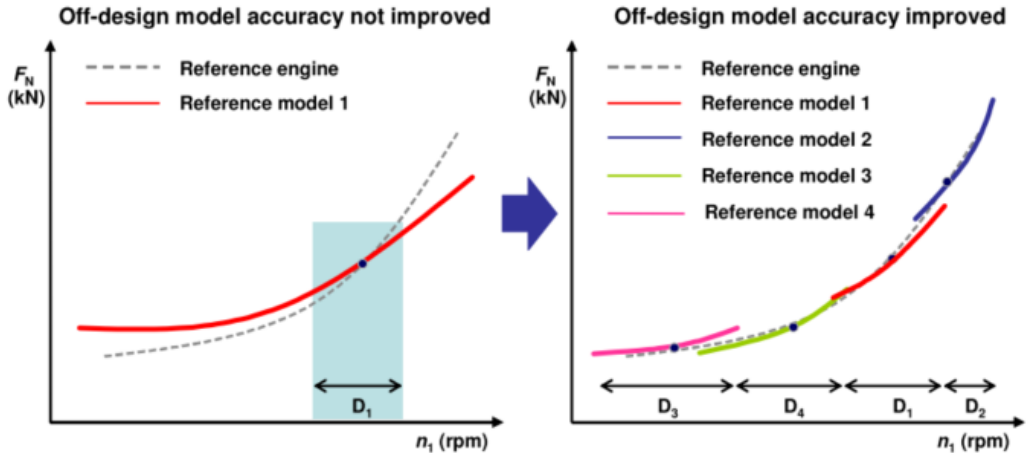

Figure 7.4: Increase in off-design model accuracy by using multiple reference models [42]

8

Application of Hybrid GPA tool on GEnx-1B Simulated Data

In this chapter, the hybrid GPA tool will be applied to simulated deteriorated data for the GEnx-1B. First, a sensitivity analysis is carried out in order to investigate each measurement sensor. Also, an optimal selection and order of health parameters is given. Then, the hybrid tool will be tested on the GEnx-1B GSP model, developed by Moorselaar [17], in order to investigate its prediction accuracy. While the GEnx-1B model is used as an example, the hybrid GPA tool can be combined with any GSP model, or even other GPA software with a few small modifications.

8.1. GEnx-1B GSP Model

In a previous research project, one of the next-generation turbofan engines in the KLM fleet, the GEnx-1B, has been modelled in GSP by Martijn van Moorselaar [17]. The model has been constructed using the already available and refined GE CF-80 model as a starting point, due to its similar architecture. The topology of this model is illustrated in Figure 8.1. The flow from the fan splits into two paths, one for the core flow and one for the bypass flow. The LPC and core portion of the fan have been modelled as a single component as this gave more stable results. The design point has been determined based on test cell results of ESN 956xxx, and Moorselaar achieved very high accuracy, 99.9958%, in replicating engine performance [17]. Off-design performance modelling has been realized by relabeling and relocating the speedlines according to Verbist's tuning method [16] and the GSP AM tool.

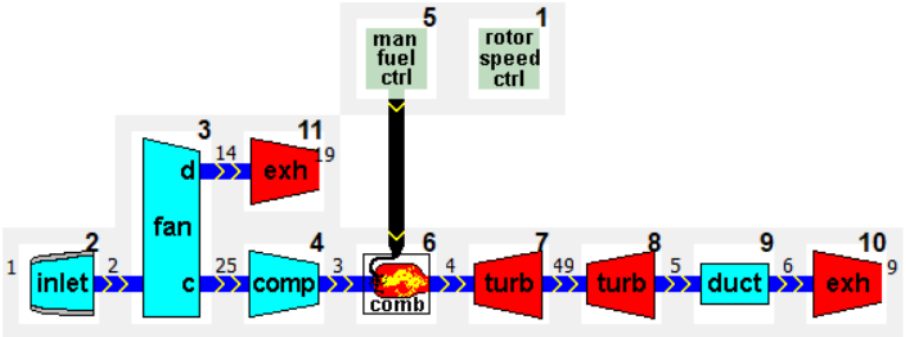

Figure 8.1: Model topology of the GEnx-1B as represented by GSP [17]

8.2. Sensitivity & Identifiability Analysis

An important part of GPA analysis is selecting the optimal measurement and health parameters. This can be achieved with a sensitivity analysis as proposed by Kamboukos et al. [36]. In this method, eigenvalues of the Jacobian matrix are calculated in order to quantify how sensitive the outputs are to changes in the inputs.

This goes hand in hand with an identifiability analysis, which determines whether the system is observable at all, and if not, filters out singular parameters.

8.2.1. Calculation Scheme

As a starting point, all variables are defined in the following sets:

- $\bar{W}$ = set of variables defining operating point ($T_{t,2}$, $P_{t,2}$, $N1$, RH)
- $\bar{X}$ = set of health parameters (η, W_c)
- $\bar{Z}$ = set of measured variables ($N2$, W_f, $T_{t,25}$, $P_{s,3}$, $T_{t,49}$)

Using these variables, we can state the following:

$$\bar{Z} = F(\bar{W},\bar{X}) \tag{8.1}$$

or that the measured values z only depend on the condition of the engine components, given an operating point u. The reference state, with a healthy engine, is expressed as:

$$\bar{Z}^{ref} = F(\bar{X}^{ref}) \tag{8.2}$$

When engine components deteriorate, it can be said that they deviate from the reference state as follows:

$$\Delta x_j = \frac{x_j - x_j^{ref}}{x_j^{ref}} \cdot 100 \tag{8.3}$$

This results in a deviation of the measured variables:

$$\Delta z_i = \frac{z_i - z_i^{ref}}{z_i^{ref}} \cdot 100 \tag{8.4}$$

This relationship between Δf_j and ΔY_i is nonlinear. For small deviations, around 1%, however, a linear relationship can be assumed. This allows for a formulation in matrix form:

$$\begin{bmatrix} \Delta z_1 \\ \Delta z_2 \\ \vdots \\ \Delta z_m \end{bmatrix} = \begin{bmatrix} a_{11} & a_{12} & \dots & a_{1n} \\ a_{21} & a_{22} & \dots & a_{2n} \\ \vdots & \vdots & \ddots & \vdots \\ a_{m1} & a_{m2} & \dots & a_{mn} \end{bmatrix} \cdot \begin{bmatrix} \Delta x_1 \\ \Delta x_2 \\ \vdots \\ \Delta x_n \end{bmatrix} \tag{8.5}$$

a_{mn} is the linear relationship between measured quantity m and health parameter n. This can also be called the sensitivity, where the higher a_{nm}, the more sensitive that sensor measurement m is to a change in health parameter n. These sensitivities are shown graphically in Figure 8.2. In this analysis, each health parameter was disturbed by -1%. These sensitivities give a useful insight in the behaviour of the GEnx-1B GSP model. First of all, a decrease in efficiency in any of the components has a relatively large effect in decreasing fuel flow, especially so for components on the N1 spool. This is the case because N1 speed is a controlling variable and kept constant. If N1 speed were allowed to increase, the fuel flow also increase, leading to a higher fuel consumption for the same thrust.

Another interesting thing to note is that changing any health parameter downstream of the $T_{t,25}$ sensor has no effect on this measurement. This lack of any upstream influence makes it a good indicator of fan and LPC performance, as any change in its value can only come from those components.

Finally, it can be noted that a deterioration in the HPC flow capacity has very little effect on any of the measured variables. This could indicate a low prediction power of this health parameter, given the current sensor set. In general, gas path sensors located at the inlet or outlet of components will have a higher sensitivity to the health parameters of those components.

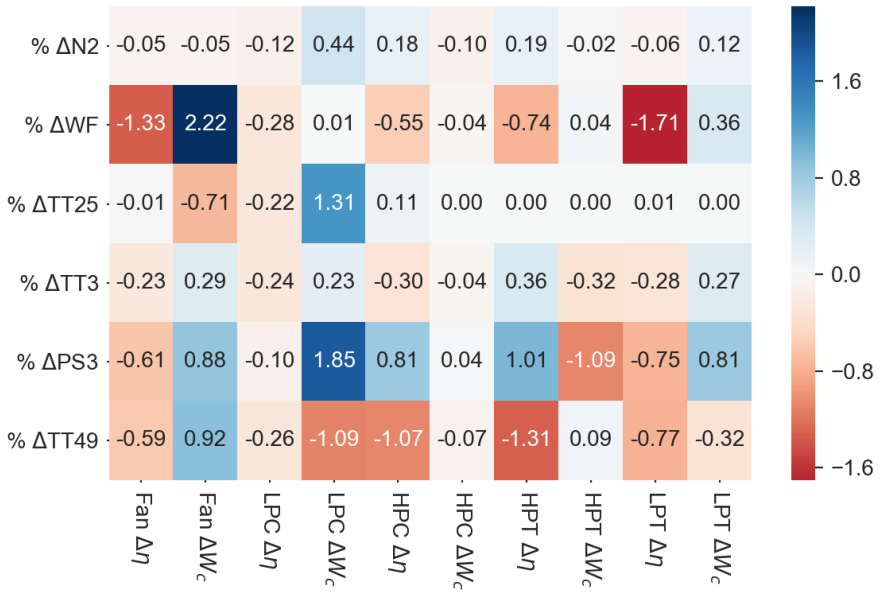

Figure 8.2: Gas path sensor measurement sensitivity

8.2.2. Overall Sensitivity Measurement

For the given set of health parameters, the measurements that are most suitable for condition monitoring are those that exhibit a high sensitivity to condition changes. The is why the overall sensitivity measure is calculated as follows:

$$S\Delta z_i = \left[\frac{1}{n} \cdot \sum_{j=1}^{n} \left[\Delta z_i^j \right]^2 \right]^{\frac{1}{2}} \tag{8.6}$$

The results for each measured variable are shown in Figure 8.3, given a 1% change in every condition parameter. Measurements with a very low sensitivity should not be selected for use in a diagnostics system. This is not the case for the measurement set on the GEnx-1B, but it is clearly visible that fuel flow, $P_{s,3}$ and $T_{t,49}$ have a much greater sensitivity than $N2$, $T_{t,25}$ and $T_{t,3}$.

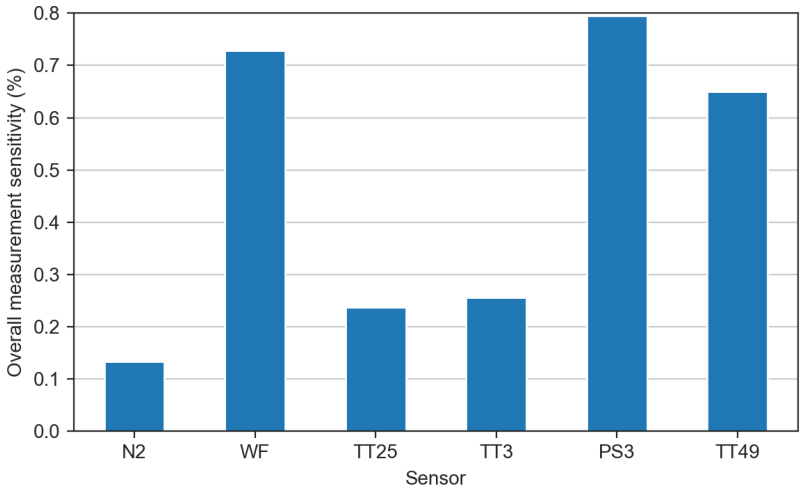

Figure 8.3: Gas path sensor measurement overall sensitivity

8.2.3. Singular Value Decomposition Analysis

It is also possible to go one step further than a sensitivity analysis and perform a Singular Value Decomposition (SVD) analysis of the Jacobian matrix. This will give an insight into the most observable system, given the measurement set available. It is also capable of demonstrating the level of linear independence between the matrix rows and columns. The method is given by Kamboukos et al.[36]:

$$J = U \cdot W \cdot V^T \tag{8.7}$$

Where the singular values of the Jacobian are contained in vector W, and each column of matrix is the singular vector of J. Then, the condition number of matrix J is defined as the ratio of the greatest singular value to the smallest:

$$CN = \frac{max(W_j)}{min(W_J)} \tag{8.8}$$

Well-conditioned matrices, indicating a well-defined parameter set, will have a small condition number [36]. As the condition number increases, the diagnostics system deteriorates. In a classical GPA problem, where n must equal m, a choice must be made as to which 6 health parameters to use. There are N_{comb} different possible combinations:

$$N_{comb} = \binom{m}{n} = \frac{m!}{n!\,(m-n)!} \tag{8.9}$$

This leads to 210 different combinations for $m = 10$ and $n = 6$. Using the condition number, the best 10 combinations are shown in Figure 8.4. Although the hybrid GPA tool allows for a complete circumvention of the $n = m$ rule, it is still useful to see which health parameters are not particularly identifiable, according to SVD theory. From Figure 8.4, it can be concluded that the GEnx-1B core is mostly well-defined, while the fan and LPC in particular have low identifiability. This will be confirmed by the simulated deterioration cases in Section 8.3.3.

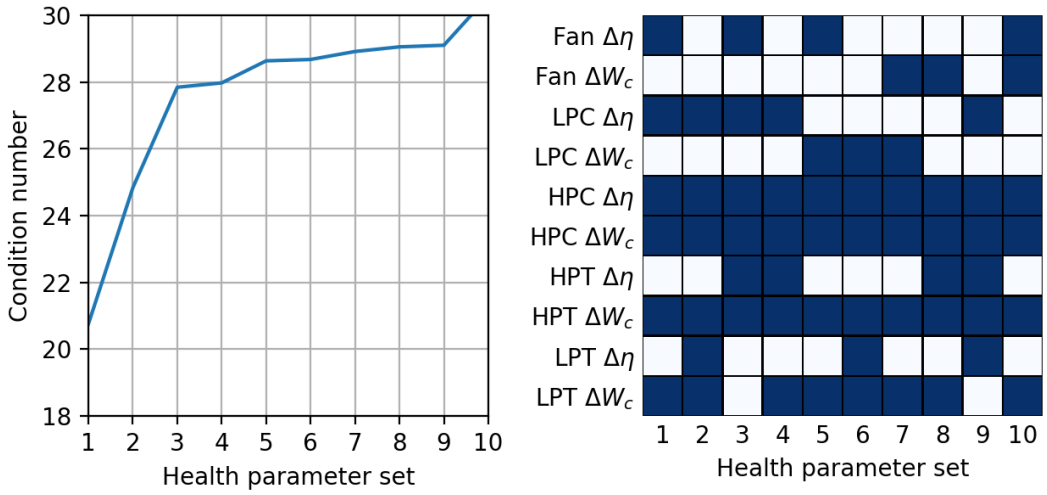

Figure 8.4: 10 best sets of 6 health parameters according to lowest condition number

An SVD analysis could also be applied from a whole different standpoint, in order to investigate the optimal choice of measurement sensors for complete identifiability of all health parameters. However, this is not very useful for KLM ES' purposes, as it does not control the number and location of sensors which are added to an engine. Ultimately, for a complete indication of all component condition deviations, sensors would need to be placed at the inlet and outlet section of every component. However, this would increase the complexity of an aero engine, introduce sources of possible malfunction, and sensors such as pitot tubes and thermocouples cause unwanted disturbances in the flow. Furthermore, in some gas path locations like the turbine inlet, placing sensors is simply not possible due to the harsh conditions.

8.3. Results

In this section, several different deterioration cases are simulated and run through the hybrid GPA tool. First, the configuration of both the evolutionary algorithm and multi-point analysis is explained. This is followed by simulated individual engine component faults. Then, more complex cases of deterioration are tested.

8.3.1. Evolutionary Algorithm Configuration

The configuration of the evolutionary algorithm is very similar to that used in the J85 model case in Section 5.2.3. The crossover constant CR is kept at 0.7, and dithering is still employed by changing F between 0.4 and 1. In order to keep the computing time to a minimum, a population size of 50 is chosen. This is at the lower end of the rule of thumb of 5-10 times the number of health parameters. The bounds for the fan health parameters is set between -1.5 and 0.1 % deviation. The HPT and LPT flow capacity bounds range from -0.5 to 2.5 %. For all other health parameters, a lower and upper bound of -2.5 and 0.5% deviation, respectively, is applied. The reason for the smaller fan condition range lies in the fact that large fan health parameter deviations greatly increase the complexity of the search space. This was discovered through experimentation, as the evolutionary algorithm would almost always get stuck in a local minimum. Therefore, it has been decided to narrow down the fan condition deviation bounds. This will not have a large effect on real turbofan engine condition monitoring, as the fan does not experience heavy deterioration.

8.3.2. MOPA configuration

The first step in a multi-point procedure is to choose the number of operating points, as well as the point spacing. If the operating points are far apart, the assumption that health parameter deviation is independent of power setting may not hold. On the other hand, if the operating points are too close together, there is the risk of inter-dependency. Also, observability is poor at low power settings [49].

A complete analysis of picking optimal operating points was deemed outside the scope of this project, and instead results published by Sampath [49] were used. In this investigation, a relative redundancy index was employed to show accuracy versus computational time for an increasing number of operating points. Additionally, tests were conducted with different bands between the operating points, with three cases: 1-3%, 5-8%, and 15-18%. It was concluded that two operating points, with a difference of 5-8% in power setting, would be the optimal composition for a multi-point procedure. More than two operating points were shown to give diminishing results. This was also confirmed by brief testing of a triple operating point procedure.

As a result, all of the simulated deterioration cases were run in a double operating point analysis, at the takeoff design point and at an N1 speed which was 5% lower, simulating an operating point closer to cruise.

8.3.3. Individual Engine Component Deterioration Cases

First, the GEnx-1B components are analysed individually by creating separate simulated deterioration cases. These deterioration cases are based on typical deterioration modes as described in Table 2.1. For the fan, lighter deterioration was simulated than for the rest of the components, due to the more restrictive bounds. In a real on-wing situation, these cases simulate a sudden fault in individual components, which can be valuable information for an MRO. The results are shown in Figure 8.5. In general, the hybrid GPA tool is very capable in predicting individual component condition, as the predicted deviation is very close to the actual deviations. However, some small differences between components prediction accuracy can be noted, as well as significant smearing in some cases.

As was already anticipated after the identifiability analysis, the fan and LPC deterioration cases, shown in Figure 8.5a and Figure 8.5b, exhibit the highest rms. Another thing that stands out is that false component deviation is contributed the most to both the LPC efficiency and LPT flow capacity. A possible reason behind this phenomenon is that both components have only one sensor at their inlets and outlets ($T_{t,25}$ at the LPC outlet and $T_{t,49}$ at the LPT inlet). For that reason, the hybrid tool could be experiencing difficulty in attaining the correct component condition deviation. On the other hand, the prediction accuracy when these two components experience deterioration (Figure 8.5b and Figure 8.5e), is quite remarkable.

8.3.4. Complex Engine Component Deterioration Cases

Now, the hybrid tool is verified with more complex engine deterioration mode. First, a deteriorated core is simulated in Figure 8.6a. This returns a high-accuracy solution with very little smearing. However, as condition deviations are introduced in all of the health parameters, as shown in Figure 8.6b, the hybrid GPA tool struggles to match the same accuracy. This result illustrates that the hybrid GPA tool is definitely able

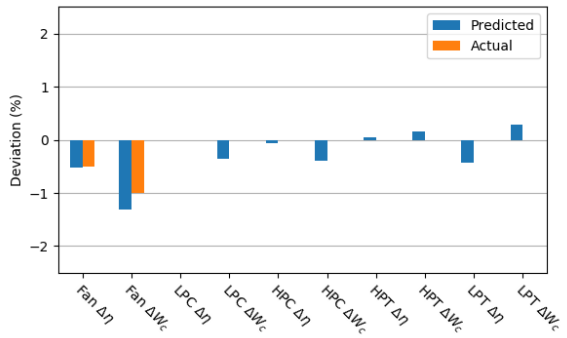

(a) Fan condition deterioration

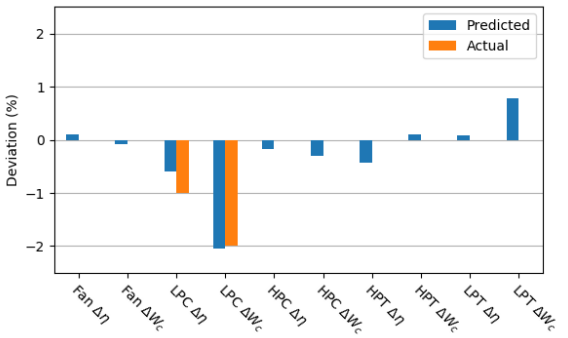

(b) LPC condition deterioration

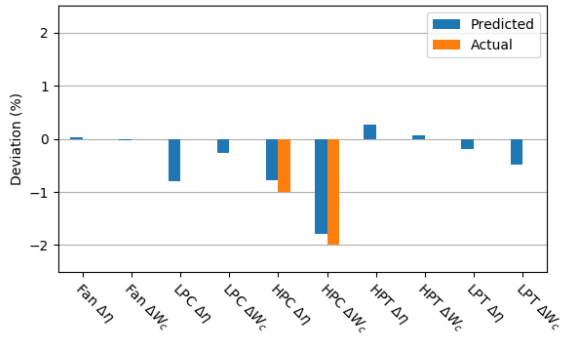

(c) HPC condition deterioration

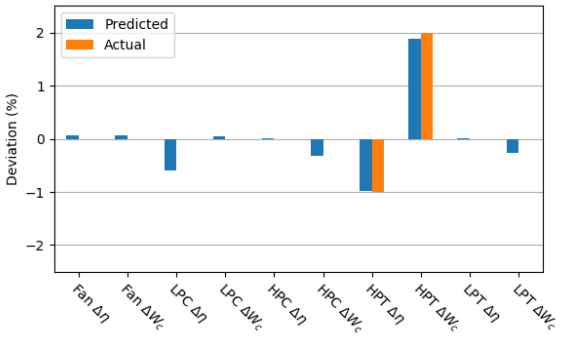

(d) HPT condition deterioration

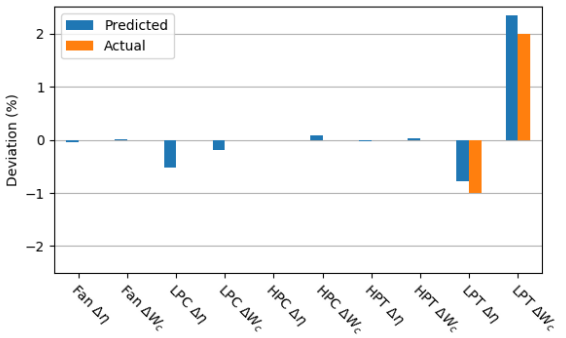

(e) LPT condition deterioration

Figure 8.5: Simulated and predicted condition deterioration of individual engine components

to predict the general direction of condition deviation for all 10 health parameters, but is not too effective in judging the exact magnitude. Nonetheless, a MOPA evolutionary algorithm procedure has proved to be adequate in predicting 10 health parameters using only 6 measurement variables.

8.3.5. Computation Time

Next to the prediction accuracy, another important aspect of the hybrid tool's performance is its computation time. A GSP AM procedure will complete almost instantly due to its deterministic solution methodology. An heuristic optimizer like a DE on the other hand has a significantly longer runtime. For the cases described above, including all 10 health parameters, the runtime amounts to around 1 hour for a single-point analysis, and double for the multi-point adaptation. If the hybrid GPA tool was to be implemented and used systematically for the entire KLM GEnx-1B fleet, this runtime would not be acceptable. There are several options which could potentially reduce the runtime:

- DE control variables optimization: it is possible to spend greater time in order to optimize the DE

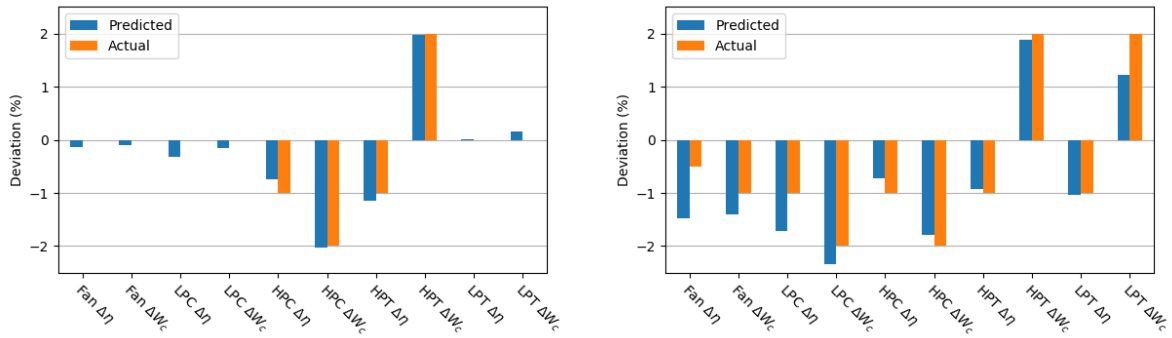

(a) Core condition deterioration

(b) Total engine condition deterioration

Figure 8.6: Simulated and predicted complex engine condition deterioration

control variables for decreased runtime.

- Multi-threading: this is currently not compatible with GSP API, but EA optimizers can be combined with multi-threading as they search for multiple solutions in parallel. Every added thread cuts the computation time in half.
- Low detail GSP run: If the chemical equilibrium calculation is reduced or turned off, GSP would converge significantly faster. Again, this option is not currently available in GSP API.
- Borland database engine: in its current form, every off-design point run is written to the same Borland Database Engine (BDE) table. Then, the DE calls the complete table every time for an output, which takes additional time if working with thousands of runs. It is expected that the hybrid GPA tool can run significantly faster by rewriting the source code to not write to the internal BDE table.

9

Application of Hybrid GPA Tool on GEnx-1B On-Wing Data

In the previous chapter, the hybrid GPA tool has successfully been verified using simulated GEnx-1B deterioration cases. In this chapter the hybrid GPA tool will be tested on real in-flight data, producing engine condition monitoring results as an engine deteriorates over time. This will answer the research question of whether the hybrid GPA tool is able to perform accurate on-wing component condition prognostics. As a starting point, only one GEnx-1B has been analysed, but the procedure can be applied on all other engines in the KLM fleet as well. First, a short background is given on the engine in question, followed by the operating point selection from the CEOD procedure. Then, the results are displayed and discussed, for both a single and double operating point procedure.

9.1. ESN 956xxx Background

This analysis has been performed on the GEnx-1B with ESN 956xxx, a long-standing member of the KLM 787 fleet. The reason why this engine was chosen is threefold. Firstly, over 4.5 years of snapshot data and 3.5 years of CEOD data is available for this engine. Secondly, it has experienced an overhaul-level workscope shop visit, as a result of a redline exceedance which will be explained in Section 9.1.1. The exact workscope overview of the shop visit is given in Appendix C. The third reason for selecting ESN 956xxx is that the design-point modelling of the GEnx-1B has been conducted using data from the 956xxx test cell run.

The lifespan of ESN 956xxx is illustrated in Figure 9.1, as a function of EGTMHD. This is an excellent measure of the overall engine condition, and it is clearly visible that between shop visits (indicated in green), a turbofan engine gradually deteriorates. The vertical orange lines indicate the occurrence of a waterwash. As explained in Section 2.2.1, a waterwash is administered primarily to combat compressor fouling. Waterwashes have a large effect on engine performance, and as seen in Figure 9.1 can restore up to 10 degrees Celsius of EGT margin.

9.1.1. Redline Exceedance Event

For every engine type, an EGT limit is decided by GE, which must not be exceeded in-flight. This is called the redline and indicates the point where an engine has zero EGT margin. A redline exceedance is thus a serious event, and warrants immediate unscheduled engine removal. ESN 956xxx experienced such an event after just 977 cycles, shown by by the red dot in Figure 9.1. It was caused by a HPT stage 1 blade mid-chord burndown. The HPT rotors and stators require blade cooling due to the high combustor exhaust temperatures. When these cooling holes are blocked, the blades will start to disintegrate causing full engine failure. This is what occurred with ESN 956xxx, illustrated in Figure 9.2. Debris from the first HPT stage also damaged the second stage. After an investigation, the failure was pinpointed to a manufacturing fault, which had blocked multiple cooling holes. Subsequently, over the course of several months, the HPT received a full performance restoration shop visit. This is an ideal case in which it can be validated if the hybrid GPA tool is able to detect this major component fault.

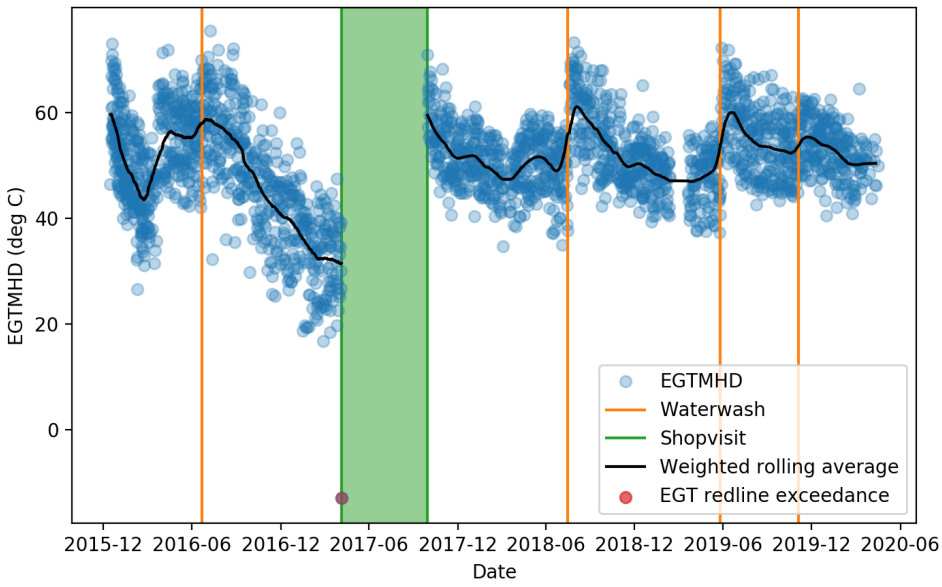

Figure 9.1: Lifespan of ESN 956xxx given as a function of EGTMHD

(a) HPT stage 1 rotor

(b) HPT stage 2 stator

Figure 9.2: Effects of a stage 1 blade mid-chord burndown on the HPT

9.2. CEOD Outlier Filtering

After obtaining a selection of CEOD data sets, one flight roughly every two weeks, the data preprocessing procedure described in Section 6.4 can be applied. The IQR outlier filtering method is utilized to create optimal steady-state operating points. Boxplots that illustrate the workings of this method are shown in Figure 9.3 and Figure 9.4 for the 8 available secondary performance parameters in a takeoff operating point. The red dots indicate all data points before and the black dots for the data set after outlier filtering. The upper whisker is drawn at the greatest value smaller than $Q_3 + 1.5 \cdot IQR$. Similarly, the lower whisker is drawn at the smallest value greater than $Q_1 - 1.5 \cdot IQR$. Any value outside of this range is classified as an outlier. This is where the program undergoes a second iteration, in order to find another operating point within the data set that lies within the IQR limits for all secondary performance parameters. It can be seen in Figure 9.3 and Figure 9.4 that after this iteration, all (black) operating points fall within the IQR boundaries.

One might note that the variability of the HPTACC and power offtake data sets are relatively high. This could introduce errors in the GPA tool, as these variations are not modelled. However, it was not possible to reduce the data set spread without eliminating a large portion of the data set. For the HPTACC system this is caused by the fact that during takeoff the engine is far from thermally stable, and thus the clearance is kept at low to mid levels by the ECU. Power off-take has a direct relation with the aircraft power demand and this too fluctuates heavily from flight to flight, depending on passenger capacity and flight destination/duration.

Another hindrance is the CAI bleed configuration. Figure 9.4 shows that for around half of the data points the valve is open (2), and for half it is close (0). The exact time the CAI system is switched on varies from flight to flight as it is regulated by the outside air temperature sensor. Usually, the valve goes from a closed position

to the open position somewhere in the takeoff/climb flight phase. This makes it difficult to pick a takeoff operating point for all flights where the CAI bleed configuration is equal, while still adhering to approximately the same N1K. On the other hand, when picking cruise operating points, the CAI valve is always open due to the low operating temperatures. It is stated in the GEnx-1B installation manual that up to 3.3% of the core airflow is extracted [6]. Due to the fact that the valve only has two positions, it can be assumed that this airflow is mostly constant. As a future recommendation, the CAI bleed valve position could be implemented directly as a bleed flow in GSP, based on its value from CEOD.

The same procedure as shown in Figure 9.3 and Figure 9.4 is conducted for the cruise operating point. Since CEOD is used, any possible combination is possible, as opposed to working with GE-provided snapshot data. However, it is important to consider the power setting range as well as the point spacing. Based on lessons learned from the simulated data analysis, an N1K power setting 5% below the takeoff design point is used as a starting point. Cruise flight has a lot of advantages compared to takeoff. First and foremost, the engine is thermally stable, and as a result both ACC systems start to regulate the casings for minimum tip clearance and maximum efficiency. There is no more heat soak which seeps efficiency from the engine, and the relative humidity is zero at high altitudes. As a result, a MOPA analysis should benefit greatly from an added cruise operating point.

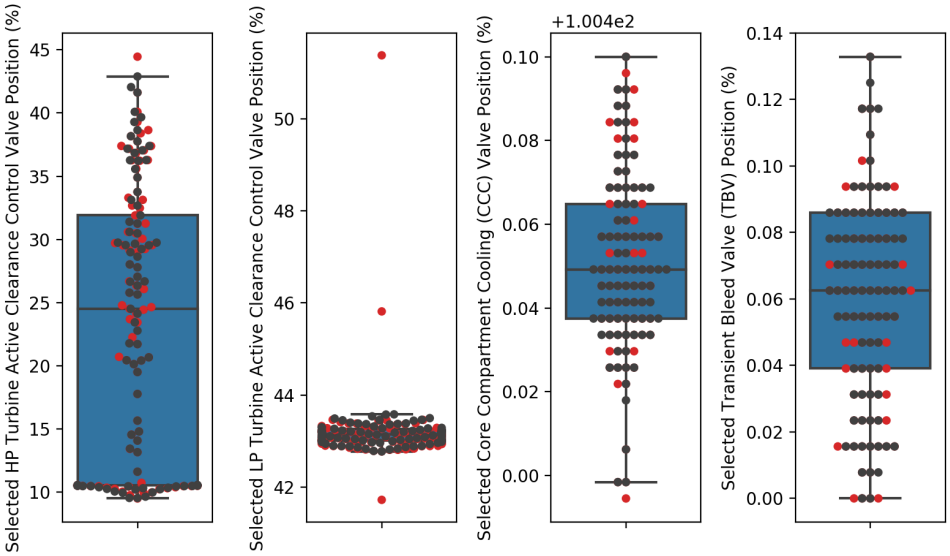

Figure 9.3: Boxplots of the HPTACC, LPTACC, CCC and TBV valves

9.3. Results

Now that the takeoff and cruise operating points have been selected, the hybrid GPA tool is applied on the historical data of ESN 956xxx. The results are split up in the following subsections per component. For all components, the GPA tool was run first in a single operating point state with takeoff data. Then, a MOPA adaptation was run for two operating points, one at takeoff and one at cruise.

9.3.1. Fan Deterioration

Figure 9.5 and Figure 9.6 illustrate the results for fan efficiency and flow capacity deterioration, respectively. The condition of the fan is fairly constant, which most likely follows reality as fan deterioration is not very severe. However, it could also be partially due to the restrictive bounds which are given by the variable bounds method from Section 6.5. Small jumps can be seen around the waterwash points, which could indicate a small performance increase from cleaning the fan blades. Another possibility is that smearing occurs, and an increase in LPC performance is incorrectly assigned to the fan. There are no large differences between the single and multi-point analyses, except for a drop in efficiency and flow capacity just before the shop visit for the latter. There are no events that suggest a quickly deteriorating fan, so this phenomenon is mostly likely the result of an incorrect shift in the model's operating point for the N1 system. This will be discussed in greater detail in Section 9.4.

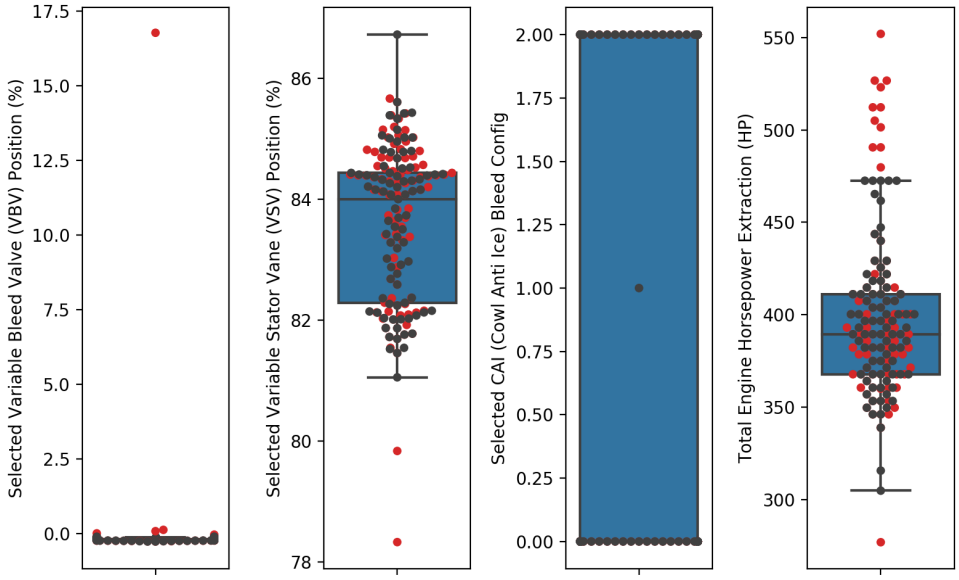

Figure 9.4: Boxplots of the VBV and VSV valves, CAI bleed configuration and power offtake

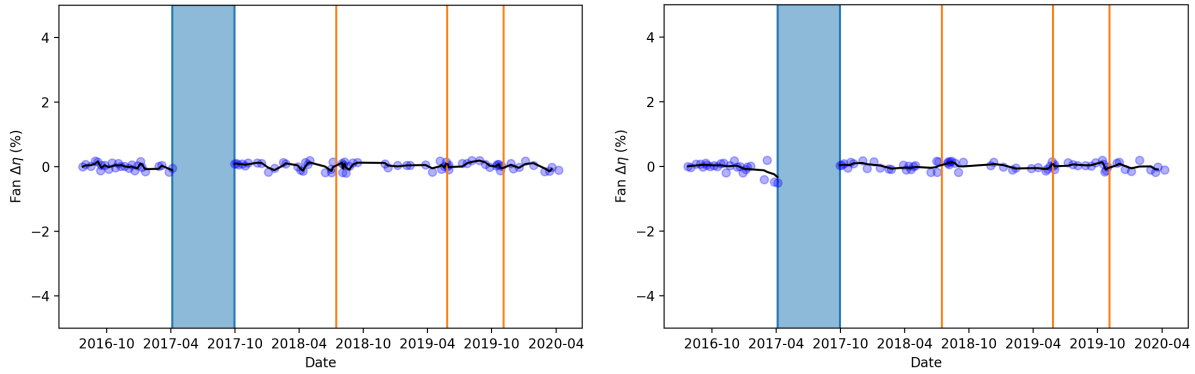

(a) Single operating point analysis

(b) Multi-point analysis

Figure 9.5: Fan efficiency deterioration

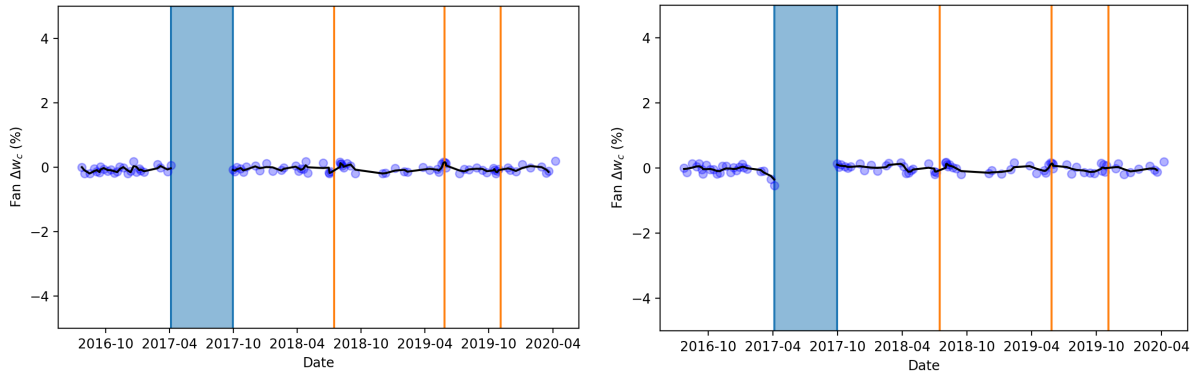

(a) Single operating point analysis

(b) Multi-point analysis

Figure 9.6: Fan flow capacity deterioration

9.3.2. LPC Deterioration

The predicted condition deviations of the LPC efficiency and flow capacity are shown in Figure 9.7 and Figure 9.8. Unlike for the fan, these results exhibit large differences between the single and multi-point analysis.

An important indicator of the validity of the tool is its ability to recognize the effect of a waterwash on the LPC and HPC, and this is clearly distinguishable. The single operating point analysis returns more distinct peaks, but a more logical downward deterioration trend is visible in the multi-point results.

In all cases except the single operating point LPC flow capacity, an upward shift is visible after the shop visit. As no maintenance work was performed on the LPC, this seems to be a faulty prediction by the hybrid GPA tool. Another trend that will continue in the rest of the components is that the multi-point results have increased scatter. This is likely due to the the GSP model itself, which is tuned in the takeoff region and has decreased accuracy outside this region.

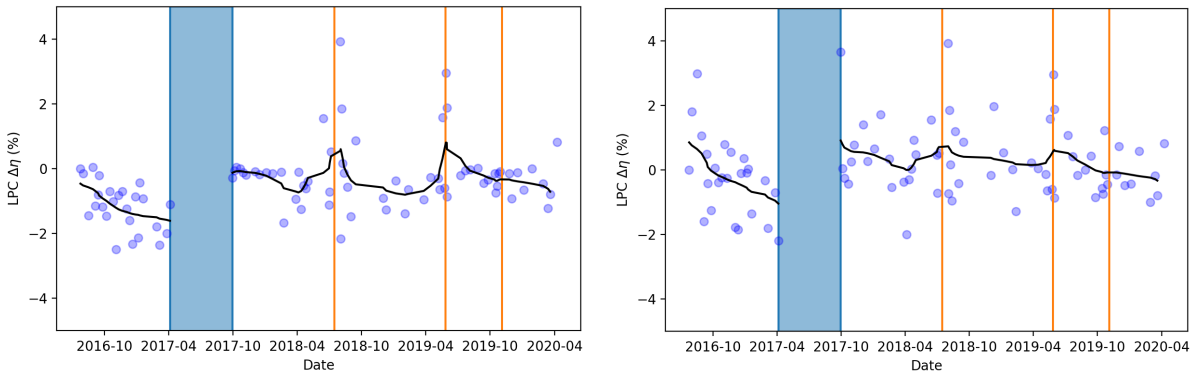

(a) Single operating point analysis

(b) Multi-point analysis

Figure 9.7: LPC efficiency deterioration

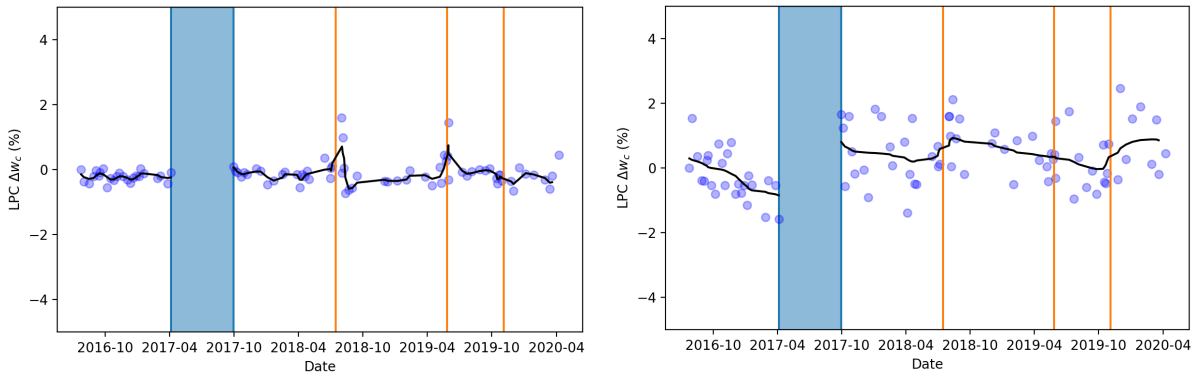

(a) Single operating point analysis

(b) Multi-point analysis

Figure 9.8: LPC flow capacity deterioration

9.3.3. HPC Deterioration

Next, the HPC deterioration results shown in Figure 9.9 and Figure 9.10 are investigated. These are very similar to the comments on the LPC deterioration, including similar waterwash peaks where performance increases by 1% and the peculiar shift in HPC flow capacity for the multi-point case. A possible explanation is that the shift is caused by VSV misrigging, or that it was adjusted for less stall margin. This would increase HPC performance. Another odd appearance is that the data points in the single-point case seem to indicate a waterwash before it has occurred, although this is likely just a coincidence.

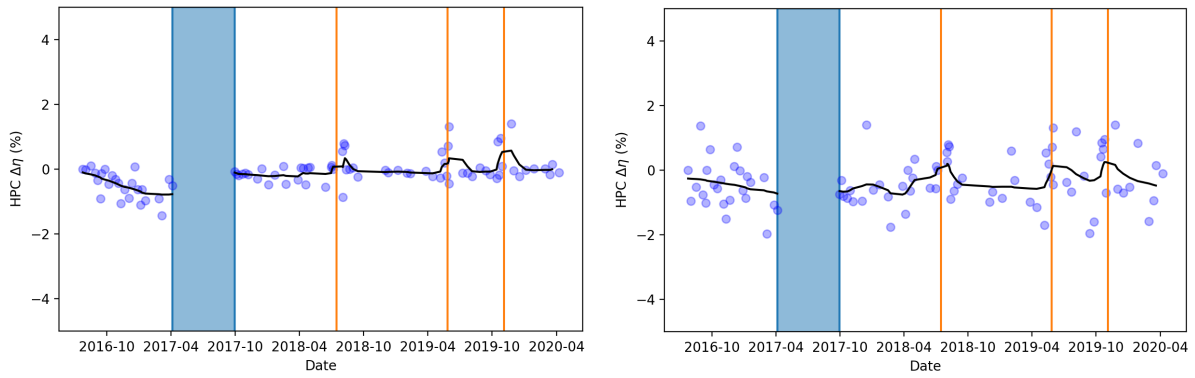

(a) Single operating point analysis

(b) Multi-point analysis

Figure 9.9: HPC efficiency deterioration

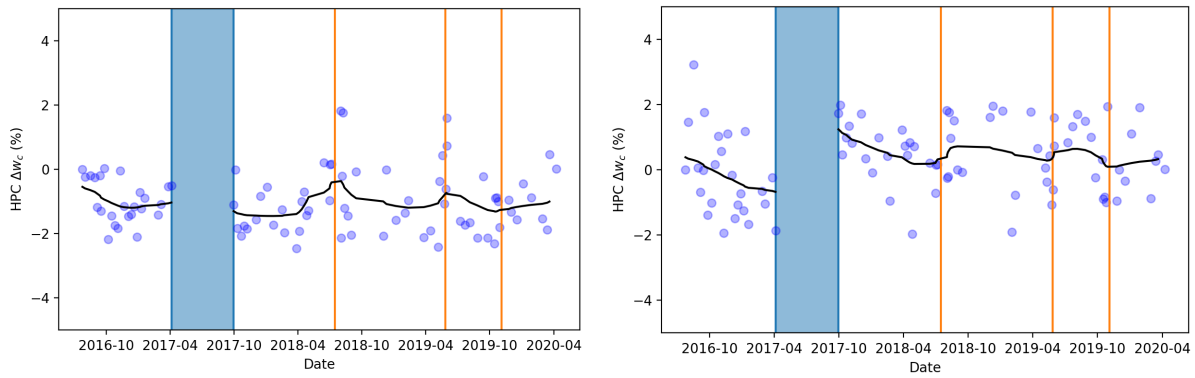

(a) Single operating point analysis

(b) Multi-point analysis

Figure 9.10: HPC flow capacity deterioration

9.3.4. HPT Deterioration

The HPT is a very interesting component to analyse due to the mid-chord burndown event that this engine has experienced. When looking at the efficiency deterioration results in Figure 9.11 a gradual downward trend is noted. Also, the final flight of the failure is indicated by a 1-1.5% drop from the moving average for both cases. The trend even more pronounced for the flow capacity condition parameter in Figure 9.12. The upward trend is indicative of excessive material erosion in the turbine, increasing the mass flow capacity. In the multi-point case, the event itself is noted by a 4.1% positive deviation from the baseline. Seeing such a clear trend is a promising sign that in the future this hybrid GPA tool could actually be employed to predict these sorts of catastrophic events before they occur. Also, the direct effect of the overhaul workscope is visible with a restoration in HPT flow capacity. The HPT efficiency remains largely unperturbed for the single operating point analysis. The multi-point case is superior in reflecting reality, with a small upward shift after overhaul and deterioration trend afterwards.

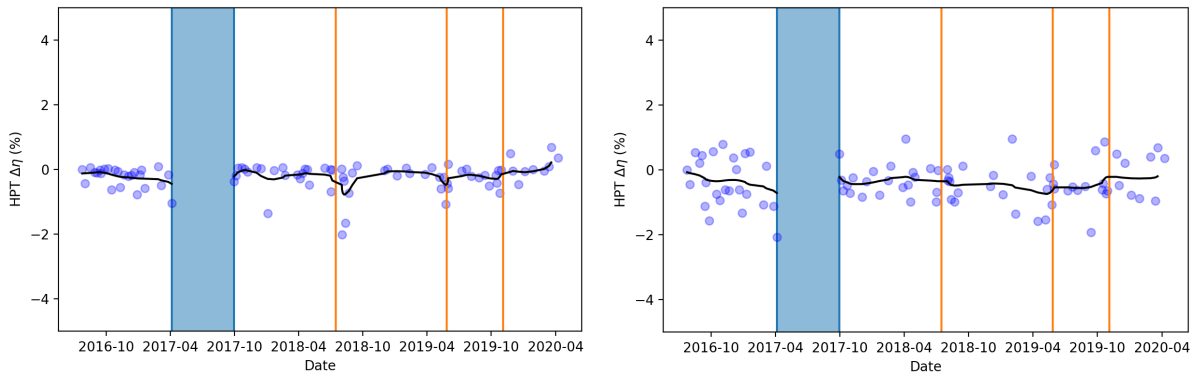

(a) Single operating point analysis

(b) Multi-point analysis

Figure 9.11: HPT efficiency deterioration

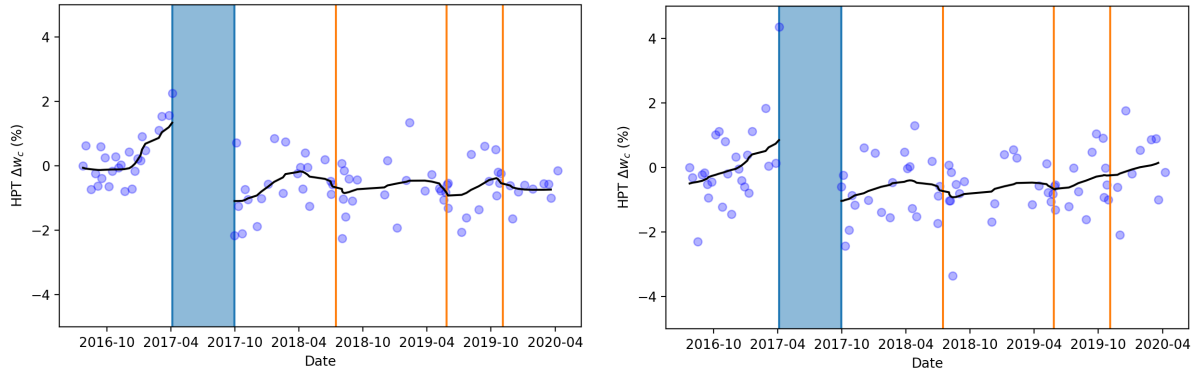

(a) Single operating point analysis

(b) Multi-point analysis

Figure 9.12: HPT flow capacity deterioration

9.3.5. LPT Deterioration

The last component is the LPT, with its deterioration trends shown in Figure 9.13 and Figure 9.8. For the efficiency there is not much difference between the single and multi-point analysis. In the time span before the first waterwash, the efficiency deviation decreases over time as expected. Subsequently, however, there is a period of close to a year where the efficiency increases. It is difficult to state with certainty that this due to an inaccurate GPA tool, or some unknown interaction in the engine between components.

A large discrepancy is also visible between the single and multi-point LPT flow capacity prediction results. According to the multi-point analysis, the shop visit has also restored the condition of the LPT, while this is not the case in the single point analysis. After consulting the workscope overview, it became clear that the LPT rotor/stator assembly experienced metal splatter on all stage 1 blades and sustained out-of-limits impact damage on three blades. The fairing was also punctured in two locations. The subsequent repair could have potentially led to the performance gain shown by the multi-point results, but likely not to the magnitude of almost 2% as shown.

Lastly, the multi-point analysis registers an extreme decrease in performance for both the efficiency (-3.7% from baseline) and the flow capacity (+4.8% from baseline) on the flight of the HPT failure event. It is possible to conclude from these results that an LPT failure took place as well, although this was not strictly the case. The impact damage and metal splatter would have caused a drop in performance, but not to the degree as shown. The model will have likely seen a shift in map operating point due to the changing inlet conditions (higher temperature and pressure). Normally this would not be seen in corrected parameter values, but this suggests GSP model inaccuracies.

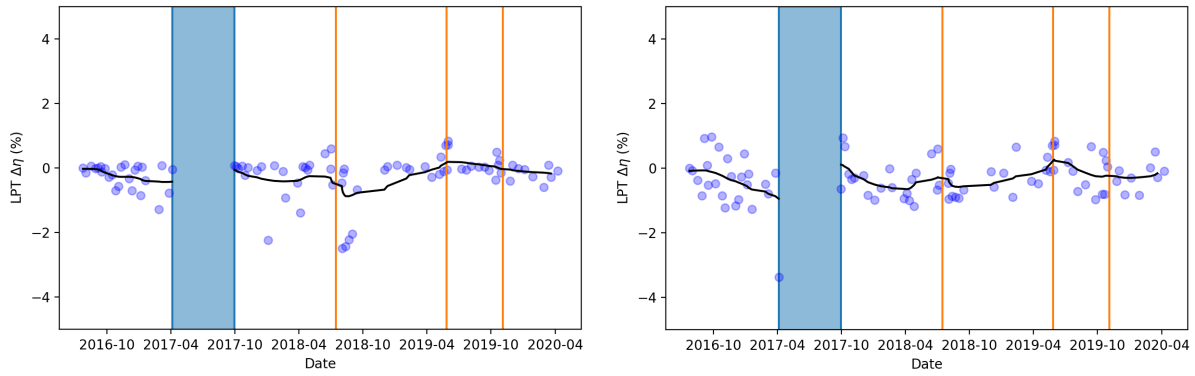

(a) Single operating point analysis

(b) Multi-point analysis

Figure 9.13: LPT efficiency deterioration

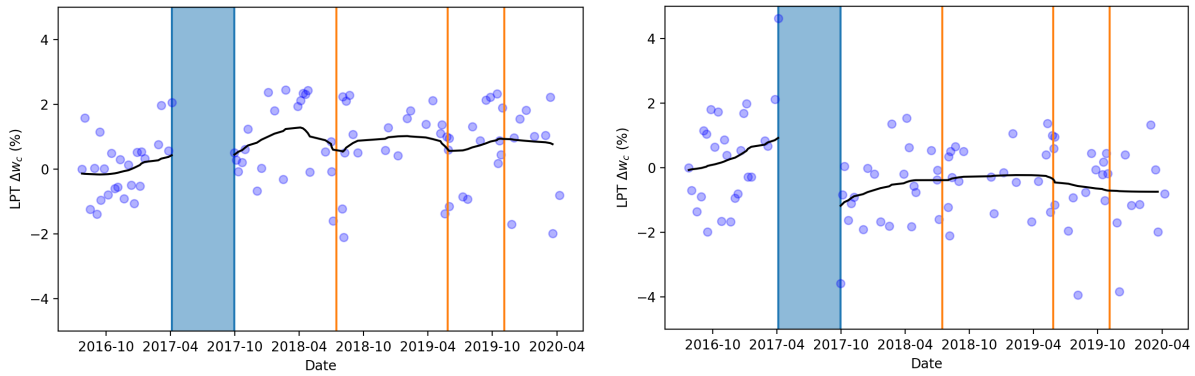

(a) Single operating point analysis

(b) Multi-point analysis

Figure 9.14: LPT flow capacity deterioration

9.3.6. Computation Time

As stated before in Section 8.3.5, runtime must also be taken into account when judging the hybrid GPA tool's performance. All of the points that have been stated for simulated data also apply for the on-wing data cases. A small increase in computation time can be seen, however, which is likely due to the increased noise of the input parameters. This leads to longer convergence times of the GSP off-design point runs, as the input data may be thermodynamically unphysical. At times, a vector parameter guess will exceed the maximum number of iterations, at which time this is declared invalid and is skipped. This phenomenon occurred frequently for on-wing data, while it was extremely rare with simulated data, even with the simulated noise included. This suggests that the maximum simulated noise was rather conservative.

9.4. Discussion

The main question is whether the results of the hybrid GPA tool are clear enough to isolate a component failure. For the case analysed in this chapter, ESN 956xxx, this meant an indication of a HPT failure. It can be concluded that this is definitely distinguishable, as the decreasing performance trend leading up to as well as the event itself was clearly registered. However, the hybrid GPA tool also predicted a significant change in LPT performance. This is partly correct, as the LPT experienced impact and puncture damage, but a portion of the deterioration must be attributed to another phenomenon. A hypothetical source is the GSP model inaccuracy. The change in inlet conditions as a result of the HPT loss in performance alters the LPT map operating point. The rotational speed is constant, as the engine is N1-controlled, but the mass flow balance must be upheld. If the component map is not completely representative of the real engine, this will introduce errors in the efficiency and flow capacity deviation results. This interaction is seen throughout the N1 system, as the fan and LPC also experience a drop in performance, especially when looking at the multi-point analysis.

The results of the hybrid GPA tool were also briefly compared to results generated by GSP AM, for the

same operating points. The AM results are shown in Appendix D, for only 6 health parameters due to the $M = N$ restriction. The performance increase of waterwashes on the LPC and HPC not distinguishable in the AM results. The upward trend for the HPT flow capacity, on the other hand, is similar to the hybrid GPA tool results. Finally, the LPT efficiency displays an substantial negative shift after the first waterwash, before recovering. It can be concluded that the hybrid GPA tool results are of better quality, not including the fact that four additional health parameters are calculated.

During the outlier detection procedure, measures were taken to control the secondary performance parameters. However, there are multiple other variables which cannot be controlled, and therefore affect the GPA results. Some of these factors, like humidity and unsteady conditions, are less prevalent at cruise altitudes. This is why, given a GSP model that is tuned correctly in the cruise region, multi-point results including cruise have the potential for highly-accurate results.

Another important thing to note is the validity of the baseline model. As stated before in Chapter 7, GPA results are heavily reliant on an accurate baseline model. The suggested approach is to take a consistent data set from the first 50 flight after entry into service, and apply the off-design calibration factor method to create the baseline model. In this analysis, the baseline data set was taken 12 months after entry into service, as CEOD did not go back any further. On the positive side, this means that run-in fluctuations are no longer present. Experimenting with different methods to create the baseline model could result in more accurate results. The best option would be to tune the component maps specifically for this engine. If the tuned portion also includes cruise power settings, the scatter of the multi-point analysis results would also decrease. This could be done in a manual fashion as proposed by Verbist [16] or using an automatic map generation method described in Appendix B.

After accuracy improvements, the next step for the hybrid GPA tool would be to automate diagnostics. By keeping track of the component health parameter trends, it is possible to alert the user of an imminent component failure. This is possible as CEOD is downloaded after every flight. This addition is included as a recommendation in Section 10.2

10

Conclusions & Recommendations

This chapter forms the end of this report, and aims to answer the research objectives and research question set out in the introduction. The main objective of this project is to make the use of Gas Path Analysis at KLM Engine Services future-proof, by developing an accurate on-wing component condition monitoring model that can operate with few gas path sensors. The key concepts introduced in this thesis are a GPA based soft-computing optimization approach, the utilization of CEOD, and the implementation of a multi-point analysis. This has culminated in a multi-point hybrid GPA tool, which is verified with the GEnx-1B GSP model, and validated with actual on-wing data. The following section will elaborate on the conclusions of this report, while Section 10.2 points out recommendations for future work.

10.1. Conclusions

Combining the key concepts described above has resulted in a novel approach of on-wing component condition monitoring, which could have an impact on the current maintenance strategy as conducted by KLM ES. If the component condition can be tracked accurately for every engine, it is possible to bridge the gap between on-wing engine operational data collection and MRO workscoping, as well as identify any engine faults when it is still installed on-wing. From the three main parts of this thesis; theoretical background, hybrid GPA tool development, and application of the hybrid GPA tool to GEnx-1B condition monitoring, the most important conclusions can be summarized:

- **Current state of the art in gas turbine diagnostics**: GSP is currently used as a non-linear GPA tool at KLM ES, predominantly for test cell acceptance test diagnostics. GSP AM is very convenient as a condition monitoring tool, due to its high adaptability, simple implementation, and high convergence speed, but it also has several limitations. The main drawback is the $M = N$ constraint, where the number of measured parameters and the number of output health parameters must be equal. The goal is to apply GSP GPA as an engine health monitoring tool, tracking component condition while the engine is on-wing. Such an advanced engine prognostics system must be able to simulate nonlinear gas turbine behaviour for a wide operating range with only a few sensors available, while dealing with measurement noise and bias. The next step, once sufficiently accurate component condition prognostics is available, is linking this information to the maintenance workscope level necessary before it enters the engine shop.

- **Existing GSP GPA research**: a review of existing GSP GPA research has shown that systematic use of GPA for condition-monitoring purposes remains limited. Most research has been conducted in a limited engine operating region, from maximum continuous to takeoff power settings. Reference model tuning is conducted using test cell data. The off-design model accuracy is limited by the availability of turbomachinery component characteristics. Finally, using a single reference data set to analyze multiple engines introduces errors. Next-generation turbofan engines have fewer gas path sensors than their predecessors, resulting in reduced AM capability.

- **Soft-computing optimization techniques investigation**: The previous point has instigated a search for alternatives that circumvent the $M = N$ constraint. In the end, it was decided upon combining GPA

with a heuristic optimizer instead of developing a purely empirical method, due to the research that has already gone into GSP at KLM ES. Subsequently, an Evolutionary Algorithm in the form of a Differential Evolution optimizer performed best for the complex gas turbine health parameter search space.

- **CEOD implementation**: the decrease in available engine measurements on the GEnx-1B is compensated by a greater quantity of available on-wing data as KLM now has access to Continuous Engine Operating Data. Relying solely on this data has several advantages: on-wing installation effects are eliminated, secondary performance parameters are available, and data points can be picked freely in order to cater the needs of MOPA and multi-point calibration. The drawbacks of CEOD include unsteady on-wing operating conditions and increased noise, requiring a form of data preprocessing and filtering. In this thesis, a procedure is proposed where selection of operating points is based on N1K and N2 rate of change measurements and subsequent IQR outlier filtering. Also, variable bounds for the optimizer search space, based on the EGTMHD, are introduced. This method is favoured over using GE snapshot data, which are not guaranteed to be (near) steady-state and have uniform secondary performance parameter values. Also, having operating points close to the model design point is beneficial for the model accuracy.

- **Hybrid GPA tool verification**: the hybrid GPA tool has been verified using simulated deterioration cases, in both a simple straight turbojet GSP model and the two-spool high-bypass GEnx-1B turbofan GSP model developed by Moorselaar [17]. In the case of the J85, four health parameters could be uniquely identified using only three measurement sensors. For the GEnx-1B, the hybrid GPA tool was able to identify the direction and magnitude of both individual component faults for 10 health parameters with 6 gas path sensors, as well as complex full engine deterioration cases. The tool can, with little modification, be applied to any GSP engine model, which makes it very versatile. One of the major downsides of the hybrid GPA tool, however, is the computation time. For multi-point analyses these exceed an hour.

- **Hybrid GPA tool validation**: the hybrid GPA tool has been validated using historical in-flight data from ESN 956xxx. Both the single and multi-point adaptations are able to track engine component condition for all 10 health parameters, and identify events such as turbine blade failure and water washes. The relatively large scatter and a few unaccountable deterioration modes indicate that the accuracy can still be massively improved.

- **MOPA vs single point analysis**: Certain differences between the single and multi-point analyses can be noted. The MOPA shows greater scatter, which can be attributed to a lack of tuning in the cruise operating region of the GEnx-1B GSP model. However, overall MOPA shows potential, picking up on deterioration trends that are not recognized by the single operating point analysis.

10.2. Recommendations

The hybrid GPA tool has shown promising results, but still requires considerable developing work. If the following recommendation are followed up, the tool can be a part of implementing a successful condition monitoring strategy as KLM ES, enabling a more cost-effective MRO approach. Indeed, the ultimate goal of GPA in aero-engine applications is that it is able to serve as the sole driver for engine removal.

- The first step would be to develop the GEnx-1B model further, and improve its accuracy in operating regions far away from takeoff. Cruise flight is a promising operating point now that CEOD is available, as the engine is thermally stable and secondary performance parameters and operating conditions do not vary widely. This would require tuning component maps, which is explained in another recommendation below.

- The numerical processes in the hybrid GPA tool can still be improved greatly in order to drastically decrease runtime. This will most likely also require some cooperation with NLR, as adaptations to make GSP itself faster necessitate changes to the Borland Database Engine (BDE) that GSP uses. This is explained in more detail in Section 8.3.5. Adding options to the GSP API version such as switching off the chemical equilibrium computation and allowing multi-threading would also benefit the tool's performance.

- Adopting an intra-engine approach can yield significant accuracy improvements, as engine-to-engine variation is eliminated. This will require automatic component map generation as manual tuning is not feasible. Two of these methods are described in Appendix B. This is where the added flight data frequency from CEOD could also aid massively. The end result would be a database of engine-specific reference models, which would be updated every time a new engine is added to the KLM fleet.
- The multi-point hybrid GPA tool must be validated with more on-wing data sets, by analyzing more flights per engine as well as different engines. This process could be made easier by also developing a system that extracts and processes CEOD.
- In the current multi-point analysis, the assumption is made that health parameters are independent of the engine operating point. This is a reasonable assumption that greatly simplifies a MOPA, but on the other hand it could potentially reduce prediction accuracy. Different engine operating points mean different aerodynamic conditions, so in this sense component efficiency and flow capacity can vary significantly [55]. In research conducted by Kamboukos [76], the distribution of each health parameter with rotational speed was expressed by a third-degree polynomial, and results show nonlinear behaviour, with condition deviation increasing with higher rotational speeds. In the future, such a procedure could be added to the hybrid GPA tool in order to increase accuracy. This would, however, necessitate a greater number of operating points, as the number of unknowns also increases in the form of extra polynomial coefficients.
- As is explained previously in Section 6.1.4, jet engines operate in highly transient conditions during takeoff, which can have a significant effect on GPA uncertainty. Putz et al.[50] proposes a method to correct for these transient deviations with a data driven method. By simulating a takeoff maneuver in a transient engine performance model for different operating conditions, correction terms for the impact of these variations on engine performance can be estimated. These can subsequently be applied to calibrate individual engines based on the operating conditions in the particular takeoff snapshot. This method could be an option in order to improve health parameter observability.

It is also possible to compile a list of recommendations that is specifically meant for application of the tool within the KLM ES environment:

- Create a Graphical User Interface (GUI) specifically for engineers at KLM ES. Currently, running the hybrid tool requires considerable knowledge of GSP, Python, Evolutionary Algorithms control variables, and API function calls. Implementing a GUI would increase its user-friendliness greatly.
- Build and maintain a database of engine-specific reference models for the GEnx-1B and LEAP. This goes hand in hand with easy access to CEOD, which is currently not available. Ideally, CEOD should be implemented in some sort of cloud-based solution.
- Implement a condition prediction method based on recent engine trending. If a certain deterioration trajectory is anticipated, it is possible to adjust initial maintenance plans. If no sudden damage or LOP end of life occurs, the engineers could decide to keep the engine on-wing for longer if the component condition is still adequate. This method could aid and eventually replace the WPG currently used by engineers at KLM. The possibility of automatic exceedance event warnings, similar to PROGNOS, could also be implemented.
- The condition prediction method could be validated and improved by comparing the initial and adapted maintenance plan. This would be an ongoing process, building towards continually greater accuracy.

Bibliography

[1] Airbus. Global market forecast 2019-2038. Report, 2019.

[2] S. Ackert. Engine maintenance management: Managing technical aspects of leased assets. Report, Jackson Square Aviation, 2015.

[3] L. Marinai, D. Probert, and R. Singh. Prospects for aero gas-turbine diagnostics: a review. *Applied Energy*, 79(1):109–126, 2004. ISSN 0306-2619.

[4] P.P. Walsh and P. Fletcher. *Gas Turbine Performance*. Blackwell Science Limited, Oxford, England, second edition edition, 2004.

[5] General Electric Aviation. GEnx-1B workscope planning guide. Report GEK 114098, 2017.

[6] General Electric Aviation. GEnx-1B turbofan engine installation manual. Report GEK 112856, 2018.

[7] S.O.T. Ogaji, S. Sampath, R. Singh, and S.D. Probert. Parameter selection for diagnosing a gas-turbine's performance-deterioration. *Applied Energy*, 73(1):25–46, 2002. ISSN 0306-2619.

[8] C.B. Meher-Homji, M.A. Chaker, and H.M. Motiwala. Gas turbine performance deterioration. In *30th turbomachinery symposium*. Texas AM University. Turbomachinery Laboratories, 2001.

[9] R. Kurz, K. Brun, and C. Meher-Homji. Gas turbine degradation. Texas AM University. Turbomachinery Laboratories, 2014.

[10] E.A. Ogiriki, Y.G. Li, T. Nikolaidis, T.G.E. Isaiah, and G. Sule. Effect of fouling, thermal barrier coating degradation and film cooling holes blockage on gas turbine engine creep life. *Procedia Cirp*, 38:228–233, 2015. ISSN 2212-8271.

[11] U. Igie, P. Diez-Gonzalez, A. Giraud, and O. Minervino. Evaluating gas turbine performance using machine-generated data: quantifying degradation and impacts of compressor washing. *Journal of Engineering for Gas Turbines and Power*, 138(12):122601, 2016. ISSN 0742-4795.

[12] H. Hanachi, C. Mechefske, J. Liu, A. Banerjee, and Y. Chen. Performance-based gas turbine health monitoring, diagnostics, and prognostics: A survey. *IEEE Transactions on Reliability*, 67(3):1340–1363, 2018. ISSN 0018-9529.

[13] E.M. Greitzer, C.S. Tan, and M.B. Graf. *Internal Flow*. Cambridge University Press, Cambridge, UK, 2004.

[14] R. Kurz, K. Brun, and M. Wollie. Degradation effects on industrial gas turbines. *Journal of engineering for gas turbines and power*, 131(6):062401, 2009. ISSN 0742-4795.

[15] W.P.J. Visser. *Generic Analysis Methods for Gas Turbine Engine Performance: The development of the gas turbine simulation program GSP*. Phd thesis, Delft University of Technology, 2015.

[16] M.L. Verbist. *Gas path analysis for enhanced aero-engine condition monitoring and maintenance*. Phd thesis, Delft University of Technology, 2017.

[17] M. van Moorselaar. *Gas Path Analysis on the GEnx-1B at KLM Engine Services*. Master's thesis, Delft University of Technology, 2018.

[18] N. Aretakis, I. Roumeliotis, A. Alexiou, C. Romesis, and K. Mathioudakis. Turbofan engine health assessment from flight data. *Journal of Engineering for Gas Turbines and Power*, 137(4):041203, 2015. ISSN 0742-4795.

[19] T.U.J. Gronstedt. Identifiability in multi-point gas turbine parameter estimation problems. pages 9–17. American Society of Mechanical Engineers, 2002.

[20] P.C. Escher. *Pythia: An Object-Oriented Gas Path Analysis Computer Program for General Applications*. Phd thesis, Cranfield University, 1995.

[21] S. Ackert. Engine maintenance concepts for financiers. *Macquarie AirFinance Mar*, 2010.

[22] M. Tahan, E. Tsoutsanis, M. Muhammad, and Z.A.A. Karim. Performance-based health monitoring, diagnostics and prognostics for condition-based maintenance of gas turbines: A review. *Applied energy*, 198:122–144, 2017. ISSN 0306-2619.

[23] M.L. Verbist, W.P.J. Visser, and J.P. van Buijtenen. Experience with gas path analysis for on-wing turbofan condition monitoring. *Journal of Engineering for Gas Turbines and Power*, 136(1):011204, 2014. ISSN 0742-4795.

[24] General Electric Aviation. The genx commercial aircraft engine. URL `https://www.geaviation.com/sites/default/files/datasheet-genx.pdf`.

[25] D.M. den Haan. *GSP Gas Path Analysis on CF6-80 Engines at KLM Engine Services*. Master's thesis, Delft University of Technology, 2010.

[26] T. W. Fowler. *Jet engines and propulsion systems for engineers*. GE Aircraft Engines, USA, 1989.

[27] H. Cohen, G. F. C. Rogers, and H. I. H. Saravanamuttoo. *Gas turbine theory*. Pearson Education Limited, Essex, England, sixth edition edition, 2009.

[28] J.P. van Buijtenen, W.P.J. Visser, T. Tinga, S. Shakariyants, and F. Montella. Reader aero engine technology ae4238. 2009.

[29] RTO Applied Vehicle Technology Task Group. Performance prediction and simulation of gas turbine engine operation for aircraft, marine, vehicular, and power generation. Report, NATO Research and Technology Organization RTO, 2007.

[30] A.D. Fentaye, S.I.U.H. Gilani, and A.T. Baheta. Gas turbine gas path diagnostics: A review. volume 74, page 00005. EDP Sciences, 2016. ISBN 2261-236X.

[31] A. Stamatis, K. Mathioudakis, M. Smith, and K. Papailiou. Gas turbine component fault identification by means of adaptive performance modeling. American Society of Mechanical Engineers Digital Collection, 1990.

[32] GSP Development Team. Gas Turbine Simulation Program 11. URL `https://www.gspteam.com/`.

[33] W.P.J. Visser, H. Pieters, M. Oostveen, and E. van Dorp. Experience with GSP as a gas path analysis tool. pages 175–182. American Society of Mechanical Engineers Digital Collection, 2006.

[34] S.Z. Boksteen, D.J. van der Vecht, R. Pecnik, and J.P. van Buijtenen. Performance modeling of a modern gas turbine for dispatch optimization. pages 835–846. American Society of Mechanical Engineers Digital Collection, 2012.

[35] Y.G. Li. Gas turbine performance and health status estimation using adaptive gas path analysis. *Journal of Engineering for Gas Turbines and Power*, 132(4):041701, 2010. ISSN 0742-4795.

[36] P. Kamboukos, P. Oikonomou, A. Stamatis, and K. Mathioudakis. Optimizing diagnostic effectiveness of mixed turbofans by means of adaptive modelling and choice of appropriate monitoring parameters. Report, National Technical University Athens Lab of Thermal Turbomachines, 2003.

[37] W.P.J. Visser, O. Kogenhop, and M. Oostveen. A generic approach for gas turbine adaptive modeling. *Journal of engineering for gas turbines and power*, 128(1):13–19, 2006. ISSN 0742-4795.

[38] H. Pieters. *Gas Path Analysis with GSP for the GEM42 turboshaft engine*. Master's thesis, Delft University of Technology, 2005.

[39] M. Oostveen. *Development of Gas Path Analysis functionality in GSP*. Master's thesis, Delft University of Technology, 2006.

[40] S. El Bouazzaoui. *Modeling of a GSP Diagnostic Tool for the CFM56-7B engines*. Master's thesis, Delft University of Technology, 2008.

[41] K. Geris. *CFM56-7B Post-Overhaul Performance Issues*. Master's thesis, Delft University of Technology, 2010.

[42] E. van Dorp. *Development and implementation of a GSP gas path analysis tool for gas turbine diagnostics*. Master's thesis, Delft University of Technology, 2009.

[43] P.A. Beishuizen. *Improving compressor maps of the GE CF6-80C2 engine*. Master's thesis, Delft University of Technology, 2012.

[44] N. Aretakis, K. Mathioudakis, and A. Stamatis. Nonlinear engine component fault diagnosis from a limited number of measurements using a combinatorial approach. *Journal of Engineering for Gas Turbines and Power*, 125(3):642–650, 2003. ISSN 0742-4795.

[45] I. Loboda. *Gas Turbine Diagnostics*, book section 7, pages 191–211. InTech, Rijeka, Croatia, 2012.

[46] A. Stamatis. Evaluation of gas path analysis methods for gas turbine diagnosis. *Journal of Mechanical Science and Technology*, 25(2):469, 2011. ISSN 1738-494X.

[47] M. Zedda and R. Singh. Gas turbine engine and sensor fault diagnosis using optimization techniques. *Journal of propulsion and power*, 18(5):1019–1025, 2002. ISSN 0748-4658.

[48] M. Zedda. *Gas Turbine Engine and Sensor Fault Diagnosis*. Phd thesis, Cranfield University, 1999.

[49] S. Sampath, S. Ogaji, R. Singh, and D. Probert. Engine-fault diagnostics: an optimisation procedure. *Applied energy*, 73, 2002.

[50] A. Putz, S. Staudacher, C. Koch, and T. Brandes. Jet engine gas path analysis based on takeoff performance snapshots. *Journal of Engineering for Gas Turbines and Power*, 139(11):111201, 2017. ISSN 0742-4795.

[51] S. Sampath, Y.G. Li, S.O.T. Ogaji, and R. Singh. Fault diagnosis of a two spool turbo-fan engine using transient data: A genetic algorithm approach. pages 351–359. American Society of Mechanical Engineers Digital Collection, 2003.

[52] S.O.T. Ogaji, Y.G. Li, S. Sampath, and R. Singh. Gas path fault diagnosis of a turbofan engine from transient data using artificial neural networks. In *IGTI/ASME Turbo Expo 2003*, 2003.

[53] Y.G. Li. A gas turbine diagnostic approach with transient measurements. *Proceedings of the Institution of Mechanical Engineers, Part A: Journal of Power and Energy*, 217(2):169–177, 2003. ISSN 0957-6509.

[54] Y.G. Li, L. Marinai, E. Lo Gatto, V. Pachidis, and P. Pilidis. Multiple-point adaptive performance simulation tuned to aeroengine test-bed data. *Journal of Propulsion and Power*, 25, 2009.

[55] A.G. Stamatis. Optimum use of existing sensor information for gas turbine diagnostics. pages 47–54. American Society of Mechanical Engineers Digital Collection, 2008.

[56] M. Kumar, P. Nallagownden, and I. Elamvazuthi. Advanced pareto front non-dominated sorting multi-objective particle swarm optimization for optimal placement and sizing of distributed generation. *Energies*, 9:982, 2016.

[57] C. Kong. Review on advanced health monitoring methods for aero gas turbines using model based methods and artificial intelligent methods. *International Journal of Aeronautical and Space Sciences*, 15(2): 123–137, 2014. ISSN 2093-274X.

[58] C. Siu, Q. Shen, and R. Milne. TMDOCTOR: a fuzzy rule- and case-based expert system for turbomachinery diagnosis. *SAFEPROCESS'97*, vol. 1:p. 556–563, 1997.

[59] G. Tang. A practical intelligent system for condition monitoring and fault diagnosis of jet engines. *AIAA 99-2533*, 1999.

[60] M.F. Abdul Ghafir, Y.G. Li, and L. Wang. Creep life prediction for aero gas turbine hot section component using artificial neural networks. *Journal of Engineering for Gas Turbines and Power*, 136(3), 2014. ISSN 0742-4795.

[61] M.A. Zaidan, R. Relan, A.R. Mills, and R.F. Harrison. Prognostics of gas turbine engine: An integrated approach. *Expert Systems with Applications*, 42(22):8472–8483, 2015. ISSN 0957-4174.

[62] R.E. Kalman. A new approach to linear filtering and prediction problems. *ASME Journal of Basic Engineering*, 1960. ISSN 0021-9223.

[63] D. Kraft. A software package for sequential quadratic programming. *Deutsche Forschungs- und Versuchsanstalt fur Luft- und Raumfahrt*, 1988.

[64] E. Tsoutsanis, Y.G. Li, P. Pilidis, and M. Newby. Part-load performance of gas turbines: Part II—multipoint adaptation with compressor map generation and GA optimization. pages 743–751. American Society of Mechanical Engineers Digital Collection, 2013.

[65] C.R. Houck, J. Joines, and M.G. Kay. A genetic algorithm for function optimization: a matlab implementation. *Ncsu-ie tr*, 95(09):1–10, 1995.

[66] R. Storn and K. Price. Differential evolution–a simple and efficient heuristic for global optimization over continuous spaces. *Journal of global optimization*, 11(4):341–359, 1997. ISSN 0925-5001.

[67] GSP Development Team. GSP API user manual. Report, Nationaal Lucht- en Ruimtevaartlaboratorium, 2016.

[68] B. Roell. *Test cell on-wing turbofan performance comparison at KLM Engine Services*. Master's thesis, Delft University of Technology, 2019.

[69] General Electric Aviation. GEnx-1B engine shop manual. Report, 2019.

[70] S. van Vuuren. *Humidity Effects on turbo-fan performance in an MRO context*. Master's thesis, Delft University of Technology, 2019.

[71] F.M. Dekking, C. Kraaikamp, H.P. Lopuhaä, and L.E. Meester. *A Modern Introduction to Probability and Statistics: Understanding why and how*. Springer Science Business Media, 2005. ISBN 1852338962.

[72] J. Kurzke. Some applications of the Monte Carlo method to gas turbine performance simulations. American Society of Mechanical Engineers Digital Collection, 1997.

[73] J. Kurzke. How to create a performance model of a gas turbine from a limited amount of information. pages 145–153. American Society of Mechanical Engineers Digital Collection, 2005.

[74] M.L. Verbist, W.P.J. Visser, R. Pecnik, and J.P. van Buijtenen. Component map tuning procedure using adaptive modeling. pages 371–379. American Society of Mechanical Engineers Digital Collection, 2012.

[75] D. Clifton. *Condition monitoring of gas-turbine engines*. Master's thesis, University of Oxford, 2006.

[76] P. Kamboukos and K. Mathioudakis. Multipoint non-linear method for enhanced component and sensor malfunction diagnosis. In *Proceedings of IGTI/ASME Turbo Expo 2006*, 2006.

[77] C. Kong, S. Kho, and J. Ki. Component map generation of a gas turbine using genetic algorithms. *Journal of Engineering for Gas Turbines and Power*, 128(1):92–96, 2006. ISSN 0742-4795.

[78] E. Tsoutsanis, Y.G. Li, P. Pilidis, and M. Newby. Part-load performance of gas turbines: Part I—a novel compressor map generation approach suitable for adaptive simulation. pages 733–742. American Society of Mechanical Engineers Digital Collection, 2013.

[79] M. Zwingenberg, F.K. Benra, and K. Werner. Improvement of performance prediction by automated assimilation of gas turbine component maps. pages 1761–1770. American Society of Mechanical Engineers Digital Collection, 2008.

A

Thesis Assignment

Gas Path Analysis on New Generation Turbofan Engines at KLM ES

MSc Assignment for Tim Rootliep, Propulsion Power (FPP), Faculty of Aerospace Engineering

Introduction
KLM Engine Services (ES) is part of Air France Industries KLM Engineering Maintenance Group, overhauling approximately 200 aircraft engines annually. The overhaul shop visit ends with a standardized performance test, to assess compliance to certification rules and customer contracts, before it is released for operation on-wing. At two different locations, the following turbofan engine types are tested:

- CFM56-7B KLM EM Testcell / Schiphol-Oost
- CF6-80E1 KLM EM Testcell / Schiphol-Oost
- CF6-80C2 KLM EM Testcell / Schiphol-Oost
- GEnx-1B Zephyr Testcell / Charles de Gaulle Airport, Paris
- CFMI LEAP-1A -1B (in gradual introduction)

Over the years KLM ES Engineering has used GSP (Gas turbine Simulation Program) as a supporting tool to analyze and evaluate engine performance data. Gas Path Analysis (GPA) techniques are used to translate engine performance data into component condition information. For optimal performance analysis accuracy, parameter inputs from all gas path sensors at the various engine stations are required. With new engine types like the GEnx and the LEAP, the OEM does no longer provide the ability to install the additional sensors at the various engine stations, hence data input is limited, resulting in reduced potential to accurately analyze performance. However, the missing information can be compensated for by using accurate and detailed system performance models, which provide relationships between measured and unmeasured parameters. For the LEAP engine, a new GSP model needs to be developed. As no test data are available yet and, once data would become available, the limited parameter set, reverse engineering methods will have to be used to obtain a model that can sufficiently represent the LEAP engine for demonstration of a GPA concept.

Key objectives

- To develop GSP a performance model of the CFMI LEAP engine.
- Assess the potential of using GSP adaptive modelling GPA for engine test cell and on-wing performance analysis and diagnostics. This applies to both the new model to be developed and the existing GSP adaptive engine diagnostics model of the GEnx engine.
- Configure the models for GPA and performance analysis purposes.

Assignment
Your work will include the following elements:

1. A literature study on turbofan engine performance modelling and test analysis, including GPA with reduced number of measured of parameters.
2. Introduction to current KLM performance and EGTM condition monitoring practice and relation to the maintenance concept.
3. Introduction to GSP (test analysis and gas path analysis models) as applied to KLM engines.
4. Development of a GSP model for the LEAP engine. The model can be derived from existing models of the CF6-80, GE90 and CFM56 engine families.
5. Assessment of options to use the models to compensate for the limited number of parameters. This involves specific analysis of the relationship of missing parameters with other parameters and operating state of the engine.
6. Development of a GSP GPA concept for the GENx and LEAP engines.

Report
Results of the work must be reported in English, with a copy of this assignment and an executive summary.

Coaching
The work will be performed in close collaboration with KLM Engine Services (Asteris Apostolidis, Michel Nollet, Rob Duivis)

Date: 1 September 2019

Professor:	Delft University tutor:	Supervisors at KLM:
Prof. dr. ir. P. Colonna	Dr. ir. W.P.J. Visser	Asteris Apostolidis
		Michel Nollet
		Rob Duivis

B

Automatic Component Map Generation

A promising way to increase the accuracy of gas turbine diagnostics is to create a specific component maps for every individual engine that is valid in a large operating range. This would require retuning component maps countless times, which is not feasible when done by hand. In this Appendix, two alternatives, which can be made fully automatic, are given: linear map scaling and speedline generation.

B.1. Linear Map Scaling

The less involved method of the two is scaling standard component maps for different operating points. This is convenient as this approach is based solely on linear map scaling, while still being able to predict performance in off-design conditions. The procedure starts by scaling the corrected parameter groups to the desired design point, which is straightforward:

$$SF_{N,DP} = \frac{N_{DP}}{N_{DP0}} = 1.0 \tag{B.1}$$

$$SF_{PR,DP} = \frac{PR_{DP} - 1}{PR_{DP0} - 1} \tag{B.2}$$

$$SF_{W_c,DP} = \frac{W_{cDP}}{W_{cDP0}} \tag{B.3}$$

$$SF_{\eta,DP} = \frac{\eta_{DP}}{\eta_{DP0}} \tag{B.4}$$

where $DP0$ is the default map design point and the rotational speed lines scaling factor is set to 1 Next, Off-Design (OD) scaling factors are introduced, which directly refer to multiple off-design points close to the design condition:

$$SF_{N,OD} = \frac{N_b}{N_a} = 1.0 \tag{B.5}$$

$$SF_{PR,OD} = \frac{PR_b - PR_{DP}}{PR_a - PR_{DP}} \tag{B.6}$$

$$SF_{W_c,OD} = \frac{W_{cb} - W_{cDP}}{W_{ca} - W_{cDP}} \tag{B.7}$$

$$SF_{\eta,OD} = \frac{\eta_b - \eta_{DP}}{\eta_a - \eta_{DP}} \tag{B.8}$$

where the chose design point remains fixed during the off-design adaptation, and a is the point on a speedline before the adaptation, while b is the new position of a after the adaptation. The optimal set of scaling factors can be found using an optimization procedure like an Evolutionary Algorithm [54]. However, as also noted by Li et al. [54], the linear nature of this method means that adapted compressor maps may lose prediction accuracy when far away from the design point, in the low speedline area. Another issue is that multiple model files with different compressor maps will need to be maintained.

B.2. Speedline Generation

Going one step further, it is also possible to automatically generate component maps by extrapolating from high-order polynomials, which has been introduced in several papers [64, 77–79]. These polynomials describe the relation between isentropic efficiency, pressure ratio and flow capacity. The unknown coefficients are then solved in an optimizing routine. Then, the performance map can be drawn for the individual components. The amount of on-wing data available for the GEnx-1B at KLM ES, including start of service life, allows

for the application of this approach. The third-order polynomials, relating isentropic efficiency, pressure ratio and flow capacity, are expressed as follows [77]:

$$W_c = a \cdot PR^3 + b \cdot PR^2 + c \cdot PR + d \tag{B.9}$$

$$\eta = a \cdot W_c^3 + b \cdot w_c^2 + c \cdot W_c + d \tag{B.10}$$

Where W_c is the mass flow parameter, PR is the pressure ratio and η the efficiency. Then the unknown coefficients a, b, c and d are found using an Evolutionary Algorithm with an objective function that minimizes the percentage error. Tsoutsanis et al. [64, 78] follow a slightly more sophisticated and complex approach, representing the speedlines with elliptic equations instead of polynomials:

$$W_{c_{a_i}} = W_1 \cdot N^{W_2} \tag{B.11}$$

$$PR_{b_i} = PR_{dp} \cdot PR_1 \cdot N^{PR_2} \tag{B.12}$$

$$\eta_b = \eta_{b_1} \cdot N^2 + \eta_{b_2} \cdot N + \eta_{b_3} \tag{B.13}$$

The first elliptical coefficient for the speedline curve, W_{c_a}, is defined by the two speedline coefficients, W_1 and W_2, and the compressor rotor speed N. The second elliptical coefficient for the speedline curve, PR_b, is also an exponential function of the design point pressure ratio PR_{dp} and two more speedline coefficients PR_1 and PR_2. The subscript i in the first two equations indicate individual speed lines. Lastly, the efficiency parameter η_b is described by a polynomial function of speed N and three unknown coefficients.

The fact that these equations are exponential and quadratic functions of the rotor speed allow them to capture nonlinear effects of compressor performance behaviour [78]. All in all, 7 coefficients determine the shape of the compressor map, and just like before these are subjected to an optimization by genetic algorithm. The advantage of this method is that the GA can also be solved with multiple operating points as data input, increasing the accuracy of off-design operating conditions further [64]. The drawback is that this procedure is a lot more involved, as it is also necessary to define the lower and upper bounds of the coefficients, along with a pressure ratio limit for the surge line.

The two approaches have the same result, namely an engine-specific compressor map, which is accurate in off-design conditions. It can be transformed into a map type recognizable by GSP with software like SMOOTH-C in Matlab [77]. Automatic map generation is a promising concept, especially when used in combination with an intra-engine approach.

C

ESN 956xxx Workscope Overview

Nomenclature	IIN	Module no.	Level of Work *				
			Serviceable remove	I	II	III	IV
Engine	**72X**	M10	X				
Fan Stator Module	**01X**	M15	X				
Fan Stator Assembly	21X	M18					
Propulsor	**02X**	M20			X		
Fan Booster Assembly	22X	M21					
No. 1 Bearing Assembly	23X	M23					
No. 2 Ball Bearing Assembly	24X	M24					
Fan Hub Module	**25X**	M30					
Fan Hub Frame Assembly	26X	M31					
Inlet Gearbox Assembly	61X	M32					
Transfer Gearbox Assembly	62X	M33					
High Pressure Compressor Module	**30X**	M53					
HPC Rotor Assembly	31X	M51					
HPC Forward Stator Assembly	32X	M52					
Combustor Diffuser Nozzle Module	**40X**	M45			X		
Combustor Diffuser Assembly	41X	-			X		
Combustion Chamber Assembly	42X	M54					X
HPT Stage 1 Nozzle Assembly	51X	M55					X
High Pressure Turbine Module	**50X**	-			X		
HPT Stage 2 Nozzle Assembly	52X	M56			X		
HPT Rotor Assembly	53X	M57					X
Turbine Center Frame Assembly	54X	M58			X		
Low Pressure Turbine Module	**04X**	M60			X		
LPT Rotor / Stator Assembly	56X	M61					
Turbine Rear Frame Assembly	57X	M63					
Fan Mid Shaft Assembly	58X	M64					
Accessory Gearbox Module	**05X**	M70	X				
AGB Assembly	64X	M71					
Lower Bifurcation Module	**03X**	M80	X				

***) Level of Work**

I Shopvisit Q/T, Continued Time
II Shopvisit Minimum workscope
III Shopvisit Performance workscope
IV Shopvisit Overhaul workscope

Figure C.1: Workscope overview of ESN 956xxx

D

Adaptive Modelling On-Wing Results

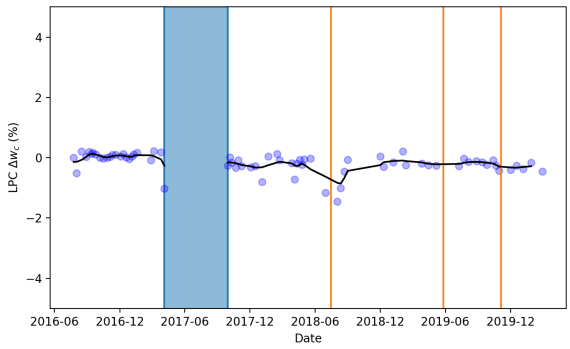

(a) LPC flow capacity deterioration

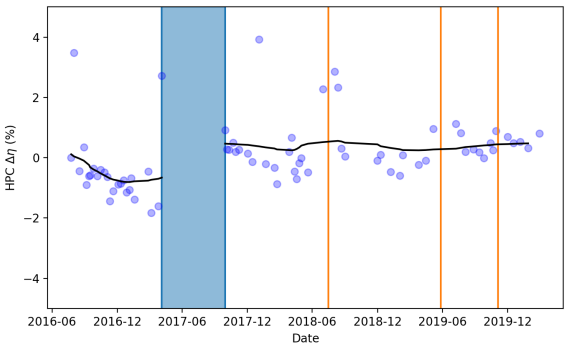

(b) HPC efficiency deterioration

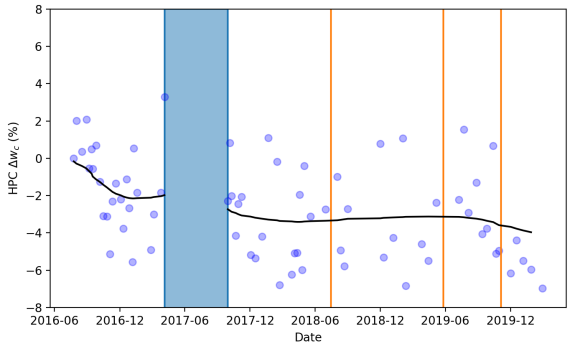

(c) HPC flow capacity deterioration

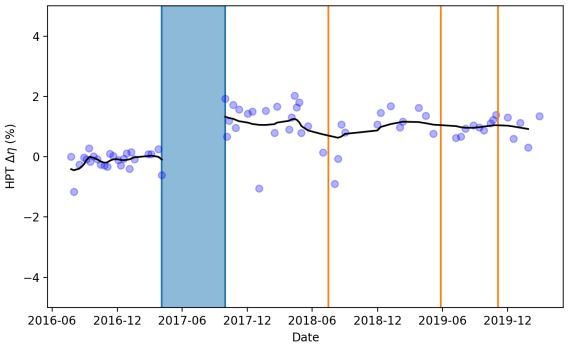

(d) HPT efficiency deterioration

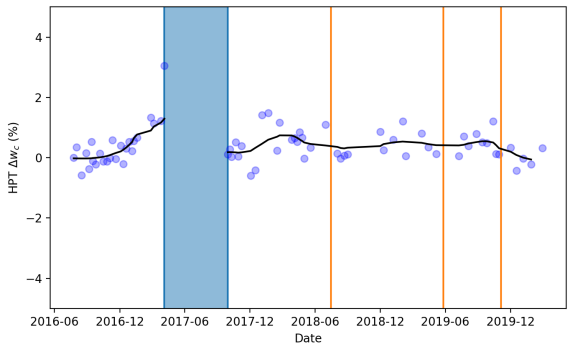

(e) HPT flow capacity deterioration

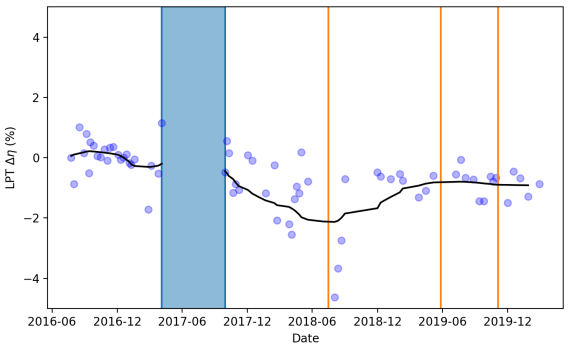

(f) LPT efficiency deterioration

Figure D.1: Engine component deterioration as calculated by GSP AM